NASA/CR—2000-210037

Development and Demonstration of Active Noise Control Concepts

R. Kraft
GE Aircraft Engines, Cincinnati, Ohio

Z. Hu
GE CR&D, Schenectady, New York

S. Sommerfeldt
Brigham Young University, Provo, Utah

B. Walker and A. Hersh
Hersh Acoustical Engineering, Westlake Village, California

H. Luo
GE CR&D, Schenectady, New York

M. Spencer
Signal Processing Solutions, Redondo Beach, California

D. Hallman
GE CR&D, Schenectady, New York

C. Mitchell
Colorado State University, Fort Collins, Colorado

D. Sutliff
AYT Corporation, Brook Park, Ohio

Prepared under Contract NAS3–27720

National Aeronautics and
Space Administration

Glenn Research Center

September 2000

Available from

NASA Center for Aerospace Information
7121 Standard Drive
Hanover, MD 21076
Price Code: A08

National Technical Information Service
5285 Port Royal Road
Springfield, VA 22100
Price Code: A08

Available electronically at http://gltrs.grc.nasa.gov/GLTRS

NASA/CR—2000-210037

Development and Demonstration of Active Noise Control Concepts

R. Kraft
GE Aircraft Engines, Cincinnati, Ohio

Z. Hu
GE CR&D, Schenectady, New York

S. Sommerfeldt
Brigham Young University, Provo, Utah

B. Walker and A. Hersh
Hersh Acoustical Engineering, Westlake Village, California

H. Luo
GE CR&D, Schenectady, New York

M. Spencer
Signal Processing Solutions, Redondo Beach, California

D. Hallman
GE CR&D, Schenectady, New York

C. Mitchell
Colorado State University, Fort Collins, Colorado

D. Sutliff
AYT Corporation, Brook Park, Ohio

September 2000

The NASA STI Program Office . . . in Profile

Since its founding, NASA has been dedicated to the advancement of aeronautics and space science. The NASA Scientific and Technical Information (STI) Program Office plays a key part in helping NASA maintain this important role.

The NASA STI Program Office is operated by Langley Research Center, the Lead Center for NASA's scientific and technical information. The NASA STI Program Office provides access to the NASA STI Database, the largest collection of aeronautical and space science STI in the world. The Program Office is also NASA's institutional mechanism for disseminating the results of its research and development activities. These results are published by NASA in the NASA STI Report Series, which includes the following report types:

- TECHNICAL PUBLICATION. Reports of completed research or a major significant phase of research that present the results of NASA programs and include extensive data or theoretical analysis. Includes compilations of significant scientific and technical data and information deemed to be of continuing reference value. NASA's counterpart of peer-reviewed formal professional papers but has less stringent limitations on manuscript length and extent of graphic presentations.

- TECHNICAL MEMORANDUM. Scientific and technical findings that are preliminary or of specialized interest, e.g., quick release reports, working papers, and bibliographies that contain minimal annotation. Does not contain extensive analysis.

- CONTRACTOR REPORT. Scientific and technical findings by NASA-sponsored contractors and grantees.

- CONFERENCE PUBLICATION. Collected papers from scientific and technical conferences, symposia, seminars, or other meetings sponsored or cosponsored by NASA.

- SPECIAL PUBLICATION. Scientific, technical, or historical information from NASA programs, projects, and missions, often concerned with subjects having substantial public interest.

- TECHNICAL TRANSLATION. English-language translations of foreign scientific and technical material pertinent to NASA's mission.

Specialized services that complement the STI Program Office's diverse offerings include creating custom thesauri, building customized data bases, organizing and publishing research results . . . even providing videos.

For more information about the NASA STI Program Office, see the following:

- Access the NASA STI Program Home Page at ***http://www.sti.nasa.gov***

- E-mail your question via the Internet to help@sti.nasa.gov

- Fax your question to the NASA Access Help Desk at (301) 621-0134

- Telephone the NASA Access Help Desk at (301) 621-0390

- Write to:
  NASA Access Help Desk
  NASA Center for AeroSpace Information
  7121 Standard Drive
  Hanover, MD 21076

Table of Contents

1 Introduction 1
1.1 Problem 1
1.2 Background 1
1.3 Overall Program Objectives 2
1.4 Previous Effort 2
1.5 Technical Approach 2
1.5.1 Develop Analytical Simulation Program 3
1.5.2 Develop ANC Concepts for High Order Radial Mode Application 3
1.5.3 Demonstrate ANC Concepts on NASA Fan in AAPL 3
1.5.4 Assess Practicality of ANC System Integration with Current Turbofan Engines 3
1.6 Summary of Results 4

2 Exhaust ANC System Design 5
2.1 Objectives 5
2.2 Background and Approach 5
2.3 Exhaust ANC System Details 7
2.3.1 Actuators 7
2.3.2 Actuator Arrays 8
2.3.3 Error Sensing Microphones 10
2.3.4 Controller 12
2.3.5 Modal Control Considerations 13
2.4 Final Exhaust ANC System Description 14

3 Exhaust ANC System Test Program 16
3.1 Hardware Preparation 16
3.2 System Calibration on ANCF 18
3.3 Actuator Array Tests 18
3.4 In-Duct Active Control Tests 18
3.5 Exhaust ANC System Test Results 19
3.5.1 Actuator Array Radiation 19
3.5.2 Active Control Performance 21
3.6 Summary of Exhaust ANC System Test Results 21

4 Exhaust System ANC Analytical Simulations 22

4.1 AANCSIM2 Model 22
4.2 Green's Function Analysis and ExhaustSim 24

5 Inlet ANC System Design 28
5.1 Inlet Sensor System Study 28
5.2 Inlet Actuator System Study 32
5.3 Overall System Performance and Passive Treatment Effects 35
5.4 Final Inlet ANC System Design 37

6 Inlet ANC System Test 39
6.1 Speaker Characteristics Test 39
6.1.1 Temperature and running time dependency of the speakers 39
6.1.2 Ambient pressure dependency of the speakers 41
6.2 Speaker Sorting 49
6.3 Mode Generation 52
6.4 Wall Microphone Sensor Performance 59
6.5 Conclusions 64

7 Inlet ANC Control System 65
7.1 Description of the BYU Controller 65
7.1.1 Controller Architecture 65
7.1.2 Controller Hardware 68
7.1.3 Controller Software 69
7.2 Verification Results For the BYU Controller 70
7.2.1 Error Sensor Calibration 71
7.2.2 Actuator Channel Calibration 71
7.2.3 Frequency Estimate 71
7.2.4 Propagation Path Calibration 71
7.2.5 Control Algorithm 72
7.3 Control Results 73

8 ANC Test Results Measured By The NASA Lewis Rotating Rake 76
8.1 Test Bed 76
8.2 Test Conditions 77
8.3 Rotating Rake Results 78
8.3.1 Modal Distortion Characteristics with Fan at Idle 78
8.3.2 Mode Reduction Performance 83

9 Evaluation of Feasibility of Application of ANC to Current Turbofan Engines 90
9.1 Objectives 90
9.2 Summary of Results 90
9.3 Approach 90
9.4 Feasibility Assessments 96
9.4.1 Ideal Case 96
9.4.2 Results from ANC System Simulations 99
9.5 Other Practical Issues 103
9.6 Conclusions and Recommendations 105
10 Appendix 1 - ANC System Analytical Simulations 107
10.1 Introduction 107
10.2 Application to Turbofan Inlet Duct 108
10.2.1 Introduction to CANCSIM 108
10.2.2 ANC Control System Implementation 111
10.2.2.1 Discussion of Gauss-Newton ANC Algorithm 111
10.2.2.2 Upgrade for Multiple ANC Actuator Rings 115
10.2.3 Examples of Control System Operation Simulation 117
10.2.3.1 Single Actuator Ring Control System Operation 117
10.2.3.2 Effects of Simulated Random Errors in Sensors and Actuators 120
10.2.4 Observations 122
10.3 Application to Turbofan Exhaust Duct 123
10.3.1 Introduction 123
10.3.2 Accommodation of Internal Noise Sources 125
10.3.3 Upgrade to Include Backward Modes Radiated from ANC Actuators 125
10.3.4 Removal of Automated Iteration Procedure 125
11 Appendix 2 - Application Of The Green's Function Technique To The Prediction Of Acoustic Fields Generated By Active Noise Control Drivers 126
11.1 Introduction 126
11.2 Analytical Approach 126
11.3 Cylindrical Inlet Duct Model 127
11.3.1 Results of Typical Calculations 129
11.4 Annular Exhaust Duct Model 132
11.4.1 Results of Typical Calculations 134
11.5 Description Of Computer Codes 136

Executive Summary

Active noise control (ANC) is proposed as a technology to overcome the limitations of passive acoustic treatment suppression anticipated for future turbofan designs. Early system noise studies of the potential of active noise control for turbofans of various fan pressure ratios have indicated that noise reductions on the order of 2 EPNdB, averaged over all flight conditions, may be expected. If these suppressions can be added to those from acoustic treatment, and if the added weight and cost of the ANC systems can be constrained to reasonable levels, the use of ANC in aircraft engines will provide added ability to meet future noise regulations or to provide the competitive advantage of added noise margins.

The practical application of active noise control for aircraft engines involves two high-risk technologies: 1) the development of a light-weight, high power actuator to generate the required high intensity sound cancellation levels in the duct; 2) the development of a control system algorithm that can be based on feedback sensors located within the nacelle itself (not in the farfield where the suppression must be achieved). An additional technical problem is that the ANC actuators would be most unobtrusively mounted flush to the surface of the nacelle inlet or exhaust duct, making it difficult to control the generation of higher order radial modes.

The primary objective of this program was to investigate design methods for and feasibility of an Active Noise Control (ANC) system for a discrete tone spinning mode generated by a turbofan engine. In particular, the case where the ANC system must use flush-wall-mounted actuators and the spinning mode tone is well cut-on, having many propagating radial modes, was considered. ANC concepts that were capable of suppressing discrete-tone spinning modes containing more than one cut-on radial mode were identified, developed analytically, and evaluated. Design goals were to develop systems that suppressed at least three radial modes in an inlet duct and three radial modes in an exhaust annulus. Requirement for placement of the actuators and sensors in the duct and for control algorithms were specified. These designs resulted in the definition of inlet duct and exhaust duct tests that were performed in coordination with NASA in the 4-ft ANC fan in the NASA AAPL facility.

An active source cancellation system was implemented at the location of stator vanes in the exhaust duct of ANCF. Effective suppression of twice blade-passing-frequency, (2BPF) spinning mode order m=2 tone noise was achieved over a range of fan speeds 1800-2450 RPM, which included sound fields with three cut-on radial order modes. Total 2BPF noise was suppressed at most fan speeds, but by a lesser degree due to actuator mode spillover and low baseline fan noise level.

For the m = 2 spinning mode, up to 15 dB PWL reduction was obtained with either two or three radial modes present in the exhaust duct. In the inlet duct, up to 18 dB PWL suppression was obtained for 2 radial modes present, up to 12 dB was obtained for 3 radial modes, and up to 4 dB was obtained with 4 radial modes. Thus, the ability to suppress multiple radial modes for tones in both the inlet and exhaust ducts has been successfully demonstrated.

Implications of ANC system design requirements on installation and system integration issues for ANC systems capable of suppressing higher order radial mode content when applied to current turbofan engines were evaluated. The predicted flyover noise benefits of an ANC engine applied to an aircraft such as a 767 using twin CF6 engines have been found to be minimal. The key problem is not that an ANC system would be predicted to not work as designed, but that the benefits gained from reductions of the tones from typical aircraft flyover spectra are small. Benefits would he higher if ANC were applied to an aircraft/engine combination for which tone levels made a higher contribution to the overall noise.

An effective ANC system design will have to attempt to minimize the loss in passive treatment area in order to maintain the suppression levels of fan broadband noise. This could be accomplished using ANC drivers and sensors that are located in treated sections of duct and have small areas open to the duct. To simplify the analysis for this study, the actuators and sensors were located in dedicated hardwall segments. Possibly, the actuators might be designed to provide some passive suppression if they are otherwise inoperable. The successful design of an aircraft engine ANC system will require a system approach that balances suppression gains and losses, possibly integrating the ANC system at the engine preliminary design phase. The integrated design must address installation, operation, and performance issues engendered by the ANC system requirements.

Development and Demonstration of Active Noise Control Concepts

1 Introduction

1.1 Problem

Two current developments in aircraft engines are confronting limitations on the amount of noise suppression that can be achieved by the use of conventional duct lining acoustic treatment. First, existing engines are being extended to higher and higher power ratings, without substantial changes in the amount of treated area. Second, advanced design ultra-high-bypass engines with thin, short outer nacelle structures will simultaneously increase the importance of tones as contributors to the radiated noise levels and make it more difficult to provide adequate passive acoustic treatment. Current passive treatment designs are near optimum, so that large gains in suppression from treatment re-designs are probably not to be expected. Added passive treatment suppression will require longer duct lengths, which will increase engine weight and cost.

Active noise control (ANC) is proposed as a technology to overcome the limitations of passive acoustic treatment suppression anticipated for future turbofan designs. Early system noise studies of the potential of active noise control for turbofans of various fan pressure ratios have indicated that noise reductions on the order of 2 EPNdB, averaged over all flight conditions, may be expected. If these suppressions can be added to those from acoustic treatment, and if the added weight and cost of the ANC systems can be constrained to reasonable levels, the use of ANC in aircraft engines will provide added ability to meet future noise regulations or to provide the competitive advantage of added noise margins.

1.2 Background

The practical application of active noise control for aircraft engines involves two high-risk technologies: 1) the development of a light-weight, high power actuator to generate the required high intensity sound cancellation levels in the duct; 2) the development of a control system algorithm that can be based on feedback sensors located within the nacelle itself (not in the farfield where the suppression must be achieved). An additional technical problem is that the ANC actuators would be most unobtrusively mounted flush to the surface of the nacelle inlet or exhaust duct, making it difficult to control the generation of higher order radial modes.

The ability to control higher order radial modes is critical to being able to apply ANC to current turbofan engines. Most fans are designed with blade-passing-frequency (BPF) tones cut-off, by using a stator vane number to rotor blade number that is just above 2.0. This give a well-cut-on second harmonic of BPF with a low spinning mode order (m-order) that is the major remaining fan noise contributor. This 2BPF tone contains multiple cut-on radial modes at its frequency of generation. A successful ANC system must address these problems.

1.3 Overall Program Objectives

The primary objective of the program was to investigate design methods for and feasibility of an Active Noise Control (ANC) system for a discrete tone spinning mode generated by a turbofan engine. In particular, the case where the ANC system must use flush-wall-mounted actuators and the spinning mode tone is well cut-on, having many propagating radial modes, was considered.

An ANC analytical simulation program was developed as a major tool and used for design and evaluation of various actuator/control system configurations. Requirements for actuator placement and control system operation will be determined. Two prototype fan rig tests, one for the inlet duct and one for the exhaust duct, was conducted on the NASA ANC Fan Rig in the AAPL to demonstrate concepts and evaluate progress for a limited increase in the number of cut-on radial modes. Assessments of feasibility of applying ANC to a typical high bypass turbofan engine were conducted based on system noise studies for a GEAE CF6-80C2 engine..

1.4 Previous Effort

In Task Order 5 NASA Contract NAS3-26617, entitled *Active Control of Fan Noise: Feasibility Study*, an evaluation of system noise was completed and a prototype piezoceramic-based, lightweight, high-power transducer was developed. The results of this effort are documented in the following NASA CR's:

NASA CR 195392 - Volume 1: Flyover System Noise Studies, Oct. 1994

NASA CR 195440 - Volume 2: Canceling Noise Source - Design of an Acoustic Plate Radiator Using Piezoceramic Actuators, Mar. 1995

Volume 3: Active Fan Noise Cancellation in the NASA Lewis Active Noise Control Fan Facility

Volume 4: Flyover System Noise Studies, Part 2

Volume 5: Numerical Computation of Acoustic Mode Reflection Coefficients for an Unflanged Cylindrical Duct

Volume 6: Theoretical Analysis for Coupling of Active Noise Control Actuator Ring Sources to an Annular Duct with Flow

1.5 Technical Approach

The program included four technical subtasks, conducted by the Prime Contractor and several Subcontractors. The subtasks are as follows:

1. Develop an analytical simulation of ANC application to engine ducts based on a modal analysis propagation program.
2. Develop inlet and exhaust duct ANC concepts for higher order radial mode application.

3. Perform two development tests on NASA ANC fan in the NASA Lewis AAPL facility, one in the inlet and one in the exhaust.
4. Assess feasibility of applying ANC to a typical high bypass turbofan engine

1.5.1 Develop Analytical Simulation Program

Analyses and computer codes were developed for analytical predictions that model the operation of an ANC system in the inlet and exhaust ducts of a turbofan engine. The model includes the fan source mode characteristics, the coupling of flush-mounted ANC actuators, the acoustic propagation through treated and hard-wall ducts with uniform mean flow, the radiation to the farfield, and the control system operation that uses pressures from duct wall sensors to drive the actuators. Control system algorithms used for the ANC test hardware and software were incorporated into the model..

1.5.2 Develop ANC Concepts for High Order Radial Mode Application

ANC concepts that were capable of suppressing discrete-tone spinning modes containing more than one cut-on radial mode were identified, developed analytically, and evaluated. Design goals were to develop systems that suppressed at least three radial modes in an inlet duct and three radial modes in an exhaust annulus. Requirement for placement of the actuators and sensors in the duct and for control algorithms were specified. These designs resulted in the definition of inlet duct and exhaust duct tests that were performed in coordination with NASA in the 4-ft ANC fan in the NASA AAPL facility. Results of testing and analyses were used to evaluate the potential for application of ANC to the second harmonic of blade passing frequency tone on a typical commercial turbofan.

1.5.3 Demonstrate ANC Concepts on NASA Fan in AAPL

Two ANC demonstration tests were performed on the 4-foot ANC fan in the NASA Lewis AAPL facility. The first test was for the purpose of demonstrating an ANC system that will suppress at least three cut-on-radial modes in an inlet duct. The objective of the second test was to suppress at least three cut-on radial modes in the exhaust duct. Testing required modification of the NASA fan rotor and stator, construction of duct spool pieces, and in-duct measurement of modal content, as well as far field acoustic measurements.

1.5.4 Assess Practicality of ANC System Integration with Current Turbofan Engines

Implications of ANC system design requirements on installation and system integration issues for ANC systems capable of suppressing higher order radial mode content when applied to current turbofan engines were evaluated. A final assessment of the practicality of a proposed ANC system design aimed at achieving a balance between suppression of higher harmonic tones with multiple cut-on radial modes and system complexity of installation and operation was made.

1.6 Summary of Results

An active source cancellation system was implemented at the location of stator vanes in the exhaust duct of ANCF. Effective suppression of 2-BPF spinning mode m=2 tone noise was achieved over a range of fan speeds 1800-2450 RPM, which included sound fields with three cut-on radial order modes. Total 2-BPF noise was suppressed at most fan speeds, but by a lesser degree due to actuator mode spillover and low baseline fan noise level.

For the m = 2 spinning mode, up to 15 dB PWL reduction was obtained with either two or three radial modes present in the exhaust duct. In the inlet duct, up to 18 dB PWL suppression was obtained for 2 radial modes present, up to 12 dB was obtained for 3 radial modes, and up to 4 dB was obtained with 4 radial modes. Thus, the ability to suppress multiple radial modes for tones in both the inlet and exhaust ducts has been successfully demonstrated.

The predicted flyover noise benefits of an ANC engine applied to an aircraft such as a 767 using twin CF6 engines have been found to be minimal. The key problem is not that an ANC system would be predicted to not work as designed, but that the benefits gained from reductions of the tones from typical aircraft flyover spectra are small. Benefits would he higher if ANC were applied to an aircraft/engine combination for which tone levels made a higher contribution to the overall noise.

If appreciable installation penalties have to be extracted for the ANC system installation due to loss of passive acoustic treatment area, the overall benefit will decrease further, due to the increase in fan broadband noise. The successful design of an aircraft engine ANC system will require a system approach that balances suppression gains and losses, possibly integrating the ANC system at the engine preliminary design phase. The integrated design must address installation, operation, and performance issues engendered by the ANC system requirements.

2 Exhaust ANC System Design

2.1 Objectives

The goal of the research project was to demonstrate global suppression of rotor/stator interaction tones in the NASA Lewis Research Center Active Noise Control Fan[1], for fan speeds resulting in a minimum of three radial order modes in both the inlet and exhaust ducts. Because of the differing duct geometries in the inlet and exhaust, the project was divided into separate elements, to be combined following demonstration of the capabilities of each. The circular inlet duct application was undertaken by General Electric Corporate Research and Development (CRD) and the annular exhaust duct application was undertaken by Hersh Acoustical Engineering, Inc.(HAE). In development of the exhaust duct application, HAE sought the following:

- Accomplish the multiple radial order noise suppression using a compact and simplified control system.
- Advance the development of tools for generalized design of active noise suppression systems for advanced turbofan engines.

2.2 Background and Approach

Figure 1 shows a cutaway diagram of the ANCF at NASA/LeRC. The annular geometry of the exhaust duct affords the possibility of control from both the inner and outer duct walls as shown, allowing axially compact arrays of actuators and error sensors.

[1] Heidelberg, L.J., Hall, D.G., Bridges, J.E. and Nallasamy, M, "A Unique Ducted Fan Test Bed for Active Noise Control and Aeroacoustics Research" NASA Technical Memorandum 107213 May, 1996

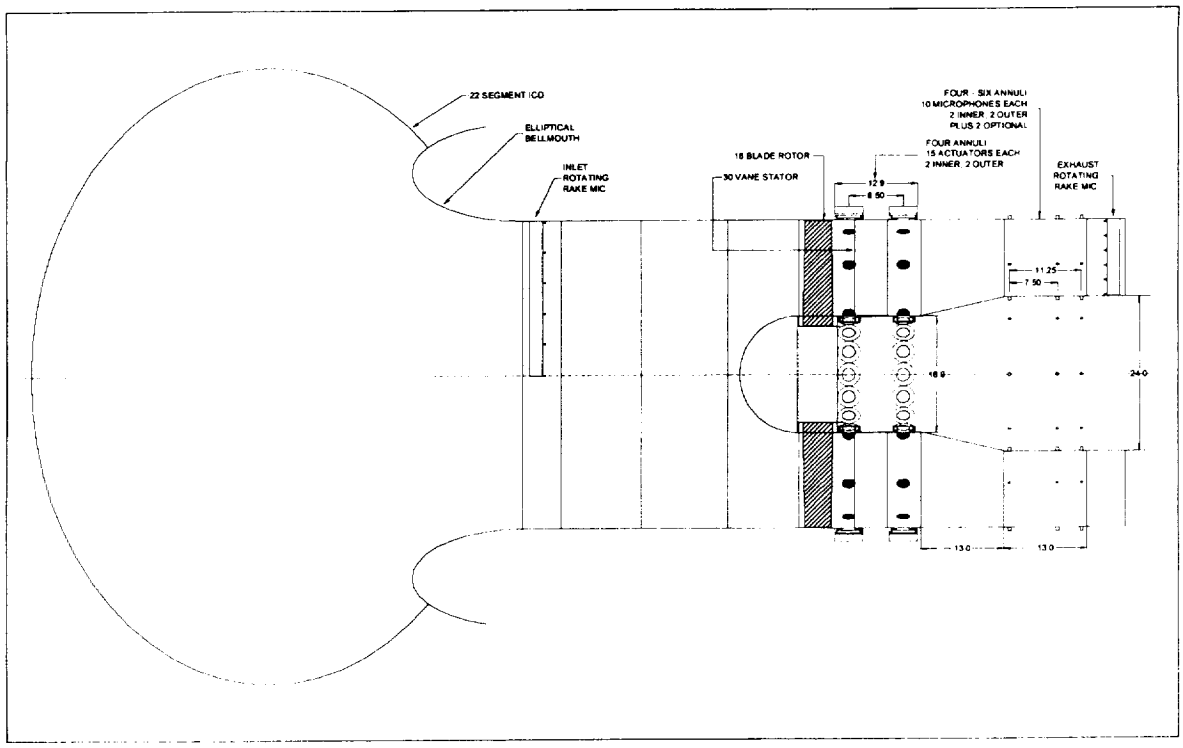

Figure 1. Schematic Diagram of HAE Source Cancellation Installation on ANCF

In 1995-96, HAE[2] developed a control system for simultaneous suppression of inlet and exhaust noise with two radial order modes. The system used arrays of actuators flanking the hubs and tips of stator vanes in ANCF, configured similarly to Figure 1 but with a 20% smaller inner duct radius. Global reduction of modes (4,0) and (4,1) was achieved, but system performance was limited by inefficient coupling of the actuators on the inner duct radius. As will be shown in a subsequent section, the problem is abated by increasing the inner radius and addressing azimuthal mode 2 instead of 4 for the current study. This results in a greatly improved predicted radiation efficiency from the inner actuator array and consequently reduced modal contamination from array imperfections.

An additional limitation encountered in the 1995-96 study was the single controller and actuator array used for simultaneous inlet and exhaust noise suppression. Because of the different geometries of the two environments, the mode mixtures in the two were disparate in a way that the simple system could only approximate. Diagnostic tests for control in one direction at a time demonstrated a high degree of suppression. In the current study, the inlet and exhaust environments are each addressed by separate control systems, alleviating this difficulty. A remaining concern is the degree to which noise in the inlet will be increased as the result of suppression in the exhaust.

---

2 Hersh, A.S., Walker, B.E., Leahy, R., Zhou, Z. and Heidelberg, L.J. "Active Control Dipole Sound Source Cancellation of Axial Fan Rotor-Stator Interaction Noise," U.S. Patent applied for, April 1994

In the 1995-96 study, error sensing was accomplished with three rows of outer wall microphones each in the inlet and exhaust ducts. Because of the potential for acoustic reflections from the exhaust and resultant contamination of the error signals, inner wall microphones were added for improved sound field resolution in the current study.

Prior to final commitment to a system design, computer simulation models indicated potential for substantial noise reduction. The design was first implemented with a modified version of the GEAE AANCSIM2[3] model. This model applies a Newton-Gauss search approach to the control function and performs full modal power balance solutions to sound propagation through the various duct elements. The program performs a modal separation at the error microphone array and uses modal power levels as errors in the controller. This model predicted approximately 17 dB suppression toward the exhaust and approximately 13 dB increase in noise toward the inlet at the design frequency 1250 Hz.

A second computer model, HAE's ExhaustSim, was used to model the actual control algorithm planned for use in the study. Modal transfer functions from the "fan" and the actuator rows to the microphone rows are "measured" and used to compute an actuator drive vector that minimizes the sum-squared error. Fan modal levels are entered from ANCF baseline data and actuator coupling factors are entered from a Greens Function model, discussed in Appendix A. The ExhaustSim model predicted approximately 25 dB exhaust suppression and 6 dB increase in noise toward the inlet.

Since both computer simulations predicted successful noise suppression (albeit with somewhat different expectations), a similar system had been successfully demonstrated in a similar program with different objectives, and the proposed system was compact and geometrically straight-forward, the axially spaced inner/outer duct actuator and error microphone array approach was selected for physical implementation on ANCF.

2.3 Exhaust ANC System Details

As discussed above, the system concept was selected on the basis of prior success, computer simulation performance conformity with the objectives of simplicity and compactness. Details of the various components were determined based on the objective of evolving the system design toward commercial implementation.

2.3.1 Actuators

Electrodynamic, fluidic and several variants of piezoelectric transducers have been explored as actuators for active noise suppression systems. Table 1 below shows several generic actuator type and relative excellence in several applicable performance categories.

---

[3] See Section 10.3.

Table 1 - Actuator Type Evaluation Summary

Actuator Type / Perfomance Criterion	Piezo/Aluminum Off Resonance	Piezo/Aluminum Near Resonance	Piezo Thin Layer Unimorph	Electrodynamic
Light Weight	+	+	++	--
Rugged	++	++	?	-
High Mech. Z	++	-	-	--
Uniformity	+	-	+	++
Mounting Vibr.	-	-	+	++
Output Sens.	-	+	-	++

As can be seen in Table 1, piezoelectric/aluminum laminate actuators excel in most categories, especially when operated away from mechanical resonance frequencies. Their ruggedness and light weight make them strong candidates for use in aircraft engine applications. They are weak in two important categories - mounting vibration excitation and output sensitivity. The former results in a need to design the actuator mounts as an integral part of the treatment structure. The latter requires use of high voltage power amplifiers.

Piezo/aluminum laminate actuators were used in three prior studies and were selected for re-use in the current program rather than redesign and fabricate new ones for the specific test conditions. This was a compromise, as the fan speeds of the current tests are up to 30% higher than those for which the actuators were originally intended.

Operation near resonance resulted in a requirement to calibrate the actuators and amplifiers carefully in an attempt to minimize modal spillover from the actuator arrays. Therefore, each actuator was driven by a separate power amplifier that could be adjusted both in gain and in feedback characteristic to trim the response near the mechanical resonance of the actuator.

2.3.2 Actuator Arrays

It was predetermined from the fan configuration of 16 rotor blades and 30 equally spaced stator vanes that the target mode was m=2. From the speed range (up to 2450 CRPM) it was determined that in the exhaust duct, up to three radial order modes would be cut on in both the 18 inch initial diameter and 24 inch final diameter sections. It is expected that multiple cutoff radial order modes would be generated in the transition regions.

In order to align well with the stator vanes, annular arrays of 15 equally spaced actuators were selected. When excited with signals advancing 48° per actuator around the annulus, mode m=2 will be radiated. Because it is composed of discrete elements, the array will also radiate modes $m \pm 15p$ where p is any integer. The nearest such *aliased* mode is m=-13, which cuts on at a frequency of 1327 Hz (2488 CRPM) in both segments of the exhaust duct, above the planned

test range (2450 CRPM) and not a significant concern. (Note that mode -12 is cut-on within the test range, so that 15 actuators per annulus represents the minimum array for the test.)

By using external circuitry as shown in Figure 2 to advance the actuator phases as required for the target mode, it is possible to limit the controller to a single output per target mode per actuator annulus, resulting is a substantial reduction in complexity relative to a totally generalized control system.

In Figure 2, the four input lines correspond to actuator arrays identified as:

U.O. Outer Wall Upstream of the Stator Tip
U.I. Inner Wall Upstream of the Stator Hub
D.O. Outer Wall Downstream of the Stator Tip
D.I. Inner Wall Downstream of the Stator Hub

Each input is buffered and split into 0° and 90° components using and analog offset delay line approach pseudo-Hilbert transform synthesizer. Inverting amplifiers are then used to provide 180° and 270° signals. Actuator signals are then derived from the four quadrature components using summing amplifiers with weighting resistances determined as

$$R_{real} = 10{,}000 / \cos(\theta_n), \quad R_{imag} = 10{,}000 / \sin(\theta_n) \tag{1}$$

When negative resistances are required, the 180° and 270° drive signals are used. It may be seen that this approach is readily adapted to any mode or actuator count.

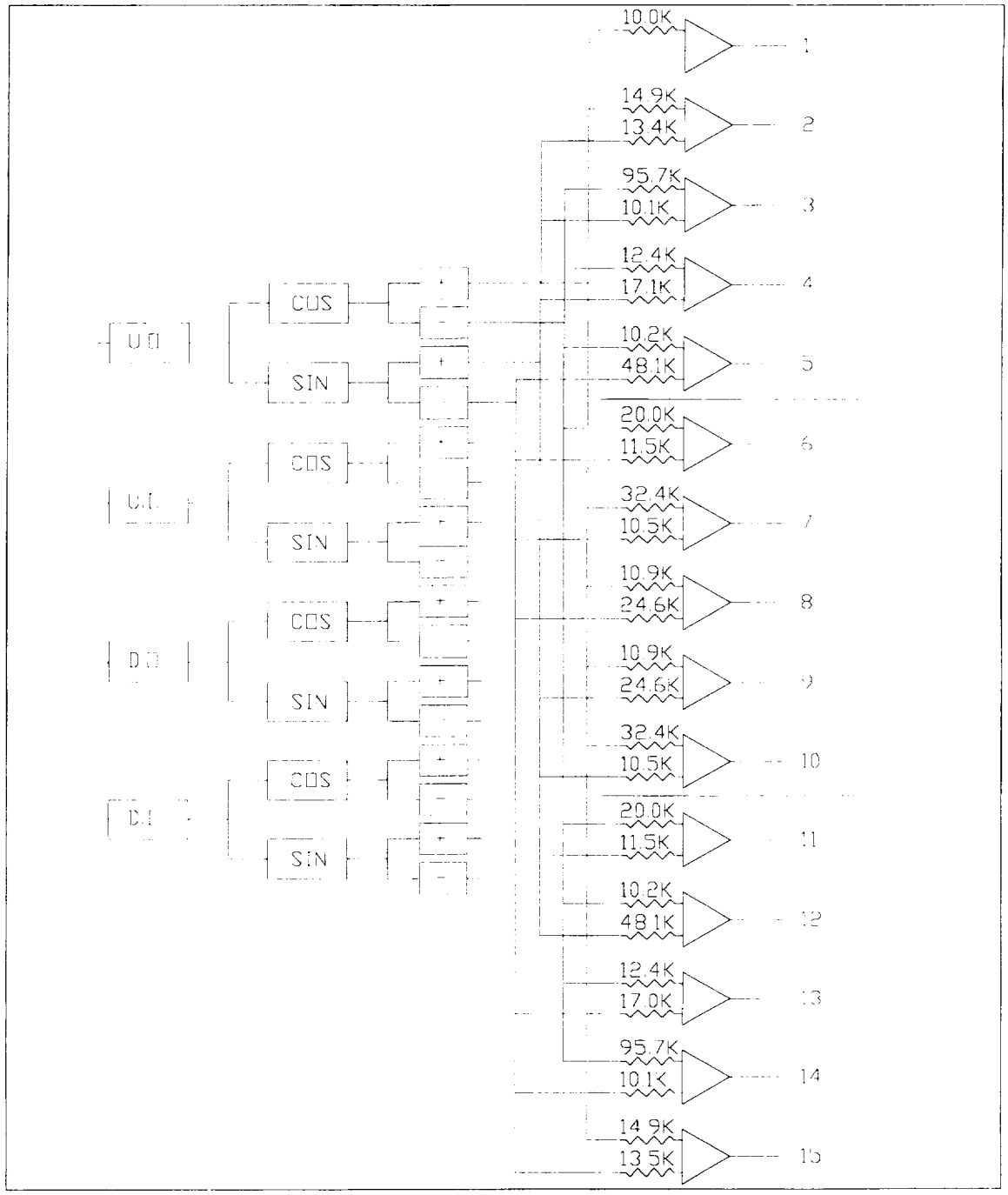

Figure 2 Schematic of Mode Distribution for 15 Actuators at Mode $m = 2$

2.3.3 Error Sensing Microphones

Conversely, in order to resolve azimuthal mode orders with microphone arrays, equally spaced annuli were installed in the duct. Similar aliasing considerations apply as with the actuators, but the minimum number is dictated only by the maximum m-order *present* rather than

the maximum *possible*. Ten microphones per annulus were selected, which resolve mode m=2 by retarding the phases 72° per microphone around the annulus and then summing the signals. Potential mode aliasing would then occur at m=-8, m=12, etc. The ANCF inlet control device is constructed in 22 segments, resulting in minor inflow distortion that generates mode m=10. The 10-microphone array was selected in lieu of an originally considered 8-microphone array to avoid contamination by this element.

Figure 3 shows the simple on-line signal processing network used to isolate mode m=2 from each of the microphone annuli. The network was implemented using all analog components to minimize digital I/O and signal processing burden. The disadvantages of this approach is that microphones must be well matched in each annulus and that a separate network is required for each mode to be resolved.

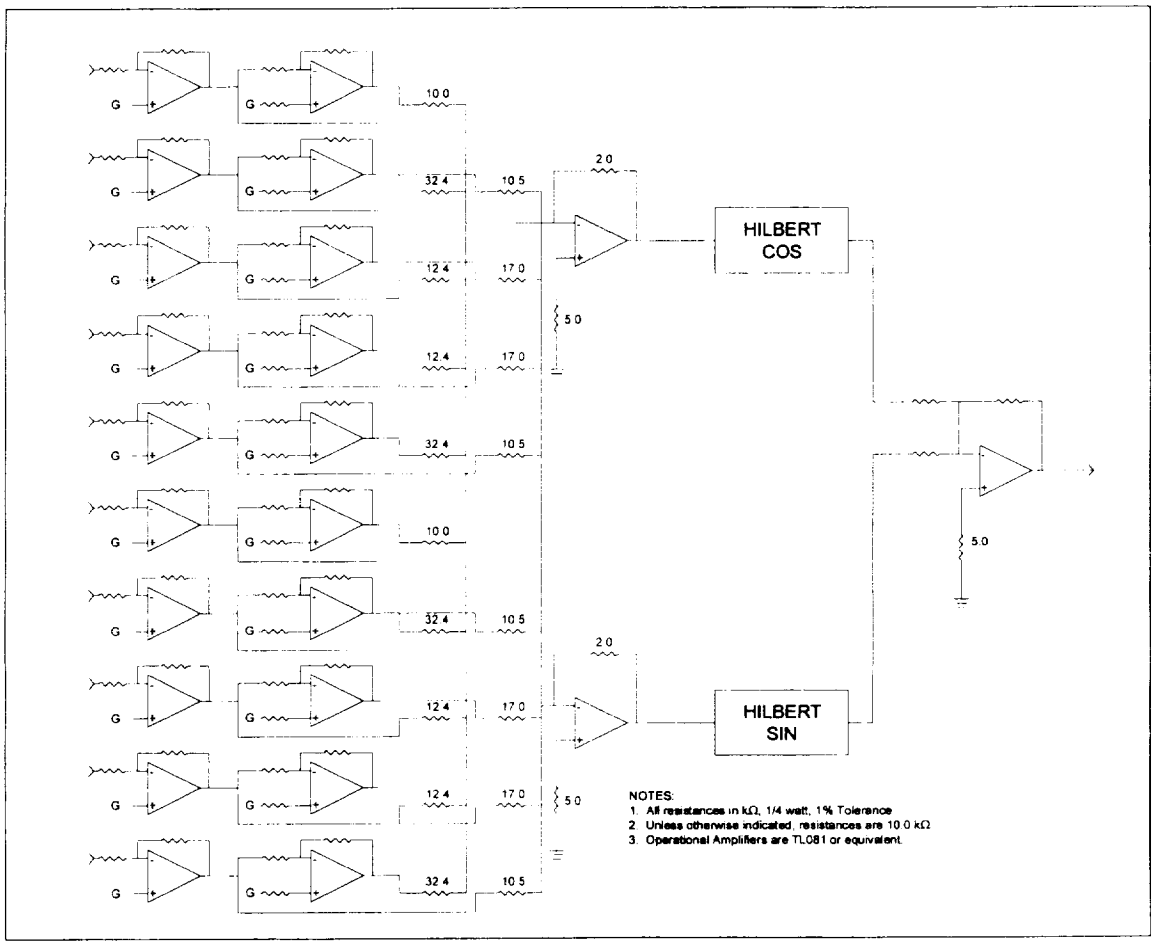

Figure 3 Schematic of On-Line Mode Separation from 10 Microphones to m = 2

In addition to the processing simplicity of the analog approach, it provides on-line modal signals that can be observed on an oscilloscope or spectrum analyzer, facilitating system diagnostics.

The network shown in Figure 2 is essentially 3 in reverse. Microphone signals are injected at the input terminals, buffered and split into positive and negative polarities. They are then combined into "real" and "imaginary" geometrical sub-sums, which are then rotated 90° phase relative to one another and added. Summing junction resistances are computed in accordance with Equation (1).

Individual microphones in the system were Knowles type BT1755 electret condenser units with integral source-followers. NASA preamp arrays of HAE design were used to buffer the microphone signals and trim the gain for uniform response.

2.3.4 Controller

The Adaptive-Quadrature (A-Q) control algorithm has been adopted for use in single and multi-tone suppression systems, based on bandwidth capability, rapid convergence and processing simplicity.

The A-Q algorithm performs the following functions in sequence:

- Measures the fan signal from all error sensor channels;
- Injects the BPF harmonic signal into each controlled actuator channel and measures the fan plus actuator signal from all error sensor channels;
- Subtracts the fan signal from each fan plus actuator to error sensor transfer function;
- Computes and applies the minimum-norm actuator channel drive vector (complex) that will combine with the fan noise to produce a minimum in the sum of the squares of the error signals.
- Following the initial adaptation, the system sequentially perturbs the real and imaginary parts of the actuator drive signals and determines on-line corrections to maintain the minimization of the error signals.

Unlike the Filtered-X or similar algorithms, which process an externally synthesized reference signal for application to the actuators, the A-Q algorithm generates the real and imaginary parts of control signals using DSP lookup tables and uses a fan tachometer only for system timing. The results of the "solver" in the algorithm are multipliers for the reference signals, so that the actual control calculations can be carried out at a slower rate than the signal I/O. Control updates must, however, occur more rapidly than fluctuations in fan parameters.

An added complexity of the ANCF duct tests is the presence of the rotating rake microphone system when measuring inlet modes. The rake is a radial strut that rotates at 1% of the fan speed. When the rake is used in the inlet duct, wakes shed by the rake interact with the fan rotor, resulting in multi-mode sound radiation at frequencies slightly displaced from BPF harmonics. To avoid confusion of the active control system by these spurious signals, the bandwidth of the active control system must be narrow enough to reject them. This was accomplished by homodyne filtering the error signals and then block averaging to synthesize $\sin(x)/x$ filters with response zeros at the rake-induced sideband frequency

2.3.5 Modal Control Considerations

For reference, Figure 4 illustrates the radial distribution of sound pressure for mode m=2, n=0,1,2 in the ANCF exhaust duct. Note that at the location of the actuators, the duct inner to outer radius ratio is 0.375 and at the microphones it is 0.500. Eigenvalues, cutoff frequencies (assuming mach 0.1 flow speed) and axial wavelengths for 2300 nominal fan RPM are given in Table 2.

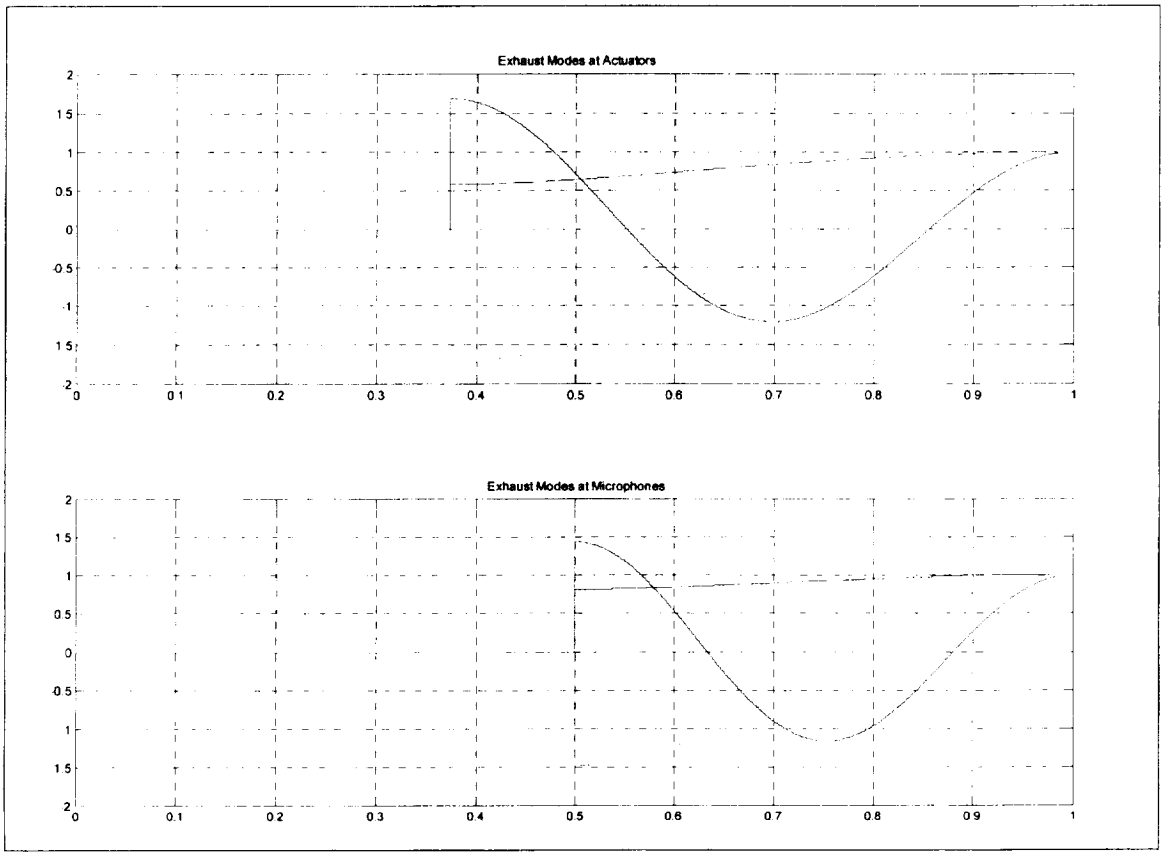

Figure 4 Annular Duct Mode Shapes for m = 2 in ANCF Exhaust

Table 2 Properties of Modes Shown in Figure 4

n	Actuator Region $R_{inner}/R_{outer} = 0.375$			Microphone Region $R_{inner}/R_{outer} = 0.500$		
	α_{mn}	F_{co}	$\lambda_{2300RPM}$	α_{mn}	F_{co}	$\lambda_{2300RPM}$
0	0.916286	253	11.2 in	0.853454	236	11.1 in
1	2.016933	558	12.3 in	2.24855	622	12.7 in
2	3.407914	942	17.1 in	4.122003	1140	29.5 in

Approaches to active control of a complex sound field include full spatial control, full modal control and mixed modal/spatial control. The ordering of the sound field in a turbofan that results form excitation by regular periodic, quasi-axisymmetric sources offers a strong motivation to use some degree of modal control. As discussed above, it was elected to address azimuthal order modes, using carefully implemented arrays of actuators to radiate the same modes as are generated by the fan. The remaining decision regards controlling the radial and axial structure of the sound field.

The full modal control approach would require radial and axial mode separation with the error sensor array and pre-weighting actuator array drive signals for single radial mode generation. Each radial mode would be treated as a separate control channel. The approach was rejected because the duct geometry is not adequately uniform to allow accurate radial and axial mode separations or reliable predetermination of individual mode actuator drive vectors (this can be done readily for idealized conditions).

The first mixed modal/spatial approach would be to separate the radial modes at the microphone array and use the modal amplitudes as error signals, but drive the actuator annuli as separate controlled sources, allowing the controller to seek the drive vector that minimizes all modes. This again was rejected because of duct geometry considerations, primarily uncertainties regarding reflections from the exhaust "nozzle" and mode scattering by the expanding inner radius just upstream of the microphone array.

The second mixed modal/spatial approach uses microphone annuli as individual error sensors and actuator annuli as individual controlled sources, each operating at a specific azimuthal order mode. To use this approach, care must be exercised in microphone positioning to avoid standing wave nodes. In addition, microphones must be far enough from actuators to allow cutoff modes to decay adequately. This approach was taken in the final system implementation. Simulations shown below illustrate the potential noise reduction capabilities.

2.4 Final Exhaust ANC System Description

A block diagram of the ANCF exhaust duct control system is shown in Figure 5. In summary, it consists of

- Six annuli of 10 error sensors, three each on the inner duct wall and outer duct wall. The first annulus is approximately 15 inches downstream of the actuators. The second and third annulus are 7 inches and 11 inches downstream of the first, respectively.
- Microphone preamplifiers and spatial filter networks to produce a mode m=2 output signal from each of the six microphone annuli.
- Six-input, four output A-Q controller, including 2-BPF sine and cosine signal synthesizer timed by the fan tachometer and processing means to seek the least mean squared sum 2-BPF error signal
- Four signal distribution systems to drive 15 actuators each with a 48° per actuator phase advance.
- Power amplifiers and piezo/aluminum actuators arranged in four annuli of 15 each flanking the stator vanes. Axial center to center spacing of the actuator annuli is 8.5 inches.

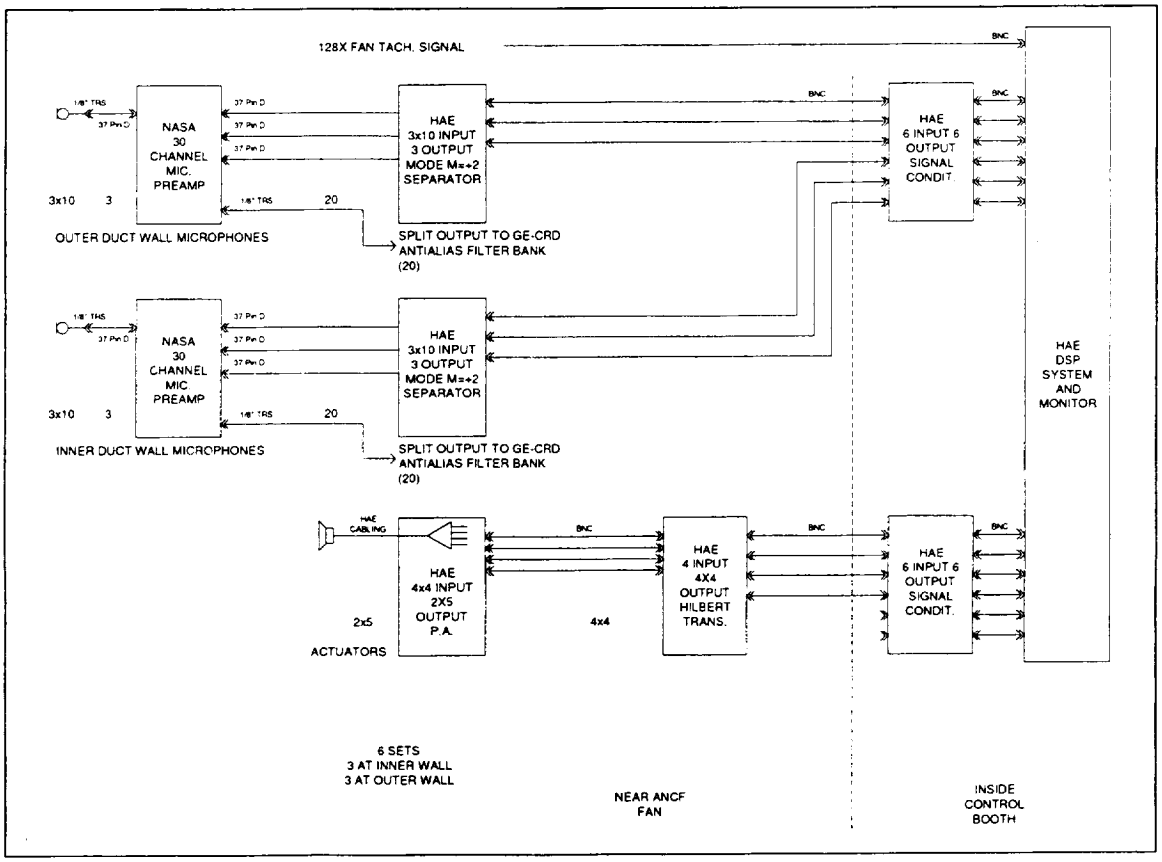

Figure 5 Block Diagram of Exhaust Duct Active Control System

Not shown in Figure 5 is a second computer and analog interface, connected to the system error, control and reference signals, used for on-line monitoring and logging of system parameters.

3 Exhaust ANC System Test Program

Tests were conducted at NASA Lewis Research Center over the time period of July, 1998 to January, 1999. The tests involved extensive preparatory, calibration and data collection procedures. Performance data was collected by NASA using the rotating microphone rake system, and data evaluation was performed by NASA.

3.1 Hardware Preparation

Mounting assemblies for the four actuator arrays were designed to provide uniform 24° azimuthal and 8.5 inch axial spacing, centered on the ANCF 30 vane stator row. For the outer duct radius, this consisted of milling mounting surface and radiation ports for 4.5-inch diameter actuators on a standard 48-inch ANCF duct spool. For the inner duct radius, mounting rings were machined from Delryn plastic in modules to receive three 3.3-inch actuators each as shown in Figure 6. In addition, a bulkhead assembly (Figure 7) was designed that could support the actuator arrays without interfering with the stator assembly.

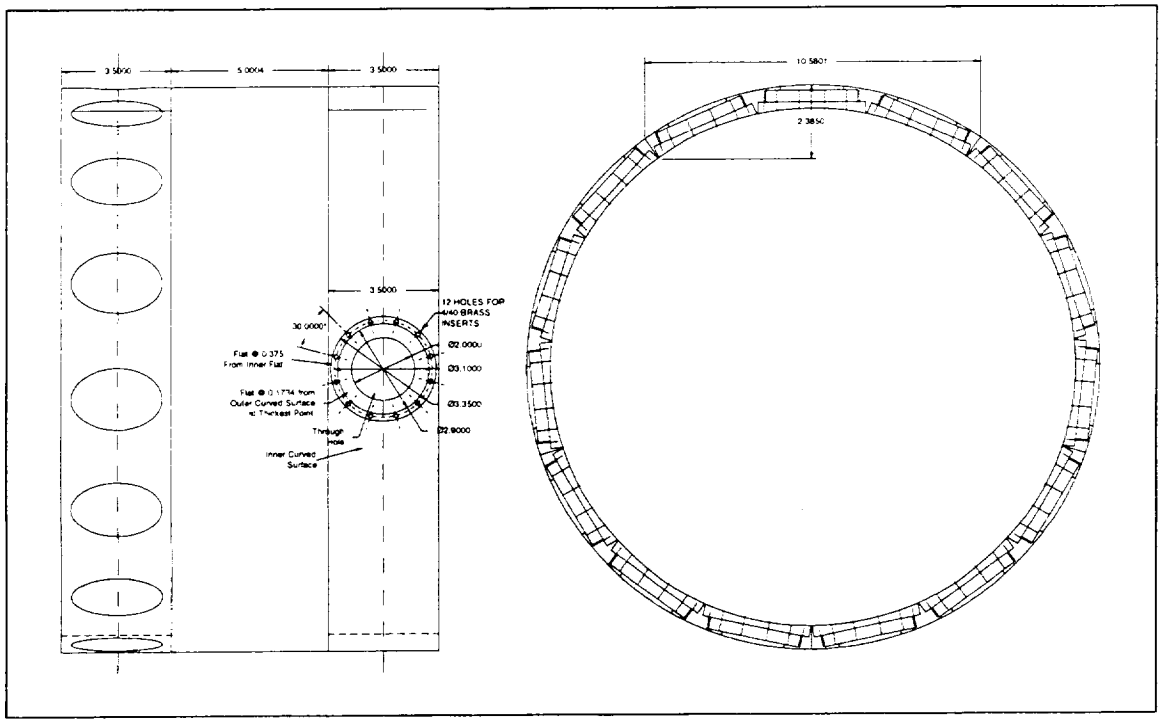

Figure 6 Diagram of Inner Actuator Modular Mounting Assembly

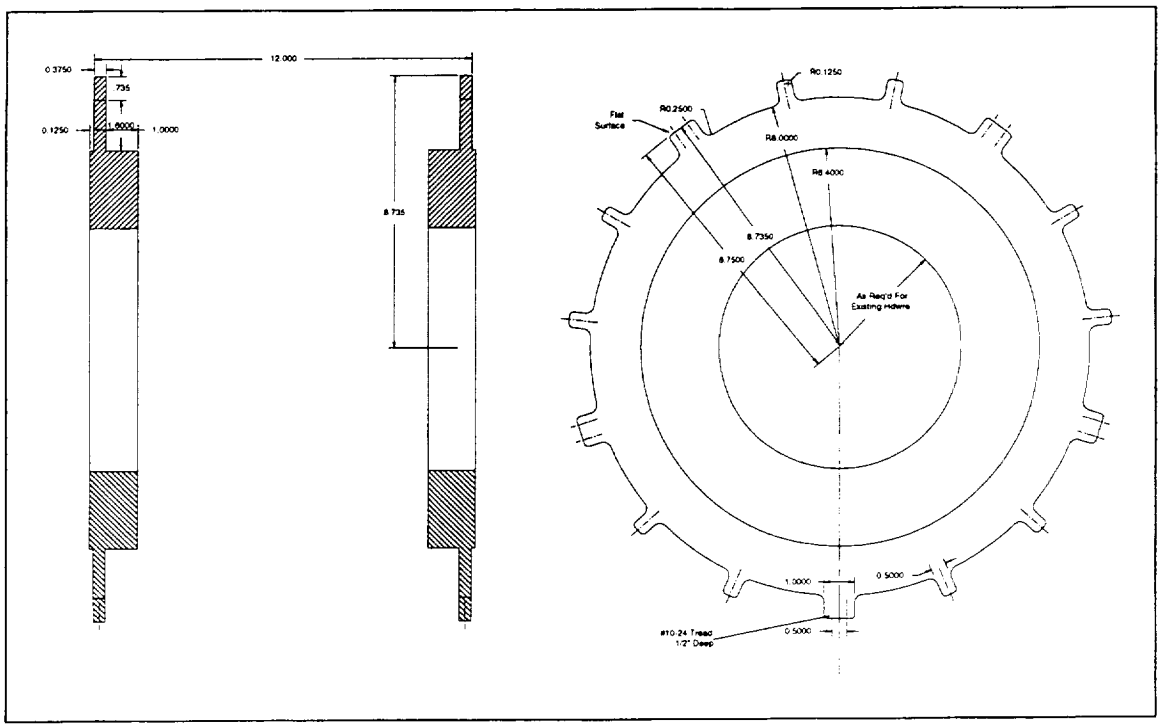

Figure 7 Mounting Bulkhead for Inner Actuator Array

Switching power amplifiers with variable current and voltage feedback capability were fabricated and matched to the characteristics of specific actuators. Cable harnesses were fabricated for connection of the amplifiers to actuators mounted on ANCF.

Actuators were mounted on the ANCF spool and the Delryn rings and installed in the 48-inch static test duct at HAE. The mode m=2 signal distribution network, power amplifiers and actuators were connected and the near-field response of each actuator was measured using a TEF-20 electro-acoustic system analyzer. Amplifier gains were set to minimize amplitude variations for each array. Current/voltage feedback ratios were adjusted to provide the required 48° per actuator position phase advance around the array. Outlying actuators or amplifier channels were identified and replaced.

Mode m=2 microphone array processors were fabricated and tested. Microphones and cable assemblies for the inner duct wall were fabricated and tested. Microphone mounting assemblies for the inner and outer duct walls and microphones for the outer walls were provided by NASA.

Controller algorithms were implemented on a PC-based Spectrum Quad-TMS320C40 DSP board, with the following Input/Output assignments:

- 6 Error Signal Inputs
- 128x Fan Shaft Pulses Timing Signal Input

- 4 Control Channel Ouputs
- Sine Reference Signal Output
- Cosine Reference Signal Output
- DC Ouput Proportional to Mean-Square Error

All signal outputs were conditioned for anti-aliasing or signal reconstruction using 8-pole lowpass filters with a passband limit of 1250 Hz.

3.2 System Calibration on ANCF

Following installation of microphone and actuator arrays on ANCF, a final calibration was conducted for each transducer.

For microphone calibration, a closed coupler was fabricated consisting of a small electrodynamic loudspeaker and electret microphone in a 3-inch diameter PVC cylinder, with a face milled to match the ANCF duct curvature (separate couplers were built for inner and outer duct walls). Using the TEF-20 analyzer, the response of each microphone was measured, including the preamplifiers and mode separation processor. Microphone preamp gains were trimmed to ±0.2 dB. Phase advance of -72° per microphone around each array was checked and verified or corrected.

Individual actuator gain and phase was calibrated in a similar procedure, using a near field microphone placed over the center of each actuator's radiation port.

3.3 Actuator Array Tests

Following transducer calibration, modal radiation was tested using the NASA rotating rake system. With the fan idling at slow speed, the fan tachometer was placed on an auxiliary electric motor shaft with variable speed control. The tachometer 128x output signal was used to synchronize the wave synthesis portion of the controller system so as to produce a 2-BPF signal (based on the auxiliary motor speed) for application to the actuator arrays. Simultaneously, the tachometer signal was used to synchronize the movement of the rotating rake in the ANCF exhaust duct. At several simulated fan speeds encompassing the program test range (up to 2450 RPM) the modal output of each of the four actuator arrays was measured and stored.

3.4 In-Duct Active Control Tests

Active control tests were conducted over a range of fan speeds including two and three cut on radial order modes. At most fan speeds, the full system was operated, i.e. with all six rows of error microphones and four rows of controlled actuators. However, system analysis indicated that a sub-set of four microphone rows would be adequate and this subset was planned for used in a combined inlet-exhaust control demonstration. At fan speed 2300 RPM, the system was tested with several combinations of the six microphone arrays taken in sets of four.

For each active control test condition, the rotating rake was used to measure the mode structure in the exhaust duct with the active control system on and off. Subsequently, the rotating rake was relocated to the inlet duct and the measurements were repeated for a representative subset of fan operating speeds and control system configurations.

3.5 Exhaust ANC System Test Results

A full compendium of the test data and active noise reduction results is presented in Section 8. Presented below are a summary of the overall results, indicating the performance potential of the system together with some of the problems that were encountered.

3.5.1 Actuator Array Radiation

An example of the modal radiation by the actuator arrays is shown for two different frequencies in Figure 8 and Figure 9 It each case the target mode m=2 is clearly dominant, but particularly for the outer duct wall actuator arrays, spurious mode radiation is high enough to be a limiting factor in the performance of the noise suppression system. (For the upstream-outer actuator array, the total non-target mode power at 2300 RPM exceeded the target mode power by about 2 dB.)

The mode spillover shown by these two plots exceeds considerably the amount predicted based on the near-field actuator response non-uniformity. A possible explanation is structural excitation of the duct wall by the actuators. The actuators were mounted using compliant screws and gaskets, but this may not have been adequate, and should be explored further.

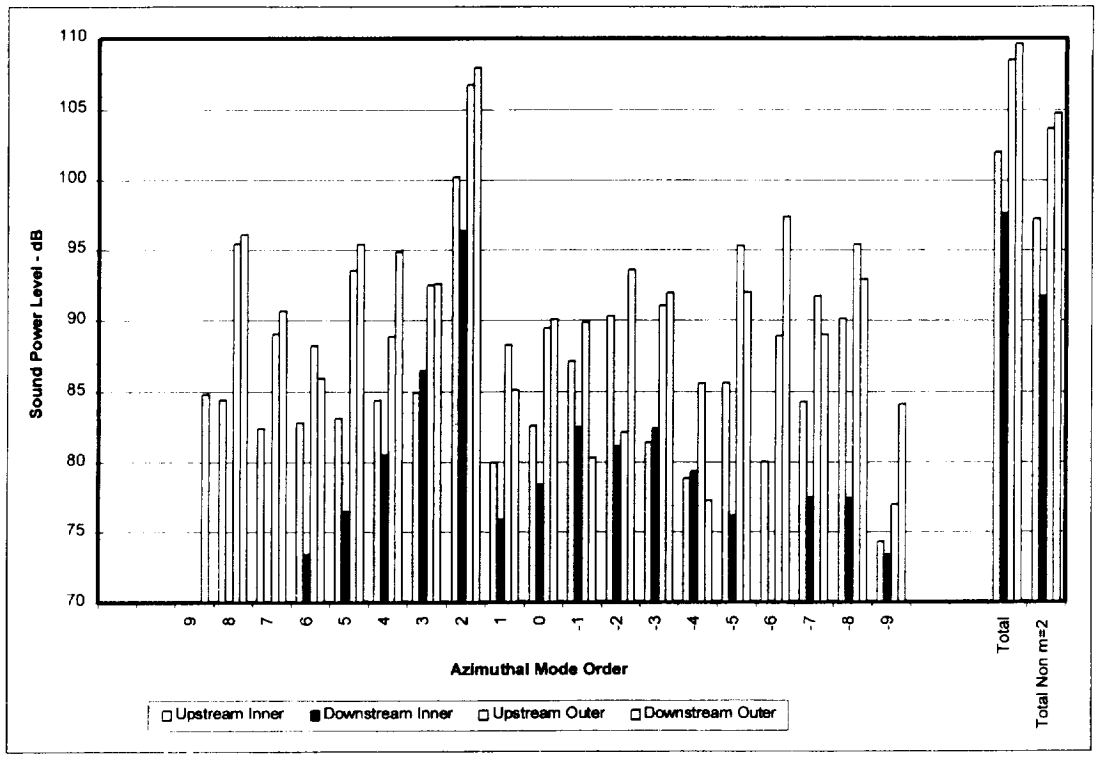

Figure 8 **Actuator Array Mode Generation *m*=2 Drive at 1800 RPM Fan Idling**

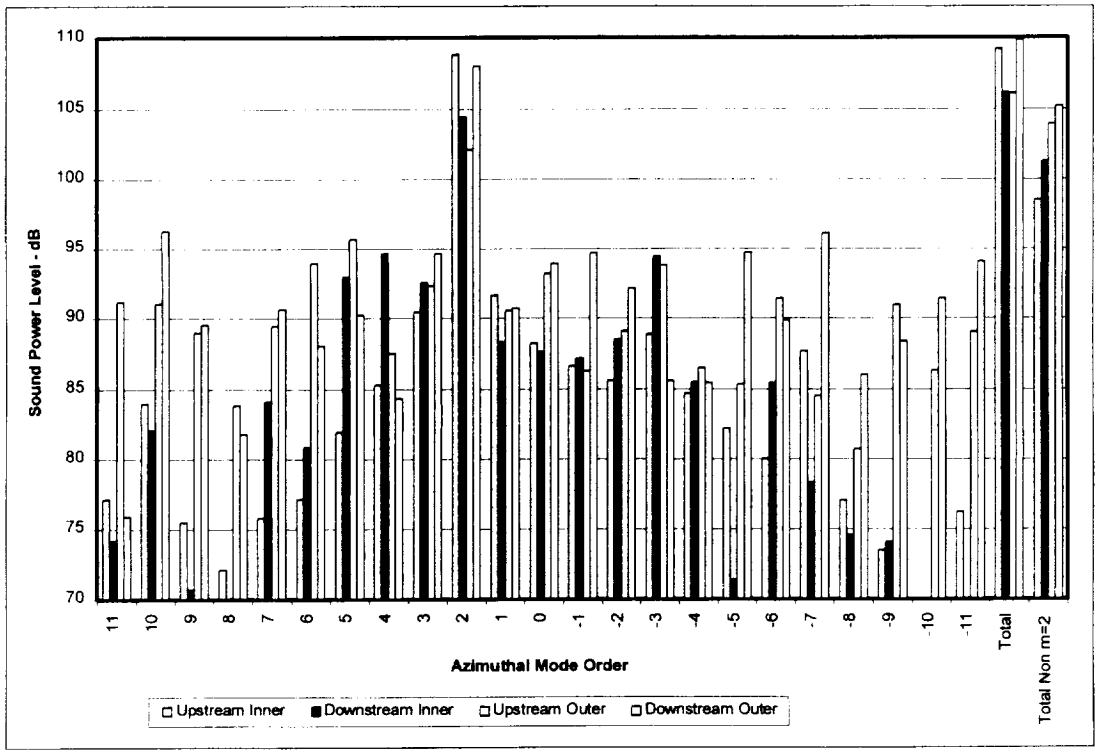

Figure 9 **Actuator Array Mode Generation *m*=2 Drive at 2300 RPM Fan Idling**

3.5.2 Active Control Performance

A summary of the test results is shown in Figure 10. In each case from 1800 to 2450 RPM (960-1307 Hz) significant attenuation was achieved in all cut-on radial orders. Total 2-BPF noise was also reduced (this data not available at 2000 and 2400 RPM) but by a smaller degree due to modal distortion in the actuator arrays and the fan output.

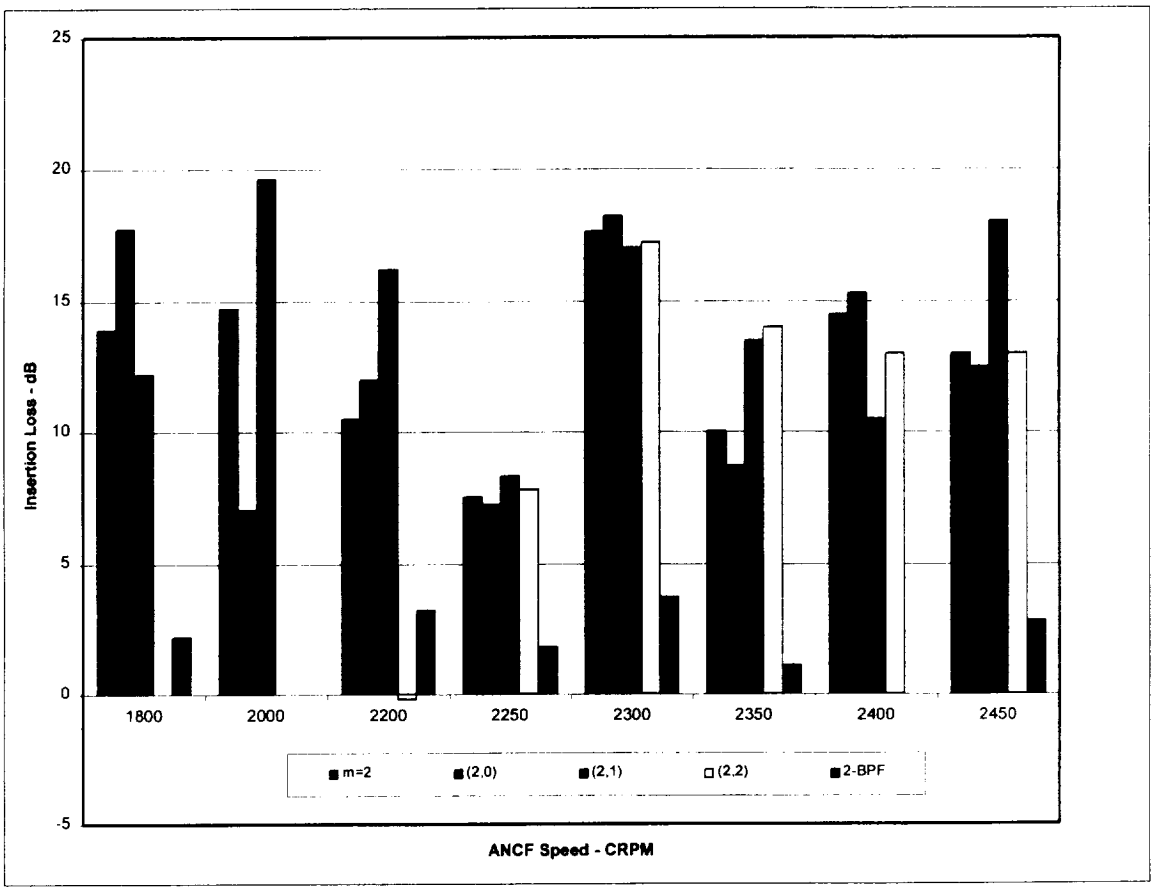

Figure 10 Summary of Exhaust Duct Insertion Loss Test Results

3.6 Summary of Exhaust ANC System Test Results

An active source cancellation system was implemented at the location of stator vanes in the exhaust duct of ANCF. Effective suppression of 2-BPF spinning mode m=2 tone noise was achieved over a range of fan speeds 1800-2450 RPM, which included sound fields with three cut-on radial order modes. Total 2-BPF noise was suppressed at most fan speeds, but by a lesser degree due to actuator mode spillover and low baseline fan noise level.

4 Exhaust System ANC Analytical Simulations

As was indicated in the previous section of the report, both the GEAE AANCSIM2 and HAE ExhaustSim computer models were used in the assessment of performance potential and establishment of parameters for the active control system.

4.1 AANCSIM2 Model

The following input NameList file was used to simulate the control system in AANCSIM2.

```
$CASEANC
  HEAD='ANNULAR ANC TEST CASE HAE SYSTEM SIMULATION'
  R1=0.75
  R2=2.0
  FREQ=1250.
  NSEG=6
  NM=6
  Z(1)=1.33 .17 .4 .4 .17 2.0
  CS=1117.
  RHO=0.00232
  MPROF(1)=-1 -1 -1 -1 -1 -1
  M0(1)=0.0 0.0 0.0 0.0 0.0 0.0
  MW1(1)=0.0 0.0 0.0 0.0 0.0 0.0
  MW2(1)=0.0 0.0 0.0 0.0 0.0 0.0
  BLTIW(1)=0.0 0.0 0.0 0.0 0.0 0.0
  BLTOW(1)=0.0 0.0 0.0 0.0 0.0 0.0
  NBLEX1(1)=0 0 0 0 0 0
  NBLEX2(1)=0 0 0 0 0 0
  SLTIW(1)=0.0 0.0 0.0 0.0 0.0 0.0
  SLEMIW(1)=0.0 0.0 0.0 0.0 0.0     0.0
  IADM1(1)=1,1,1,1,1,1
  IADM2(1)=1,1,1,1,1,1
  BETA1(1)=(0.0,0.0) (0.0,0.0) (0.0,0.0) (0.0,0.0) (0.0,0.0) (0.0,0.0)
  ZETA1(1)=(0.0,0.0)
  BETA2(1)=(0.0,0.0) (0.0,0.0) (0.0,0.0) (0.0,0.0) (0.0,0.0) (0.0,0.0)
  ZETA2(1)=(0.0,0.0)
  NDELM=10
  NEXP=2
  NBLS=10
  IDGN=0
  EVIMAX=15.0
  INAX(1)=1 1 1 1 1 1
  IEVR=0
  ICHK=0
  IPODTL=1
  IIPO=0
  IMPO=0
  IENPO=0
  IPRINT=0
  NSPF=7
  NSPB=6
  QVF(1,1)=(20.,0.0),(10.0,0.0),(10.0,0.0),(10.0,0.0)
```

```
 QVB(1,1)=(20.,0.0),(10.0,0.0),(10.0,0.0),(10.0,0.0)
 $END
 $PRSNS
 NSEGPS=6
 NPSENS=36
 ZPS(1)=10*1.25,10*1.8,10*1.25,10*1.8
 THPSD(1)=0.,36.,72.,108.,144.,180.,216.,252.,288.,324
 THPSD(11)=0.,36.,72.,108.,144.,180.,216.,252.,288.,324
 THPSD(21)=0.,36.,72.,108.,144.,180.,216.,252.,288.,324
 THPSD(31)=0.,36.,72.,108.,144.,180.,216.,252.,288.,324
 NPSWALL(1)=20*1,20*2
 SIGSPL=0.0
 SIGPHS=0.0
 SCALSPL=0.0
 SCALPHS=0.0
 SPLBKGD=40.
 NRANDSEED=3408
$END
$ANCIN
 NANC=4
 NACT(1)=15,15,15,15
 NANCSEG(1)=2 2 5 5
 SLDTY(1)=0.5,0.5,0.5,0.5
 IWALLACT(1)=1,2,1,2
 NUMSPNM=1
 ICFWDBK=2
 MSMANC=2
 NRDANC=4
 MSMC(1)=2
 JRDL(1)=4
 CMU=0.5
 CLAM1=0.05
 CLAM2=0.05
 VMGIN=1.
 WFAC=1.E-6
 ACTVLSD(1)=0.0,0.0,0.0,0.0
 ACTPHSD(1)=0.0,0.0,0.0,0.0
 ACLMVSD(1)=0.0,0.0,0.0,0.0
 ACLPHSD(1)=0.0,0.0,0.0,0.0
 ITROUT=0
 NACTOUT1(1)=0,0,0,0
 NACTOUT2(1)=0,0,0,0
 NELEMOUT1(1,1)=0,0,0
 NELEMOUT2(1,2)=0,0,0
 NUMITR=100
$END
$RFMAT
 MSMR=2
 RS= 36*(0.,0.)
 RT= 36*(0.,0.)
$END
```

Using the above input data, AANCSIM2 predicted 20-25 dB suppression but 11 dB increase in noise toward the inlet, as shown in Figure 11.

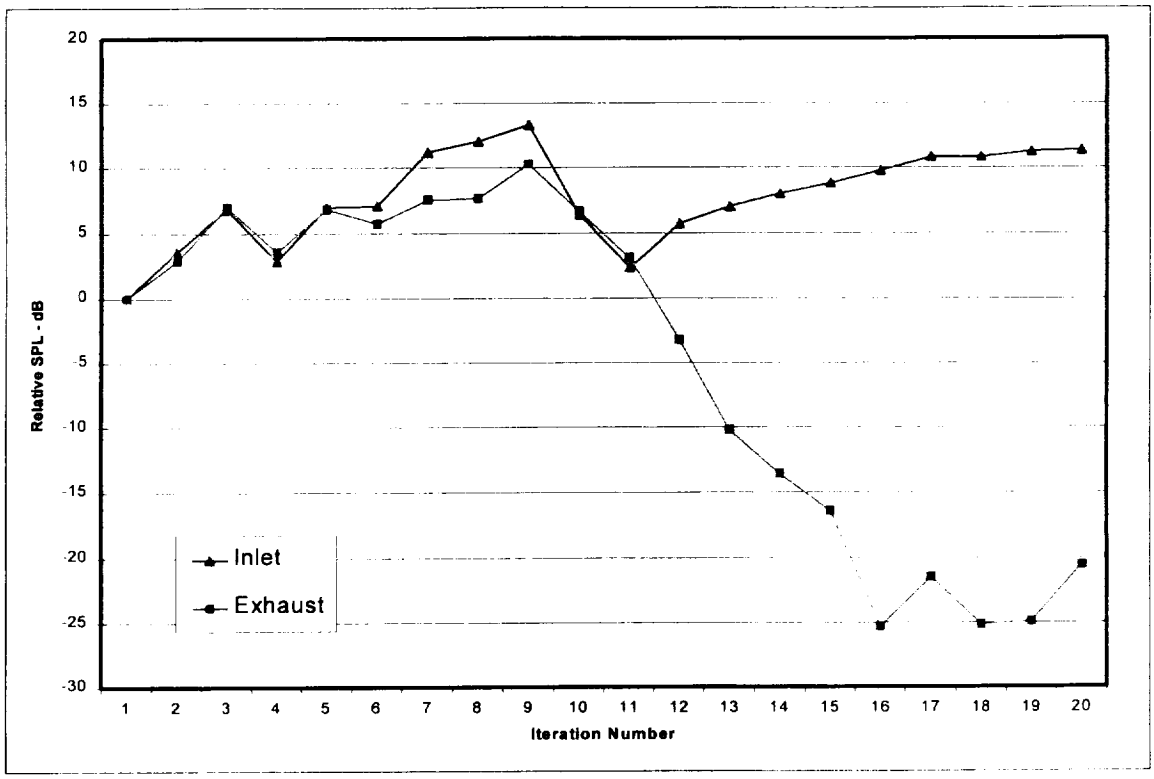

Figure 11 Plot of Predicted Exhaust ANC Convergence from AANCSIM2

The large predicted increase in sound in the inlet direction did not agree well with prior experience with the source-cancellation control concept. Examination of the actuator modal coupling results within AANCSIM2 indicated a higher weighting toward lower radial order modes from both inner and outer wall actuators than had be measured in previous source-cancellation tests.

4.2 Green's Function Analysis and ExhaustSim

In an effort to resolve this question, a Green's Function analysis of the source coupling issue was undertaken. Section 3 of the report presents the details of this investigation. A summary of results for one test case is shown in Table 3.

Table 3 **Mode m=2 Pressure Coefficients for 15 Actuators in ANCF: Outer Diameter 48-inches, Inner Diameter 18-inches, Frequency 1250 Hz**

Radial Order n	Outer Wall Drive		Inner Wall Drive	
	Real Pressure	Imaginary Pressure	Real Pressure	Imaginary Pressure
0	5.21512	0	1.70067	0
1	-6.805244	0	6.521056	0
2	11.64984	0	11.10549	0
3	0	-18.18206	0	17.03019
4	0	8.534701	0	7.930752

Using the above complex coupling factors η for inner and outer wall actuators discussed above, the following idealized actuator to microphone transfer function was obtained:

$$H_{act,mic} = \sum_n \eta_{mn,act} * \left[J_m(\pi\alpha_{mn}\frac{r_{mic}}{R}) + \beta_{mn} Y_m(\pi\alpha_{mn}\frac{r_{mic}}{R}) \right] * \exp(ik_{zmn}(z_{mic} - z_{act})) \quad (2)$$

Consequently, the drive vectors required to cancel the fan signal at all microphone annuli is:

$$\begin{pmatrix} D_{UO} \\ D_{UI} \\ D_{DO} \\ D_{DI} \end{pmatrix} = -\begin{pmatrix} H_{UO,1} & H_{UI,1} & H_{DO,1} & H_{DI,1} \\ H_{UO,2} & H_{UI,2} & H_{DO,2} & H_{DI,2} \\ H_{UO,3} & H_{UI,3} & H_{DO,3} & H_{DI,3} \\ H_{UO,4} & H_{UI,4} & H_{DO,4} & H_{DI,4} \end{pmatrix}^{-1} \times \begin{pmatrix} P_{Fan,1} \\ P_{Fan,2} \\ P_{Fan,3} \\ P_{Fan,4} \end{pmatrix} \quad (3)$$

Solving for the drive vector and then computing the sound field in the duct results in contour of the type shown in Figure 12 and Figure 13.

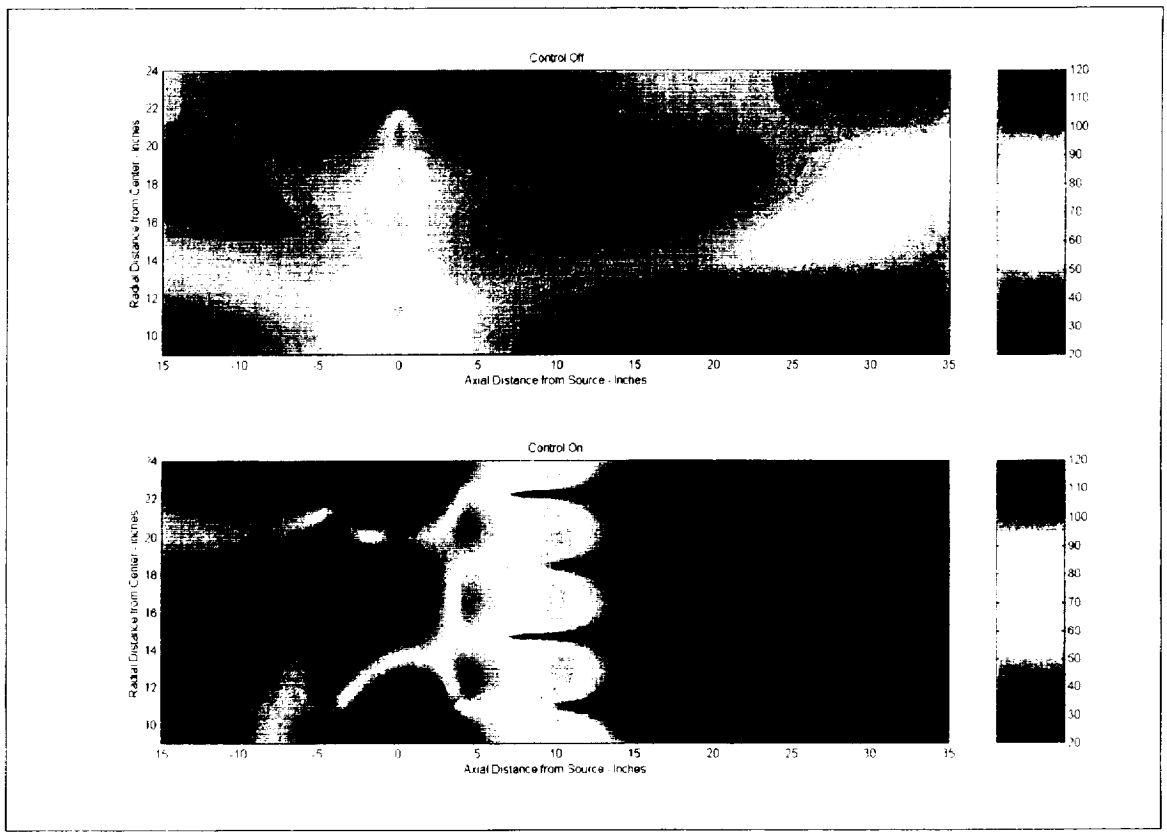

Figure 12 **Idealized Simulation of Exhaust Duct Active Noise Control with Actuator Rows at ±4.25 In., Error Microphone Rows at 23 and 30 In. - 2300 CRPM**

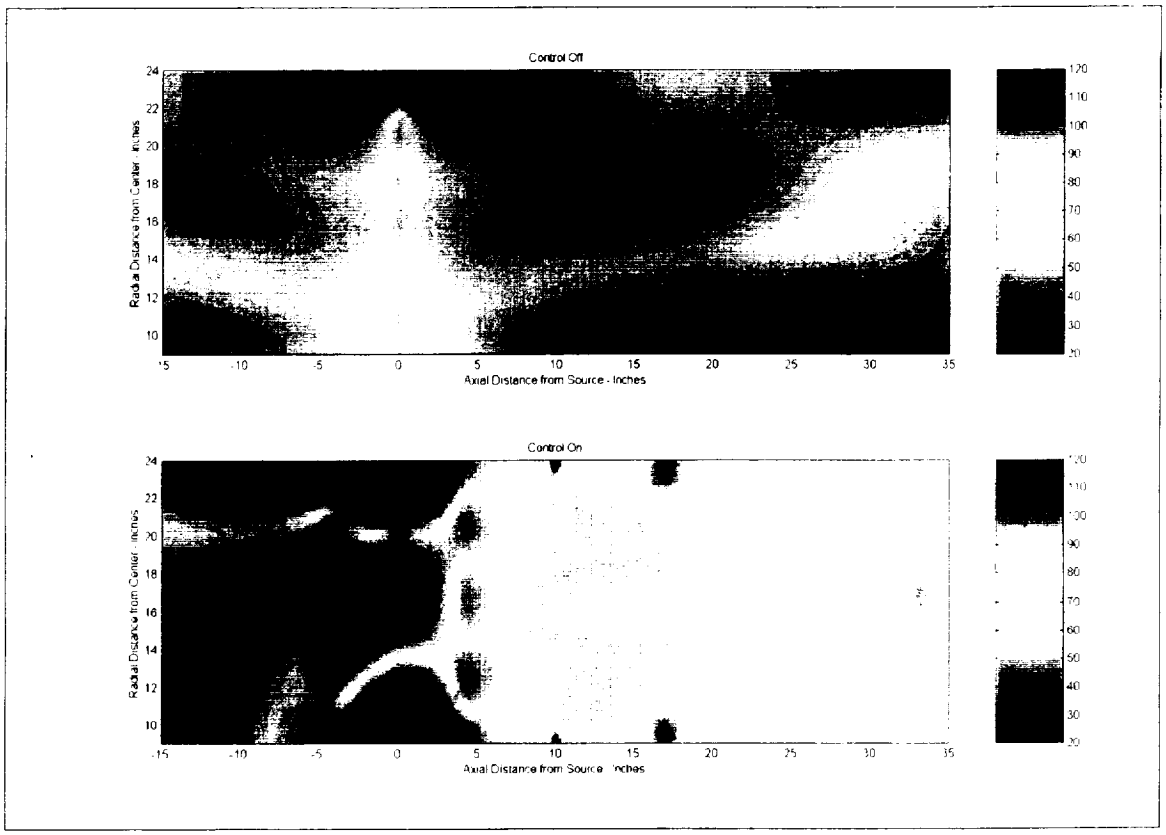

Figure 13 **Idealized Simulation of Exhaust Duct Active Noise Control with Actuator Rows at ±4.25 In., Error Microphone Rows at 10 and 17 In. - 2300 CRPM**

The two contour plots illustrate the importance of adequately separating the actuators and error sensors. In Figure 13 the error microphones respond to a combination of the three cut-on modes plus residual cutoff radiation from the downstream actuators. The controller acts to minimize this mixture at the error sensors and as a result, gives the wrong drive for the cut-on modes.

5 Inlet ANC System Design

This section discusses the design study performed to determine the most appropriate layout of the sensors and actuators for the ANC system to be deployed at NASA Lewis on the 4 foot fan rig. It was decided in mid-year 1997 to develop a system to target the m=2 mode in the inlet in a frequency range nominally centered on 1300 Hz based on the tone at 2BPF. At this frequency, it can be shown that a total of four radial modes propagate down an ideal, hard-walled duct with a diameter of 4 foot. Therefore, the minimum design for modal-based control must be able to sense and generate four radial modes with arbitrary amplitude and phasing.

In this section, some general design parameters were held constant while usually a single parameter was varied. The nominal constant parameters used (unless otherwise specified) are listed in Table 4.

Table 4 Nominal design study parameters

Frequency	1300 Hz
Sensor Section Length	2'
Actuator Section Length	2'
Transition Section Length	1'
Modal Distribution	Equal Energy in the modes
Noise Level (standard deviation)	1 dB amplitude, 5°phase
Actuators/ring	16
Number of sensors per ring	12
Number of sensor rings	4

In addition it was assumed that no reflections are generated at the duct exit. The design study was performed using both the CANCSIM (version 2.1A) program developed as a part of the active noise control project as well as a set of Matlab routines which had functionality equivalent to modules of the CANCSIM program.

5.1 Inlet Sensor System Study

The first part of the system to be studied was the sensor system. The primary measure of the effectiveness of the sensor system is how accurately the individual modal amplitudes can be measured based on the noise level of the in-duct pressure field and the geometrical layout of the sensors. The results presented herein are expressed in terms of the error (in dB) of the measured modal amplitudes for each of the four modes as a function of the parameter under study. The sensors were assumed to be mounted in circular rings of even circumferential and axial spacing at the duct wall. From the modal distribution, it is known that a minimum of four sensor rings will be required to be able to separate the modes mathematically.

First, the number of sensors placed circumferentially within each ring was studied. Since there are only 4 modes, a minimum set of 4 sensors at any set of axial locations can detect the

modes, but in practice, this is usually not achievable. To study the effect of the number of sensors per ring, a simulated duct pressure was "measured" at the duct wall four rings of sensors consisting of 2 to 16 sensors per ring incremented by 2 sensors each time. The standard deviation of the error in the "measured" pressure in each mode was calculated base on the results of 100 error distributions of the nominal error values in Table 4. The results are shown in Figure 14.

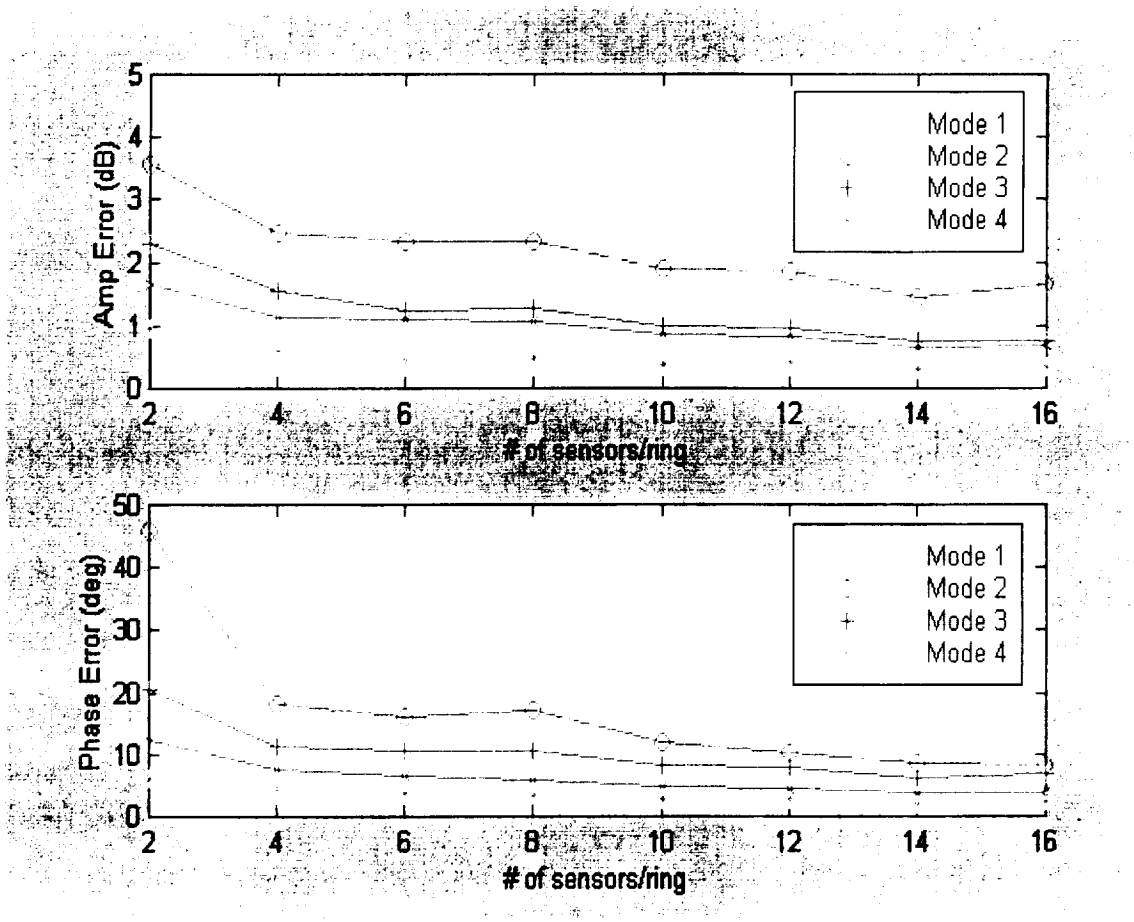

Figure 14. Standard deviation, by mode of the measured pressure for four axial rings with a varying number of sensors per ring

Significant gains in the estimated data are achieved from 4 sensors after which a flat region predominates until the tenth sensor is added. Beyond the tenth sensor, the gain achieved by increasing the number of sensors is very small. The use of ten sensors also has an advantage with the combined system, since it is not evenly divisible into the number of actuator used per row, so that aliased modes produced by the actuators are not coincident with aliased modes detected by the sensors. For these reasons, 10 sensors/ring was chosen for the design.

The next study involved the number of rings used. The primary focus here was to determine if additional rings, beyond the four required, could provide additional accuracy in the estimation of the modal amplitudes. The study was conducted in the manner described

previously with the nominal system values used except for the number of rings, which was varied from 4 to 7. The results of the modal amplitude estimation errors are shown in Figure 15.

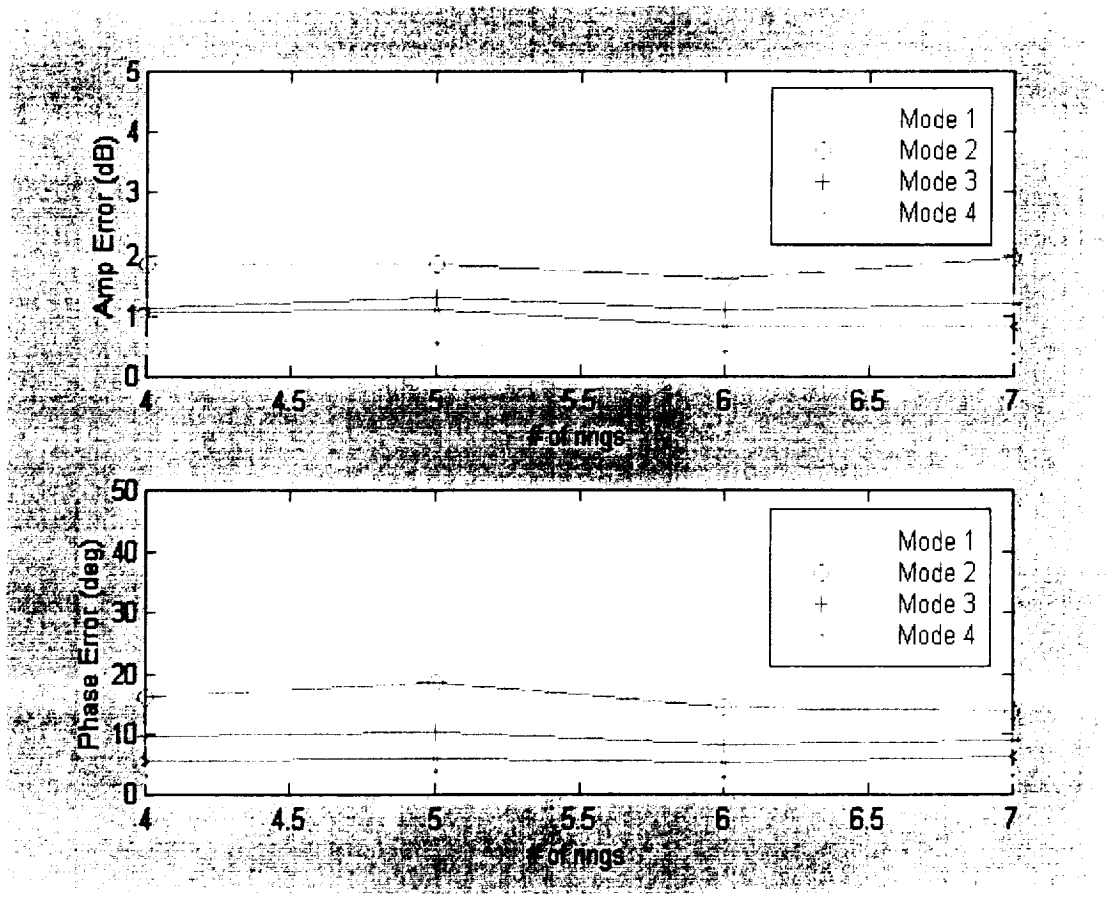

Figure 15. Standard deviation, by mode of the measured pressure with a varying number of axial rings

From Figure 15, it is evident that little or no gain is achieved by increasing the number of rings. Therefore, it was decided that unless significant reflections are measured in the testing phase, 4 rings will be sufficient for the sensor system. The only benefit of additional rings will be the possible detection of independent reflections from the duct end, which are not considered in this study.

The final parameter studied in the sensor section was the axial spacing between the sensor rings. The sensor ring spacing was varied from 0.3' to 0.8' in 0.1 ft increments. The study was again conducted with 100 error distributions at the nominal error values placed on the data with the standard deviation of the estimated modal amplitudes plotted in Figure 16 against sensor ring spacing.

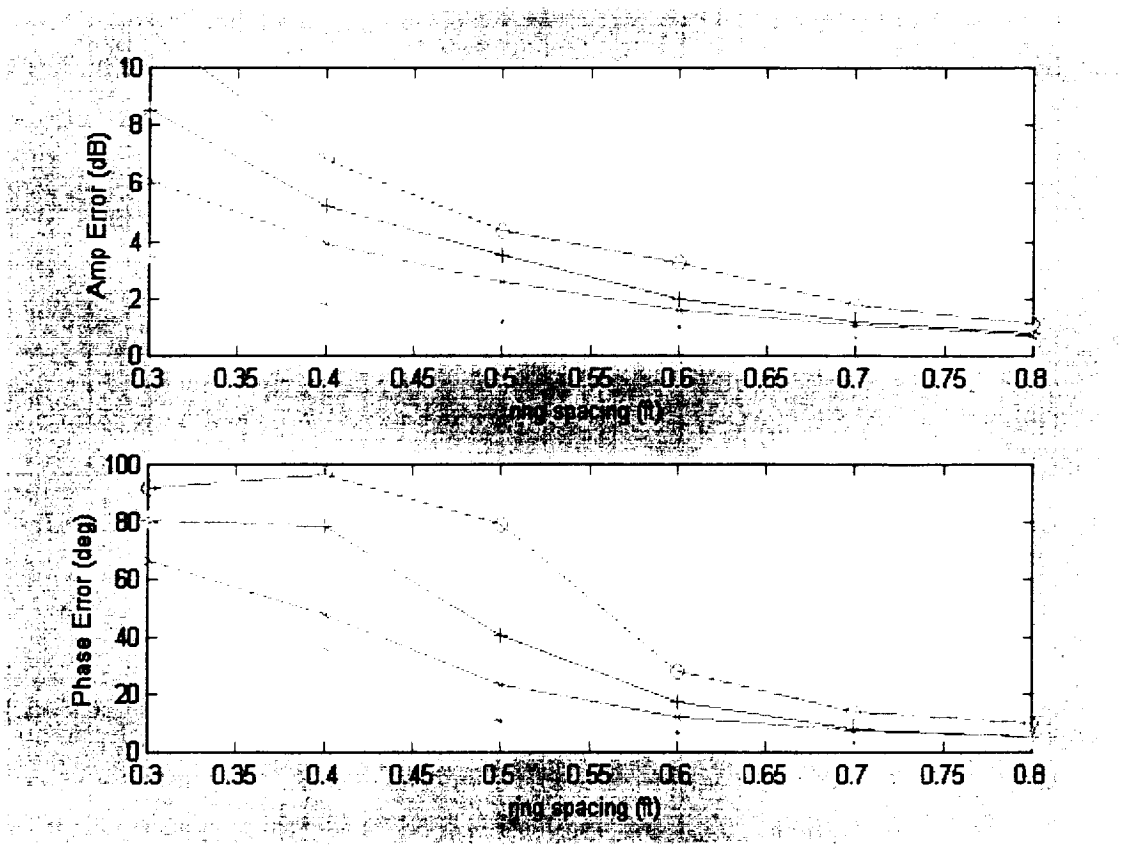

Figure 16. Standard deviation, by mode of the measured pressure with a varying axial ring spacing

From Figure 16, it is observed that sensor ring spacing has a very large effect on the performance of the sensor system. Significant gains in accuracy are achieved up until about 0.65, at which point the gain increases, but at a much slower rate. This indicates, as might be expected, that since it is the difference in modal wavelengths that distinguishes the modes, that the axial length of the sensor system will be the most important parameter in the design of the sensor system. Based on the results of this study, and the practical limitation of the duct, a sensor spacing of nominally 0.65 ft was used. This corresponded to a sensor section of 2.05 ft. A slightly uneven spacing was also used, since the Bessel functions do not have even periods, which also slightly improved the results.

The results of this section are then:

1.) Actuator section length has a big effect on the sensor system performance. A design length of 2.05 ft has been specified.

2.) Only one ring of sensors per mode is required to obtain required system performance and no benefit is gained from adding more rings unless significant reflections exist.

3.) A ring of ten sensors will provide good performance for the sound field under study.

5.2 Inlet Actuator System Study

The design of the actuator system will determine both the useable frequency range for the ANC system as well as the ability to generate cancellation on a mode-by-mode basis. The first study will determine the number of actuators used per ring in order to attain a design at the frequency range specified by NASA Lewis. The second study will evaluate the performance of the actuators in generating energy at each mode. Since the actuator size is large relative to the section length allotted to the actuators, it is not practical to assess parameters such as actuator spacing since they will have to be packed as close as possible in order to fit the four rings required.

For the purpose of determining the number of actuators required per ring, it must be observed that for a ring of N actuators, the generation of the m=2 mode will also generate energy in the m=-(N-2) mode due to spatial aliasing. Thus the cut-on frequency of the m=(N-2) mode (which is identical to the cut-on frequency for the m=-(N-2) mode) must be above the frequency range of the system, since the modes cannot be generated independently for cancellation. This way, no aliased modes will propagate in the duct. Non-propagating modes can be effectively ignored provided a transition section of about 1 ft length is placed between the sensor and actuator system. Those modes will decay more than 20 dB over this transition section. The cut-on frequencies for the modes in a 4 foot diameter duct as a function of m-order are plotted in Figure 17.

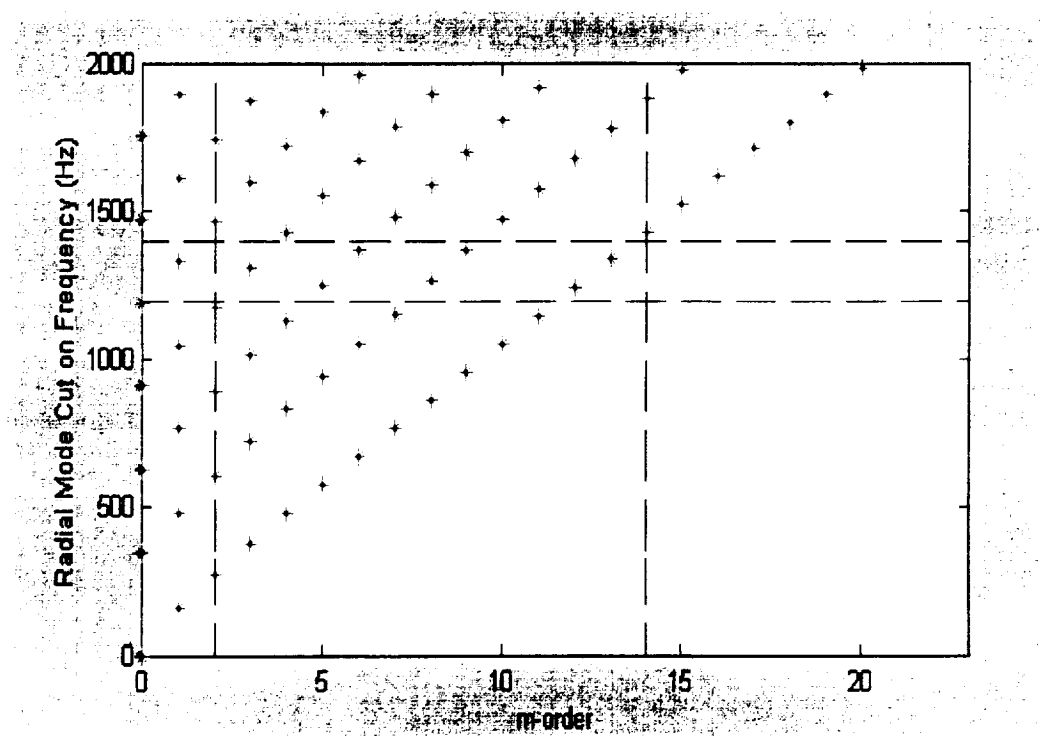

Figure 17. Cut-on frequencies in a hard-walled duct of 4 foot diameter as a function of m-order

From Figure 17, it is clear that in order to obtain a frequency range centered on 1300 Hz, aliasing must be into at least m=-14, so that a minimum of 16 actuators are needed to avoid generation of propagating modes at aliased m-orders. This will give a nominal frequency range of 1200 Hz to 1400 Hz with 4 propagating modes at m=2 and no aliased modes for 16 actuators/ring. The lower bound of the frequency range is defined by the cut-on frequency of the fourth mode at m=2. Based on the results of this study, 16 actuators were used in each ring.

The effectiveness of the actuator system is defined as its ability to generate a single radial mode without spillover into the other radial modes. This governs its ability to actively cancel a single mode. The effectiveness against an arbitrarily weighted sum of the modes is simply the sum of its ability to cancel each individual mode with the proper weight. In principle, the system can generate each mode independently in the presence of no errors. However, errors in the weights will cause spillover of energy into the other radial modes at the same m-order.

In order to assess the effects of spillover due to noise, it was first determined what the correct modal distribution produced by a single ring of actuators is assuming a uniform axial velocity distribution of correct m-order over the ring surface. Then, the correct weights on the set of four rings to generate each of the modes individually with an amplitude of 1.0 (94 dB) was calculated exactly based on an actuator ring spacing of 6 inches axially and a system of four rings. Noise at the nominal values was added to the "exact" weighting factors and passed through the same actuator system. The resulting spillover into the neighboring modes was calculated.

Those results are summarized in Figure 18. The phasing for individual modes are indicated by different color bars while the resulting spillover due to the correct phasing plus error is indicated by bars of the same color at the appropriate mode number of the x-axis.

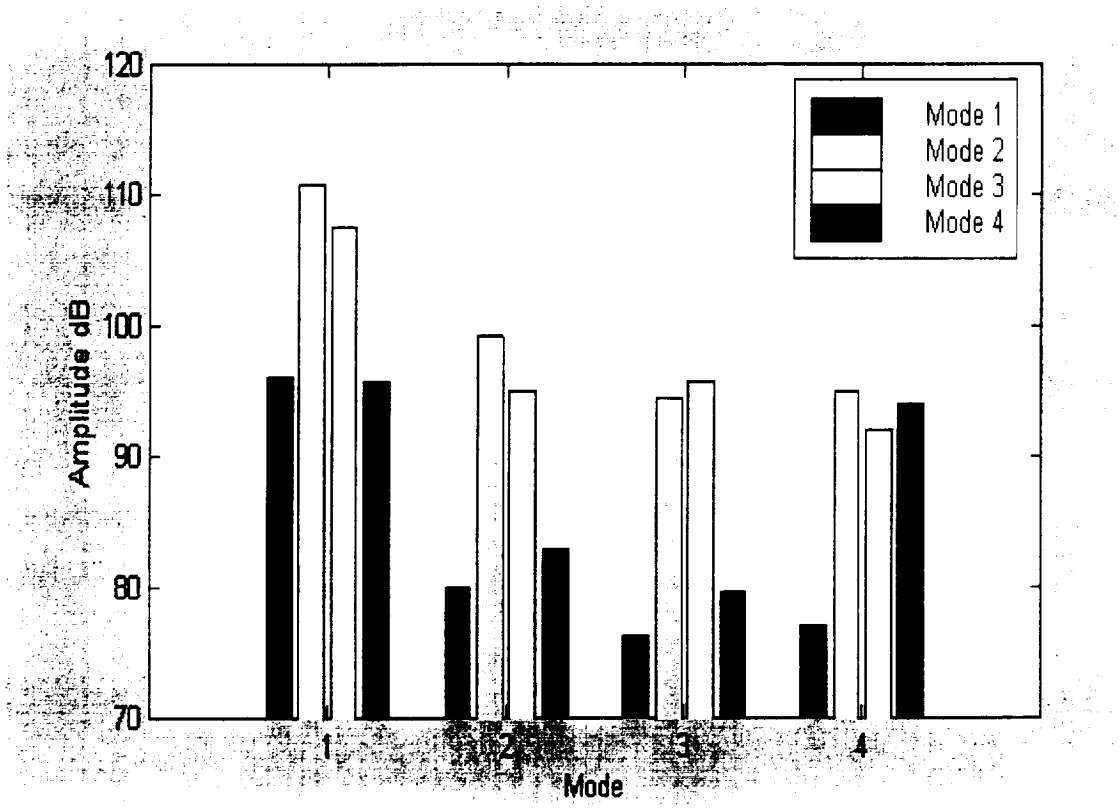

Figure 18 Modal spillover based on random errors in the correct modal weighting for individual mode generation

Based on Figure 18, it appears that the actuators will handle Mode 1 best, but significant spillover will result in the generation of the other modes. In particular spillover dominates in Modes 2 and 3 and both require a lot of power (indicated by the high amount of spillover to achieve the same modal amplitude at the desired mode) to get the same modal amplitude. Mode 4 is generated relatively cheaply, but still has significant spillover into Mode 1. Results were improved as the errors decreased, however significant spillover problems were still observed in Modes 2 and 3.

The results of this study indicate the following.

1.) At least 16 actuators are required per ring to avoid the generation of propagating modes at aliased m-orders.

2.) A nominal frequency range of 1200 Hz - 1400 Hz can be obtained with 4 rings of 16 actuators based on the assumption of 4 radial modes at m=2.

3.) The system may experience difficulty in canceling energy in the second and third radial modes due to spillover.

4.) The actuator needs to have significant energy capacity over that of the source in order to generate some of the modes.

5.3 Overall System Performance and Passive Treatment Effects

The optimal design formulated in the previous two sections was tested using the CANCSIM program developed by GEAE in order to assess the total system performance. The system performance was determined as the total sound power reduction (NR) in the duct at a series of frequencies from 1200 Hz to 1400 Hz. An error distribution of standard deviation 1 dB in magnitude and 5° in phase was placed on the sensors. The results are plotted in Figure 19.

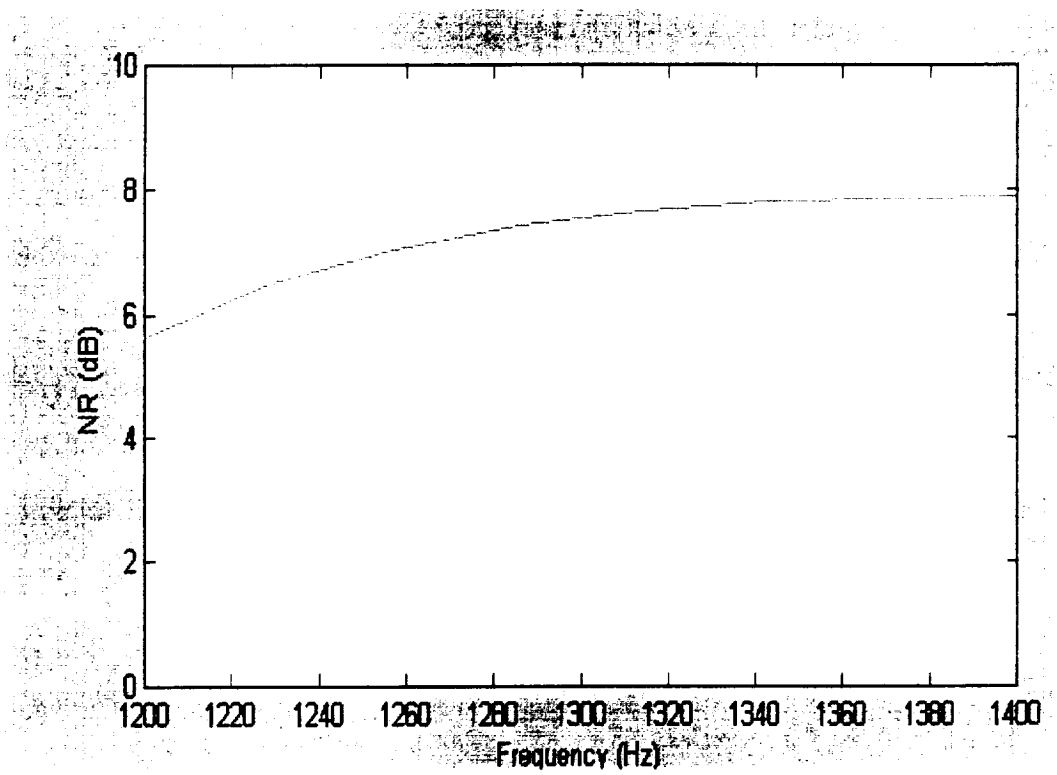

Figure 19. System performance as a function of frequency for the optimal system with nominal errors on the sensors

The simulation predicts a nominal sound power reduction near 7 dB at 1300 Hz. The system performance increases with frequency. This is due to the shortening of the acoustic wavelength of each mode in the axial direction, which in effect "increases" the sensor section length relative to the sound field, thereby improving system performance as in Figure 16.

It was found that system performance could be significantly increased by adding an passive liner in the 1 ft transition section between the sensors and actuators. This liner/transition section length and impedance was also optimized for system performance. Since liners are generally designed for passive tonal cancellation in the presence of no ANC system, the results of an optimally passive liner were also studied. The optimized impedance for the liner based on a passive only system and combined passive-active system are shown in Figure 20(a) and the overall system performance based on passive only system and the combined system is shown in

Figure 20(b). The notation for Figure 20(b) refers to the (impedance used)-(system used), so that the optimal passive liner in the combined system is denoted as passive-comb.

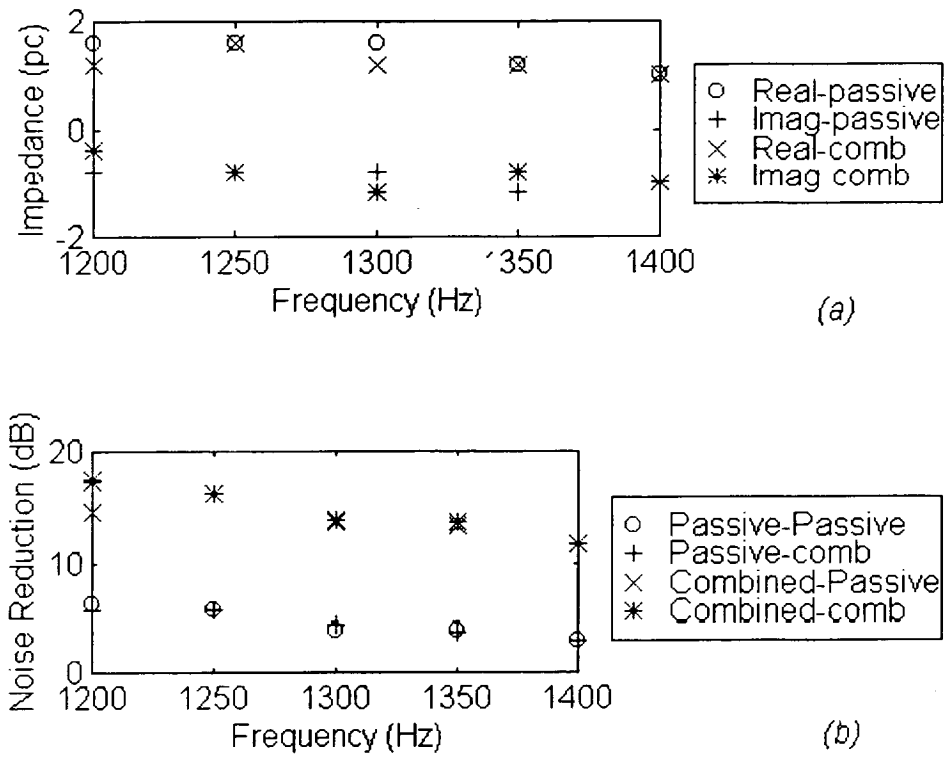

Figure 20. (a) Optimal liner impedance and (b) system performance for a passive only or a combined passive-active system in the duct

Based on Figure 20, two important observations can be made. First, the optimal liner for a passive-only application delivers performance comparable to the liner optimized for a combined system. This indicates that liners already designed for passive treatment can be incorporated directly into the active system with little or no performance loss. Second, it can be shown that the performance of the combined system is slightly better than the simple sum of the active system only and the passive system only. In this about 2 dB of additional benefit of performance is gained by using a combined system over the summed result of active and passive systems acting independently.

Even greater gains were observed in a similar study for m=4 with 3 active modes (about 5 dB performance enhancement). This occurs because of the scattering effect at the treatment interfaces. The combination of the two systems allows the creation of a new sound field at the duct interface which is optimized to scatter energy into higher order modes. This increases the liner performance, since higher order modes are more easily attenuated by the liner. This was clearly observed by looking at intermediate results in the CANCSIM program which showed significant changes in the scattered energy distribution with the presence of the active system. A

thorough study of this effect is beyond the scope of this program, but may be an area for future research.

The results of this section are summarized as follows:

1.) The active system will give a reduction in the in-duct sound power of about 7 dB.

2.) Significant improvements can be used by adding an optimally designed passive liner to the transition section between the actuators and sensors.

3.) The liner can be designed for a passive only application, i.e., a standard nacelle liner can be used without modification

4.) The combined effect of the active-passive system is greater than the sum of the individual systems acting independently. This is due to an enhancement of the scattering effect at the treatment interface.

5.4 Final Inlet ANC System Design

Based on the above system study and practical limitations of the NASA ANC test rig, the inlet system was designed and fabricated. Figure 21 show the final system design. The ANC system includes four rings of actuators and five rings of sensors. Each actuator ring has 16 actuators and each sensor ring has 10 microphone sensors. The last two sensor rings have been installed in the inlet bellmouth because of practical limitations of duct length and sensor axial distance required sensing the modes. The last actuator ring and first sensor ring distance were designed to be one foot apart. However, because of the practical limitation of the duct length, only 9.7 inches of space was available and this was implemented into the design and will result in above 15 dB reduction of cut-off mode components.

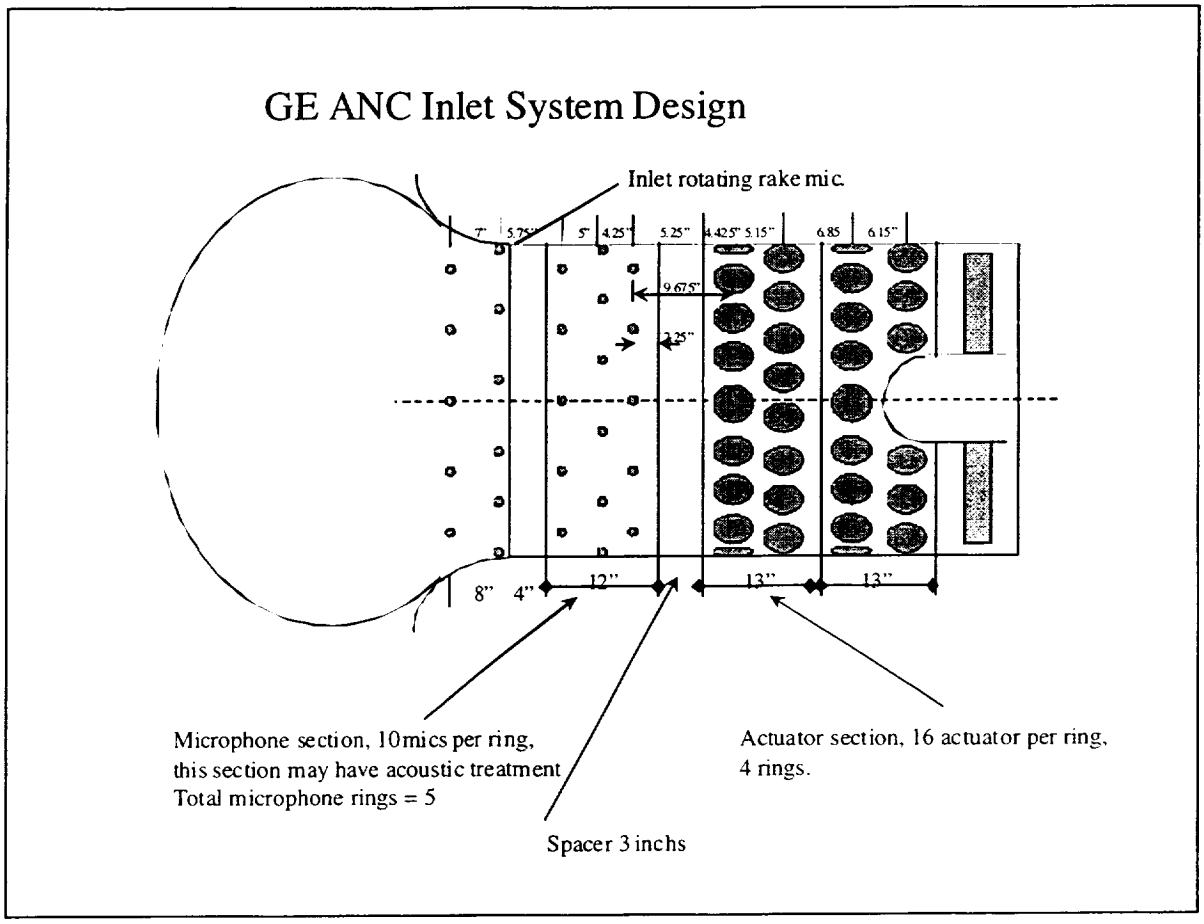

Figure 21. GE ANC inlet system design

6 Inlet ANC System Test

6.1 Speaker Characteristics Test

Speakers were chosen as the actuators used for active noise cancellation in the system designed by GE CRD. Due to the nature of the engine duct environment, the stability of the speaker characteristics under the harsh environment is very important for active noise cancellation. Tests were designed to measure the dependency of speaker characteristics to the ambient temperature, the running time, and the ambient pressure.

6.1.1 Temperature and running time dependency of the speakers

The first test was designed to check the stability of speakers under different running time and temperature. The test setup is shown in Figure 22. In this test, the transfer function (TF) was defined as the acceleration at the center of the speaker over the voltage to the speaker.

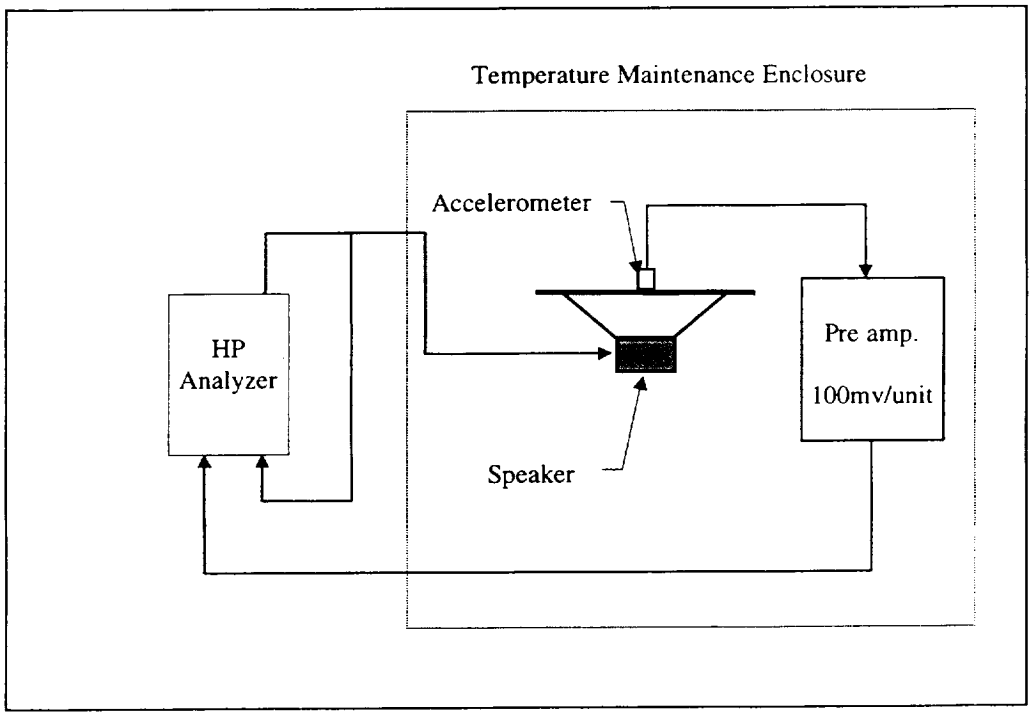

Figure 22. Speaker test setup

In Figure 23 and Figure 24, we have shown the dependency of the transfer function (TF) amplitude and phase with the running time. The TFs at 0.0s, 10.0s, 20.0s, 30.0s, and 40.0s were recorded. No significant variation was identified.

In Figure 25 and Figure 26, the dependency of the TF amplitude and phase with the ambient temperature is shown. The TFs at 0.0°F, 42.0°F, 59.0°F, and 86.0°F were recorded. Only negligible changes were identified.

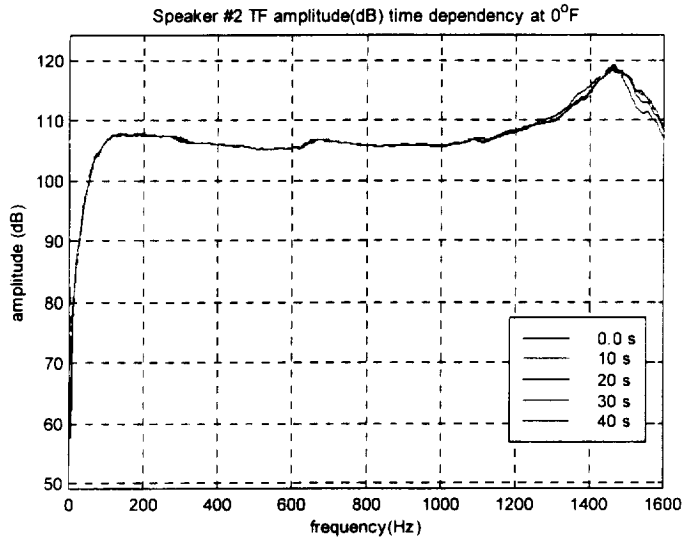

Figure 23. Running time dependency of the TF amplitude

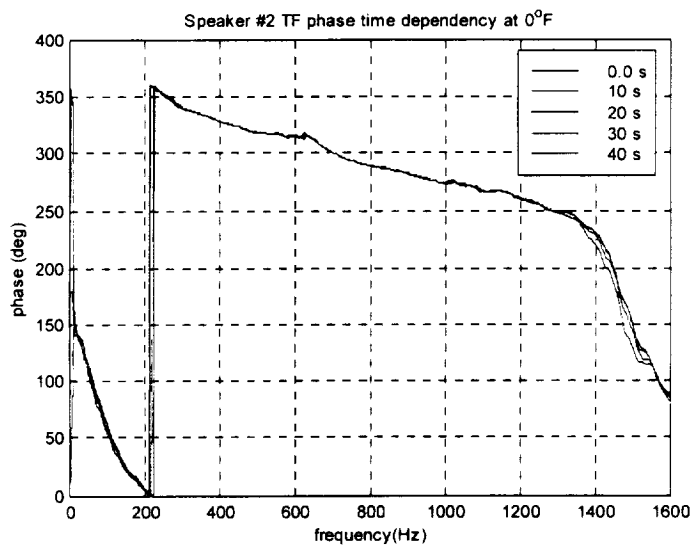

Figure 24 Running time dependency of the TF phase

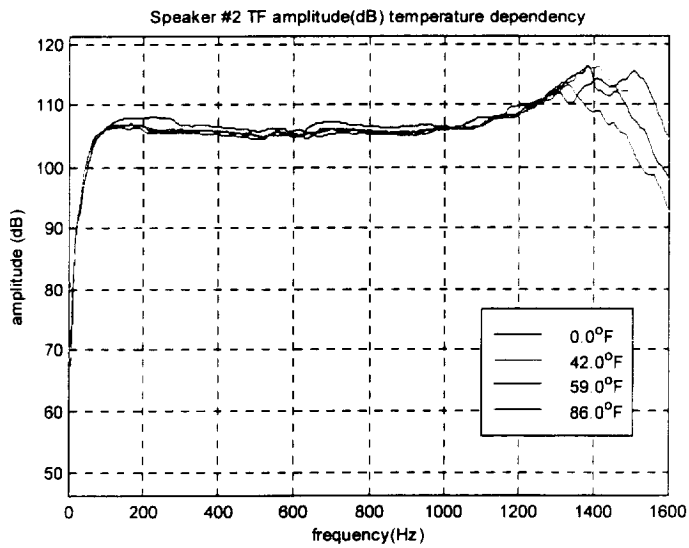

Figure 25 Environment temperature dependency of the TF amplitude

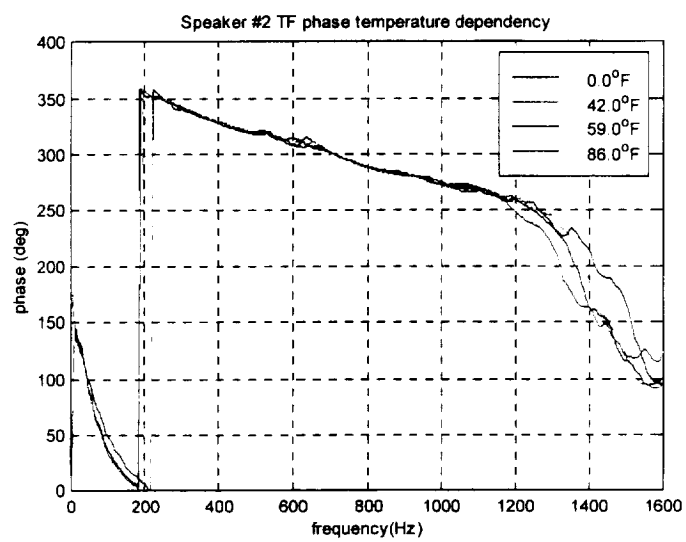

Figure 26 Environment temperature dependency of the TF phase

6.1.2 Ambient pressure dependency of the speakers

In the engine duct, the actuator may experience up to 1.0 inch water pressure difference from the outside of the duct. To protect the speaker diaphragm from excessive displacement, the speaker back was sealed. A laser displacement sensor and an airflow rig were used to measure the speaker diaphragm displacement. The laboratory setup is shown in Figure 27.

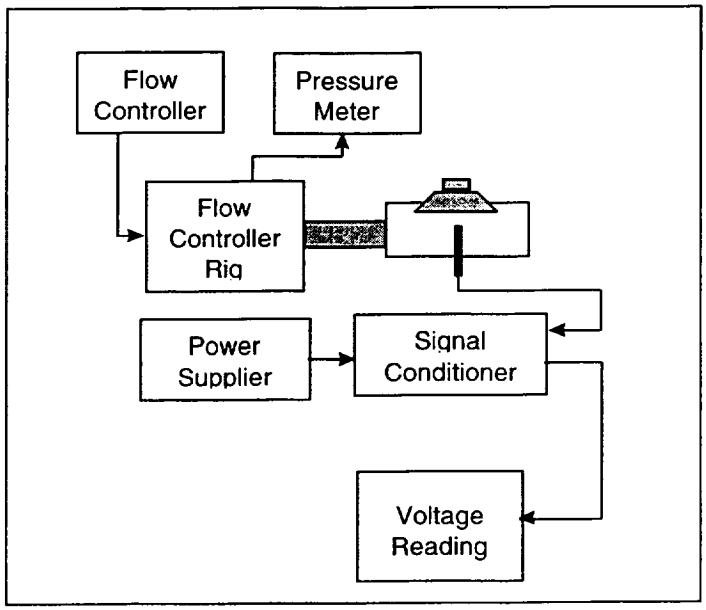

Figure 27 Speaker diaphragm displacement measurement

The sensitivity of the laser sensor was calibrated first. The calibration data are shown in Table 5 and the curve fitting is shown in Figure 28.

Table 5 Sensor calibration data

Gap (mils)	Output (mv)
5	78
52	162
105	302
158	436
206	517

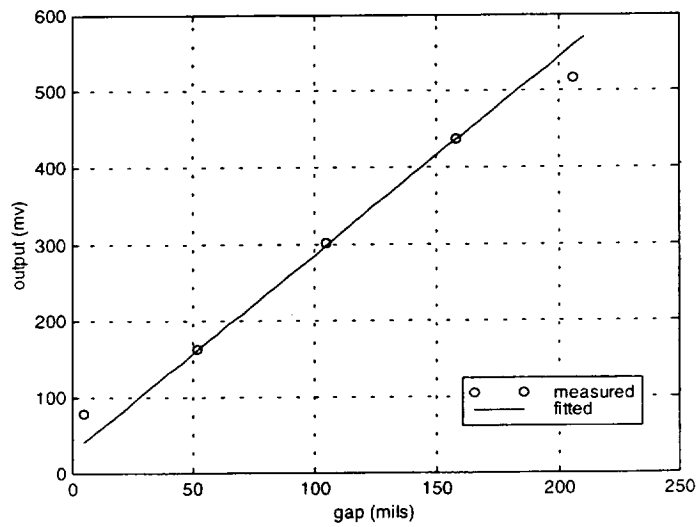

Figure 28 Sensor calibration

From the calibration data, it was identified that the linear region is from about 50mils to 160mils. In this region, the sensitivity is about 0.387 mil/mv. Thus, the initial gap was set at 152 mils.

Speaker static displacement under zero pressure and one inch water pressure levels were measured. The speaker diaphragm is not a pure linear spring material, pressure increasing and pressure decreasing measurements were conducted for comparison. The data are listed in Table 6. The averaged displacement at one inch water pressure is about 27.66 mil.

Table 6 Static measurement data

P (inch water)	pressure increasing		pressure decreasing	
	sensor output (mv)	Displacement (mil)	sensor output (mv)	Displacement (mil)
0	407	0.0	383	0.0
1	335	-27.8540	312	-27.4672

The back seal can protect the excessive displacement of the speaker diaphragm under static pressure. The effect of the back sealing on the speaker dynamic characteristics was examined by another experiment. The test setup diagram is shown in Figure 29.

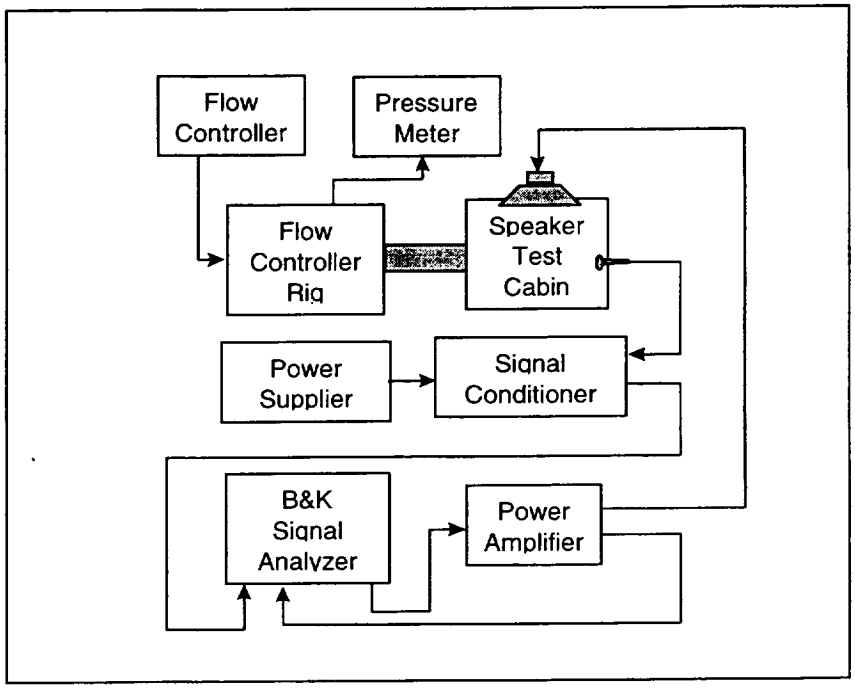

Figure 29 Test setup for speaker dynamic characteristics with back sealing

Similar to the previous tests, the transfer function is defined as the relation between the microphone inside the test cabin and the voltage to the speaker. To examine the effect of the pressure release of the speaker back sealing, the dynamic characteristics of the speaker with different hole sizes on the speaker diaphragm were also tested. Three speakers, numbered B9, B1 and B3, with zero and one inch water pressure were tested. The B1 and B3 speakers were considered as well sealed while the B9 was not well sealed.

The input signal to the speaker was random noise with an amplitude of 3.0V rms. The test microphone sensitivity was unknown and set at 20μV/Pa. The input sensitivity was set at 1V/Pa. Thus the TF measured is relative. Discrete measurements are recorded in Table 7. The difference in the TF amplitude and phase due to the one inch water pressure are shown in Figures 30 and 31 for the B9 speaker, in Figures 32 and 33 for the B1 speaker, and in Figures 34 and 35 for the B3 speaker.

As can be seen from Figure 30 through Figure 35, the pressure releasing hole can reduce the difference due to the static pressure for speakers which have a poorly sealed backing. For speakers with a well sealed back, the effect of the pressure releasing hole is negligible.

Table 7 Transfer function under the static pressure

Hole (in)	Speaker #	P (in.W.)	1200 Hz		1250Hz		1300Hz		1350Hz		1400Hz	
			dB	deg	dB	deg	dB	deg	dB	deg	dB	deg
0.00	B9	0	49.2	-9.3	47.5	-26.9	45.8	-39.6	44.1	-54.1	42.8	-68.4
		1	47.8	5.2	46.5	-17.2	44.4	-37.6	42.2	-54.1	40.3	-67.6
	B1	0	49.7	-11.9	47.7	-29.8	45.9	-42.9	44.1	-55.7	42.6	-67.4
		1	49.1	-7.5	47.6	-23.6	45.9	-38.6	44.2	-52.4	42.7	-64.4
	B3	0	49.5	-11.7	47.4	-28.6	45.8	-39.6	44.4	-52.8	43.2	-66.5
		1	49.0	-7.8	47.2	-24.0	45.6	-36.5	44.1	-49.3	43.0	-63.0
0.07	B9	0	49.1	-7.3	47.4	-24.6	45.8	-37.6	44.3	-52.7	42.9	-66.5
		1	47.6	7.0	46.4	-16.3	45.3	-36.7	42.1	-52.8	40.3	-67.7
	B1	0	49.9	-11.9	47.7	-30.0	45.8	-43.2	43.9	-55.6	42.6	-67.4
		1	49.2	-7.0	47.6	-23.7	45.8	-39.1	44.2	-52.5	42.6	-63.8
	B3	0	49.5	-11.4	47.5	-27.6	45.9	-40.1	44.3	-53.5	43.1	-66.5
		1	48.9	-6.0	47.3	-22.4	45.3	-39.1	44.3	-49.1	43.1	-62.0
0.10	B9	0	49.2	-7.5	47.5	-24.8	45.9	-38.2	44.2	-53.3	42.8	-66.9
		1	47.8	5.6	46.5	-17.9	44.3	-37.9	42.0	-53.5	40.3	-67.3
	B1	0	49.9	-12.7	47.7	-30.0	45.7	-41.8	44.0	-55.0	42.5	-67.0
		1	49.4	-6.4	47.6	-24.5	45.6	-38.3	44.0	-51.3	42.6	-63.0
	B3	0	49.5	-10.2	47.5	-26.7	45.9	-39.0	44.2	-52.4	43.0	-64.6
		1	49.0	-6.4	47.3	-21.6	45.7	-34.9	44.3	-48.4	43.1	-60.8
0.143	B9	0	49.2	-6.7	47.5	-23.3	45.9	-37.4	44.2	-51.8	42.7	-64.9
		1	48.1	3.0	46.5	-19.9	44.3	-37.8	42.2	-51.7	40.5	-64.7
	B1	0	49.9	-11.3	47.6	-28.7	45.8	-40.8	44.0	-54.6	42.5	-65.4
		1	49.4	-5.1	47.5	-23.2	45.7	-37.1	44.0	-51.1	42.5	-61.6
	B3	0	49.4	-9.2	47.5	-26.0	45.7	-37.5	44.3	-51.1	43.0	-64.5
		1	49.0	-3.6	47.3	-20.8	45.7	-33.7	44.4	-46.9	43.2	-60.9
0.200	B9	0	49.2	-5.0	47.5	-22.7	45.8	-35.8	44.3	-50.9	42.6	-64.6
		1	48.5	-0.3	46.7	-20.3	44.7	-35.4	43.0	-49.1	41.5	-62.9
	B1	0	49.9	-10.3	47.7	-28.3	45.6	-40.3	43.9	-53.0	42.5	-64.5
		1	49.5	-4.9	47.5	-23.2	45.6	-37.1	43.9	-50.1	42.5	-61.6
	B3	0	49.5	-8.7	47.4	-25.1	45.6	-36.8	44.1	-50.1	43.0	-62.9
		1	49.0	-2.9	47.3	-20.0	45.7	-32.9	44.4	-46.8	43.1	-61.0
0.279	B9	0	49.2	-2.6	47.6	-20.3	45.8	-34.6	44.3	-50.6	42.8	-62.9
		1	48.5	0.7	47.0	-17.0	45.3	-32.4	43.8	-47.1	42.2	-59.4
	B1	0	49.9	-8.7	47.4	-26.8	45.7	-39.0	44.0	-52.2	42.6	-64.2
		1	49.5	-3.5	47.6	-22.2	45.6	-36.1	44.1	-49.2	42.5	-60.6
	B3	0	49.3	-6.6	47.5	-23.5	45.7	-36.1	44.2	-49.8	42.8	-62.1
		1	49.0	-1.1	47.4	-18.8	45.7	-32.3	44.2	-46.2	42.9	-59.2
0.279 ×2	B9	0	49.1	4.1	47.8	-14.4	46.2	-30.9	44.5	-46.5	43.1	-60.7
		1	48.6	7.9	47.4	-10.3	45.8	-27.6	44.3	-43.6	42.8	-57.1
	B1	0	50.1	-2.4	48.1	-21.0	46.1	-35.9	44.3	-50.8	42.7	-62.8
		1	49.8	3.0	48.0	-16.4	46.1	-32.5	44.3	-46.9	42.6	-59.5
	B3	0	49.5	0.5	47.8	-17.9	46.0	-32.6	44.4	-46.8	43.0	-59.7
		1	49.2	5.6	47.7	-13.0	45.9	-29.1	44.5	-43.0	43.0	-56.9
0.279 ×3	B9	0	48.8	10.6	47.9	-8.3	46.3	-25.5	44.9	-42.8	43.3	-58.3
		1	48.4	14.6	47.5	-4.6	46.0	-22.5	44.7	-39.1	43.2	-54.9
	B1	0	49.7	5.2	48.1	-14.0	46.3	-30.4	44.6	-45.6	43.1	-59.0
		1	49.4	9.8	48.0	-10.0	46.3	-27.7	44.6	-42.6	43.0	-56.0
	B3	0	49.2	8.5	48.0	-10.2	46.4	-27.3	44.6	-42.9	43.1	-57.3
		1	48.9	13.0	47.8	-6.2	46.3	-24.6	44.7	-40.5	43.1	-54.6
0.279 ×4	B9	0	48.6	19.0	48.0	0.3	46.7	-19.5	45.1	-39.2	43.5	-54.9
		1	48.1	22.8	47.6	4.0	46.5	-16.4	45.0	-35.5	43.4	-51.8
	B1	0	49.8	12.5	48.5	-7.9	46.7	-26.2	44.9	-42.7	43.2	-56.5
		1	49.4	16.6	48.3	-2.7	46.8	-21.4	45.1	-39.3	43.1	-54.4
	B3	0	49.0	15.0	48.0	-3.6	46.6	-21.5	45.0	-39.9	43.3	-55.3
		1	48.7	19.4	47.9	0.1	46.5	-19.3	45.0	-37.0	43.3	-51.3

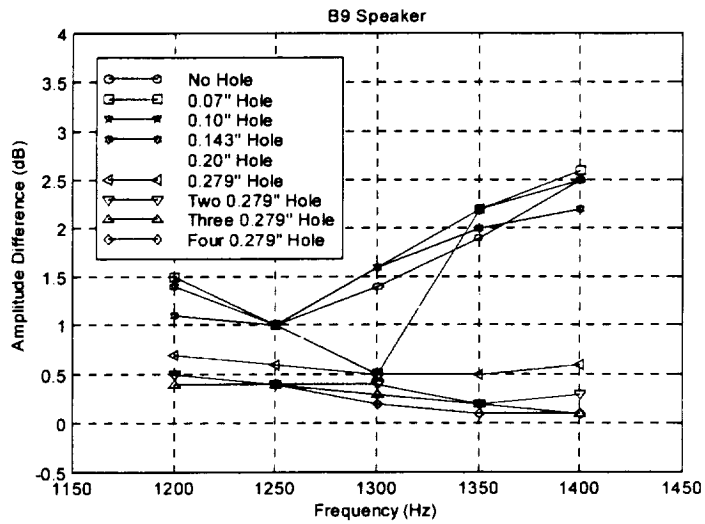

Figure 30 TF Amplitude difference due to the pressure, B9 speaker

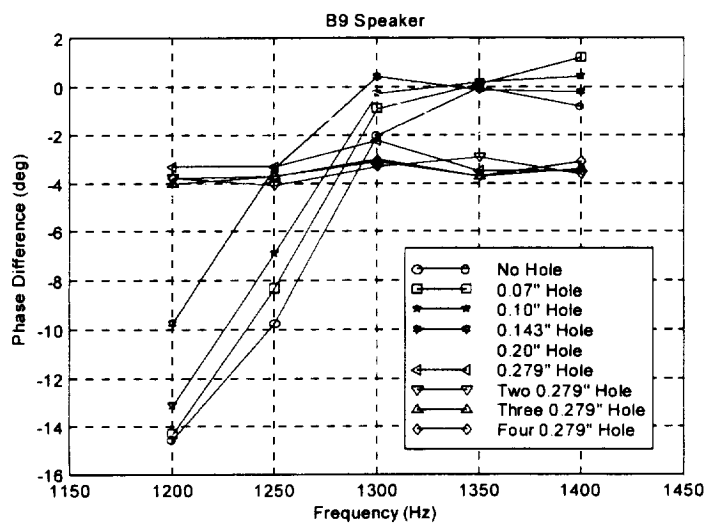

Figure 31 TF Phase difference due to the pressure, B9 speaker

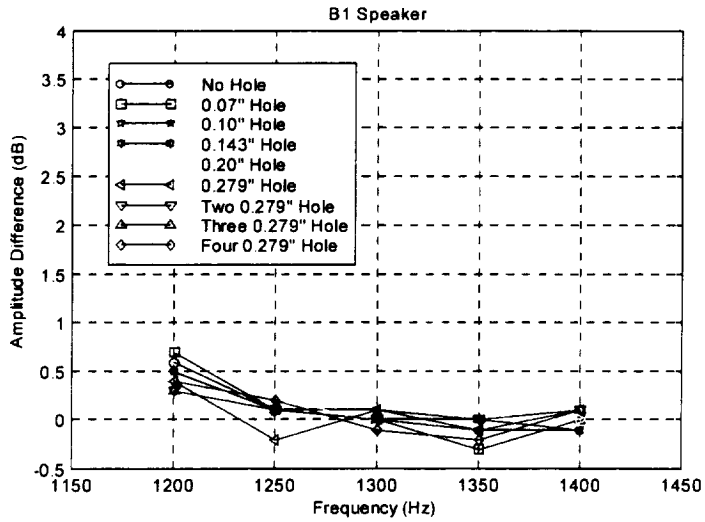

Figure 32 TF Amplitude difference due to the pressure, B1 speaker

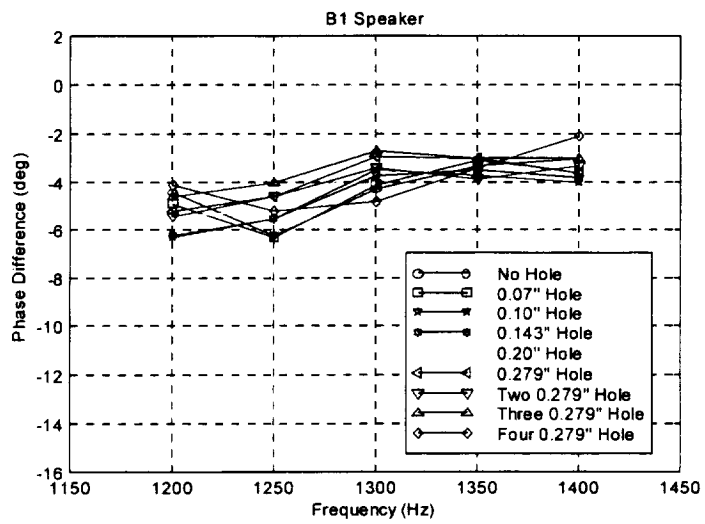

Figure 33 TF Phase difference due to the pressure, B1 speaker

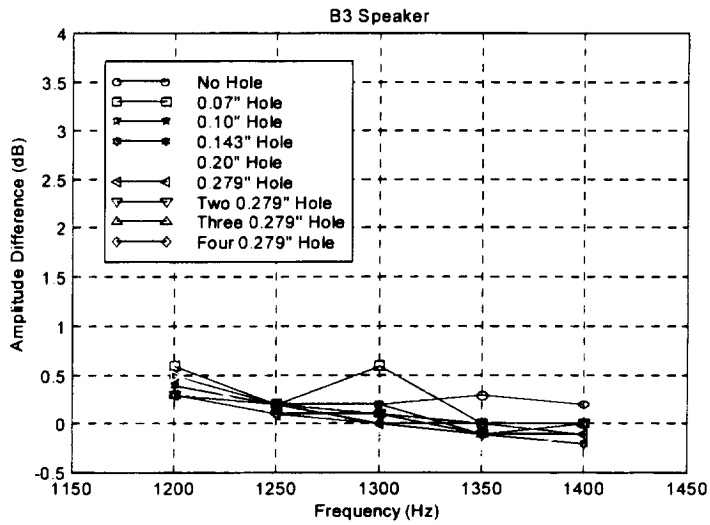

Figure 34 TF Amplitude difference due to the pressure, B3 speaker

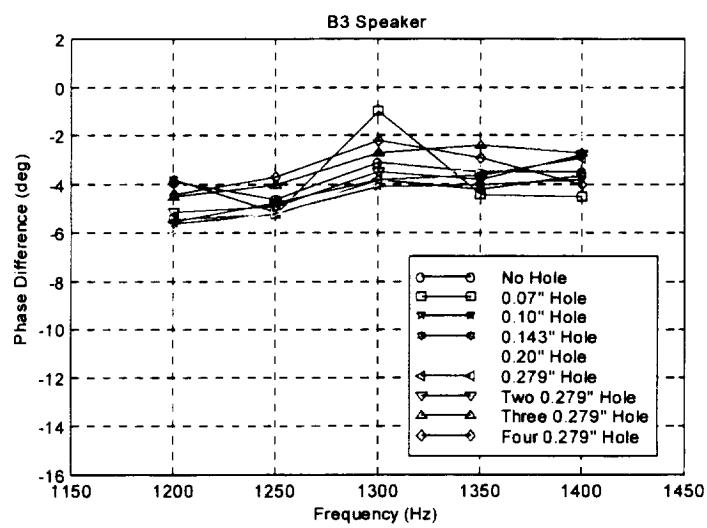

Figure 35 TF Phase difference due to the pressure, B3 speaker

Based on the speaker test information, it is concluded that the characteristics of the selected speakers are stable with the ambient temperature, running time, and ambient pressure. Speakers with back sealing and without pressure releasing holes were determined to be used as actuators for the active noise cancellation system. To further reduce the speaker mechanical variation and back sealing difference in an actuator ring, a speaker sorting was conducted and is presented in the next section.

6.2 Speaker Sorting

To reduce the calibration requirements in real control applications, the speakers on the same actuator ring need to be as similar as possible. We conduct the speaker sorting by measuring the speaker amplitude and phase at five discrete frequencies. Seventy-five speakers were tested. Then the speakers were grouped into 4 groups according to the phase characteristics (see Table 8). Each group had 16 speakers. The amplitude difference within a group was compensated by fine tuning of the speaker amplifier.

Table 8 Phase-Based Sorting

group #1										
Mark	1200A	1200P	1250A	1250P	1300A	1300P	1350A	1350P	1400A	1400P
B-34	98.60	-32.8	97.30	-54.2	95.90	-70.7	94.70	-83.8	93.90	-96.7
B-55	99.20	-30.2	97.80	-53.9	96.20	-70.9	95.00	-85.0	94.20	-97.6
B-73	98.60	-33.6	97.10	-54.0	95.60	-69.4	94.70	-82.4	94.00	-95.9
B-65	98.80	-32.0	97.40	-53.6	95.90	-69.7	94.70	-83.0	94.00	-95.8
B-50	98.90	-29.2	97.90	-52.0	96.50	-70.3	95.20	-84.8	94.30	-97.8
B-44	99.00	-28.7	97.90	-52.0	96.50	-70.3	95.20	-84.8	94.30	-97.8
B-63	97.90	-32.5	96.70	-52.6	95.50	-68.6	94.50	-82.8	93.70	-96.2
B-71	98.40	-28.4	97.50	-50.6	96.20	-68.7	95.00	-84.6	94.00	-98.6
B-61	98.20	-29.1	97.30	-50.8	96.30	-69.1	95.00	-82.9	94.20	-98.6
B-37	98.70	-30.6	97.60	-51.6	96.20	-69.2	95.00	-82.8	94.30	-96.2
B-21	99.20	-29.4	98.10	-52.7	96.30	-69.8	95.10	-82.5	94.50	-95.3
B-45	98.90	-28.1	97.80	-50.9	96.30	-69.2	95.10	-83.9	94.40	-96.9
B-15	97.40	-30.7	96.50	-51.0	95.20	-67.9	94.20	-82.9	93.40	-96.2
B-59	97.80	-29.5	96.70	-50.8	95.50	-67.8	94.50	-82.9	93.60	-96.9
B-60	98.10	-29.6	97.10	-50.5	96.00	-68.2	94.80	-82.9	94.00	-96.6
B-57	98.10	-31.4	97.00	-50.8	95.90	-67.1	94.90	-81.9	94.20	-96.3
Ave.	98.48	-30.3	97.35	-52.0	96.00	-69.1	94.85	-83.3	94.06	-96.8
Min.	97.40	-33.6	96.50	-54.2	95.20	-70.9	94.20	-85.0	93.40	-98.6
Max.	99.20	-28.1	98.10	-50.5	96.50	-67.1	95.20	-81.9	94.50	-95.3
group #2										
Mark	1200A	1200P	1250A	1250P	1300A	1300P	1350A	1350P	1400A	1400P
B-29	97.90	-31.7	96.90	-49.8	95.90	-66.6	94.90	-80.6	94.30	-94.7
B-33	98.40	-29.4	97.30	-49.4	96.20	-66.9	95.10	-81.5	94.40	-95.8
B-11	99.10	-26.3	98.10	-49.7	96.90	-67.1	95.80	-82.6	94.90	-97.2
B-52	98.10	-30.9	96.90	-50.7	95.70	-66.3	94.80	-80.5	94.10	-94.4
B-68	98.20	-28.7	97.30	-49.4	96.20	-66.6	95.20	-81.6	94.40	-96.2
B-51	98.30	-27.9	97.40	-49.4	96.20	-66.8	95.30	-81.7	94.50	-95.9
B-18	98.40	-28.7	97.20	-50.2	96.00	-66.6	95.00	-80.8	94.30	-94.6
B-49	97.50	-31.6	96.40	-49.7	95.60	-65.3	94.70	-80.0	94.10	-94.0
B-14	98.80	-27.5	97.70	-49.5	96.40	-66.6	95.30	-81.7	94.60	-95.1
B-05	98.40	-28.3	97.40	-47.6	96.50	-65.2	95.70	-81.6	94.70	-97.1
B-25	97.80	-29.9	96.80	-49.0	95.80	-65.5	94.80	-80.4	94.10	-94.1
B-62	98.40	-26.8	97.50	-48.6	96.40	-66.0	95.40	-81.3	94.70	-96.0
B-53	98.20	-31.2	96.90	-50.9	95.60	-65.0	94.90	-78.6	94.20	-93.0
B-58	98.40	-24.2	97.60	-47.1	96.40	-67.0	95.10	-83.2	94.10	-96.6
B-19	98.40	-26.7	97.50	-48.3	96.30	-66.0	95.30	-81.2	94.50	-95.3
B-12	98.90	-26.5	97.70	-49.6	96.30	-66.6	95.10	-80.2	94.40	-93.8

Ave.	98.32	-28.5	97.28	-49.3	96.15	-66.2	95.15	-81.0	94.39	-95.2
Min.	97.50	-31.7	96.40	-50.9	95.60	-67.1	94.70	-83.2	94.10	-97.2
Max.	99.10	-24.2	98.10	-47.1	96.90	-65.0	95.80	-78.6	94.90	-93.0

group #3

Mark	1200A	1200P	1250A	1250P	1300A	1300P	1350A	1350P	1400A	1400P
B-41	98.10	-25.6	97.30	-47.0	96.30	-65.4	95.30	-81.6	94.40	-96.9
B-35	99.00	-24.8	98.20	-47.1	97.00	-66.0	96.00	-81.7	95.00	-96.9
B-28	97.90	-29.8	96.90	-49.1	95.80	-64.6	95.00	-79.4	94.30	-93.5
B-10	98.00	-30.7	96.80	-49.0	95.80	-64.2	95.00	-78.1	94.40	-92.1
B-64	97.80	-26.6	97.00	-46.6	96.20	-63.5	95.40	-80.3	94.70	-95.9
B-54	97.90	-28.7	96.90	-47.2	96.00	-63.8	95.10	-79.0	94.50	-94.1
B-75	98.00	-28.9	97.10	-47.6	96.00	-63.7	95.30	-78.8	94.70	-93.6
B-20	98.20	-27.3	97.30	-47.8	96.10	-64.6	95.20	-79.5	94.60	-93.4
B-40	98.10	-29.4	96.80	-48.4	95.70	-63.7	95.10	-78.2	94.50	-92.7
B-39	98.40	-25.2	97.60	-46.8	96.50	-64.2	95.60	-80.3	94.80	-95.7
B-01	97.80	-27.8	96.90	-46.8	95.90	-64.0	95.00	-79.8	94.20	-93.8
B-47	98.10	-27.8	97.20	-47.3	96.10	-64.0	95.30	-78.9	94.60	-93.7
B-07	98.20	-24.9	97.60	-46.1	96.40	-65.0	95.40	-80.7	94.60	-94.3
B-32	97.70	-26.4	96.90	-47.0	95.80	-64.4	94.90	-79.2	94.20	-94.0
B-27	98.30	-25.5	97.40	-46.3	96.30	-65.1	95.30	-79.6	94.50	-94.2
B-56	97.90	-27.7	97.00	-46.8	96.10	-63.1	95.20	-79.4	94.50	-93.4
Ave.	98.08	-27.3	97.18	-47.3	96.12	-64.3	95.25	-79.6	94.53	-94.2
Min.	97.70	-30.7	96.80	-49.1	95.70	-66.0	94.90	-81.7	94.20	-96.9
Max.	99.00	-24.8	98.20	-46.1	97.00	-63.1	96.00	-78.1	95.00	-92.1

group #4

Mark	1200A	1200P	1250A	1250P	1300A	1300P	1350A	1350P	1400A	1400P
B-67	98.40	-25.2	97.60	-45.7	96.60	-64.2	95.70	-80.3	94.80	-94.8
B-13	97.80	-29.3	96.60	-47.8	95.70	-62.9	94.90	-77.1	94.30	-91.3
B-69	98.60	-25.0	97.70	-46.0	96.60	-63.6	95.70	-79.5	94.90	-93.5
B-30	97.30	-27.4	96.50	-46.4	95.70	-62.7	94.90	-77.8	94.20	-93.0
B-42	98.60	-25.4	97.50	-46.7	96.30	-63.5	95.60	-78.3	94.80	-93.4
B-26	97.30	-27.4	96.50	-45.5	95.70	-62.5	94.90	-78.4	94.10	-92.9
B-03	97.50	-26.6	96.80	-45.6	95.90	-62.4	95.20	-78.6	94.40	-93.4
B-23	97.40	-26.6	96.70	-45.6	95.80	-62.4	95.00	-77.9	94.30	-92.3
B-70	98.10	-27.3	97.10	-46.8	96.00	-61.3	95.10	-77.4	94.50	-91.5
B-66	97.60	-25.3	97.00	-44.3	96.20	-62.0	95.40	-78.5	94.60	-93.7
B-06	97.70	-27.3	96.90	-44.6	96.10	-61.6	95.40	-77.5	94.70	-92.4
B-17	97.50	-26.4	96.70	-45.3	95.80	-62.3	95.00	-77.5	94.30	-91.8
B-24	98.40	-25.2	97.50	-45.6	96.40	-63.2	95.40	-77.5	94.80	-91.5
B-22	97.60	-25.2	96.80	-44.4	95.90	-61.3	95.00	-77.4	94.20	-92.0
B-16	98.20	-24.2	97.40	-44.5	96.30	-61.8	95.50	-77.2	94.80	-91.6
B-72	96.70	-25.7	96.40	-41.7	95.80	-60.0	95.00	-75.3	94.40	-90.7
Ave.	97.79	-26.2	96.98	-45.4	96.05	-62.3	95.23	-77.8	94.50	-92.4
Min.	96.70	-29.3	96.40	-47.8	95.70	-64.2	94.90	-80.3	94.10	-94.8
Max.	98.60	-24.2	97.70	-41.7	96.60	-60.0	95.70	-75.3	94.90	-90.7

The amplitude fine-tuning was carried out based on a test setup shown in Figure 36. A sine signal at 1300Hz was generated by a signal generator. The signal was amplified and then fed into a speaker of a ring actuator. The microphone boom tip was pointed to the center of the speaker. The amplifier gain was tuned such that the output level at the microphone was a

constant. After the tuning, the TF between the boom tip microphone and the signal to the speaker was recorded.

As shown in Figure 37 and Figure 38, after the tuning, all speakers of the five ring actuators are expected to have the same amplitude under the same input. The phase difference among the speakers inside a ring should be within ±4°. Note that the averaged phase angle of each actuator ring is different. This difference needs to be compensated by calibration.

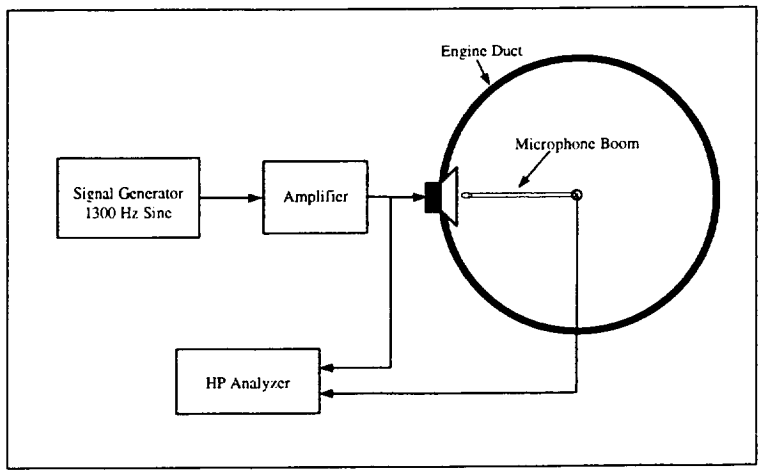

Figure 36 Speaker fine-tuning test setup

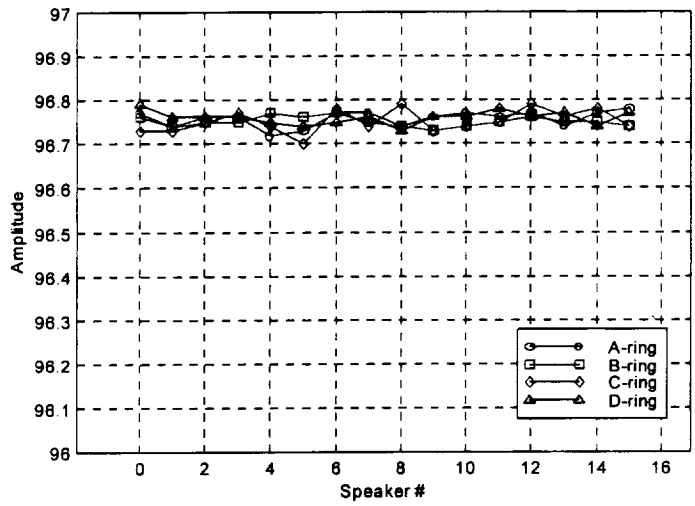

Figure 37 Actuator ring speaker amplitude variations

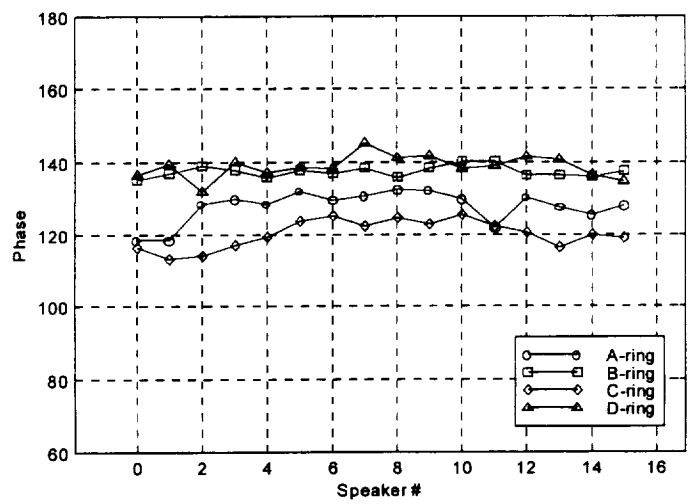

Figure38 Actuator ring speaker phase variations

6.3 Mode Generation

Though the individual speaker characteristics of a ring actuator were sorted to be similar, the most important thing is to make sure that the actuator ring can generate desired acoustic modes at the sensor location in the duct. Thus the noise components generated by noise source can be eliminated or reduced. To demonstrate this, a rotating boom with 15 microphones was placed in the duct to measure the sound pressure distribution over a duct cross-section (see Figure 39). The signal was then decomposed in the circumferential direction to examine the modal components.

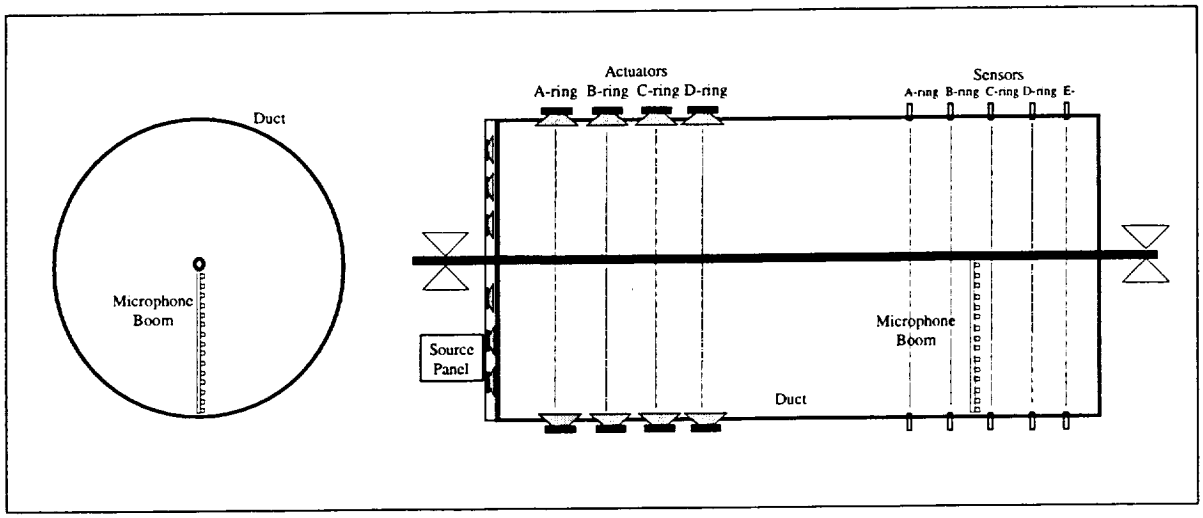

Figure 39 Mode generation measurement setup

In the tests, the control signal was set to generate a 1300 Hz signal with circumferential mode M=-2. In Figure 40, the real and imaginary parts of the SPL at the tip mic are shown. Figure 41 is the real part of the SPL at different radial positions. In Figure 42, the FFT in the circumferential direction is shown. It is seen that M=-2 mode stands out from the other modes by more that 16 dB.

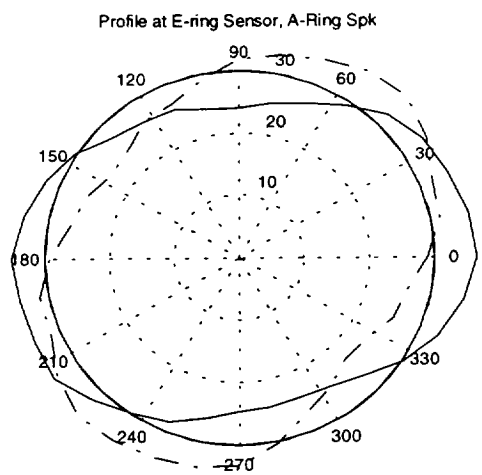

Figure 40 Real and imaginary parts of the SPL at the tip mic, A-ring

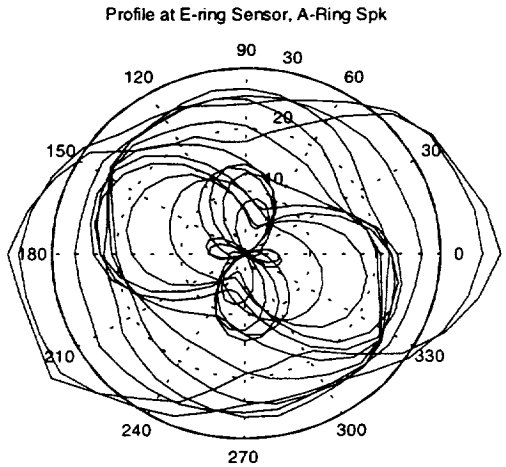

Figure 41 SPL real part for different radial positions, A-ring

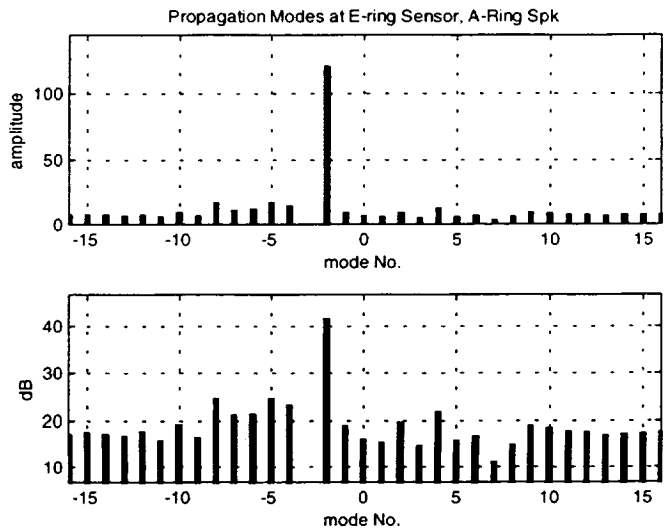

Figure 42 Circumferential modal decomposition, A-ring

Similar results were obtained from the B-ring, C-ring, and D-ring actuators. The FFT analysis results are shown in Figure 43 through Figure 45.

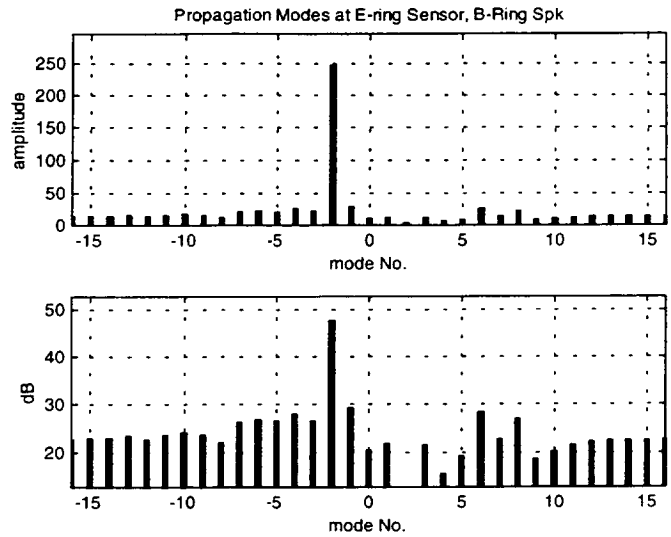

Figure 43 Circumferential modal decomposition, B-ring

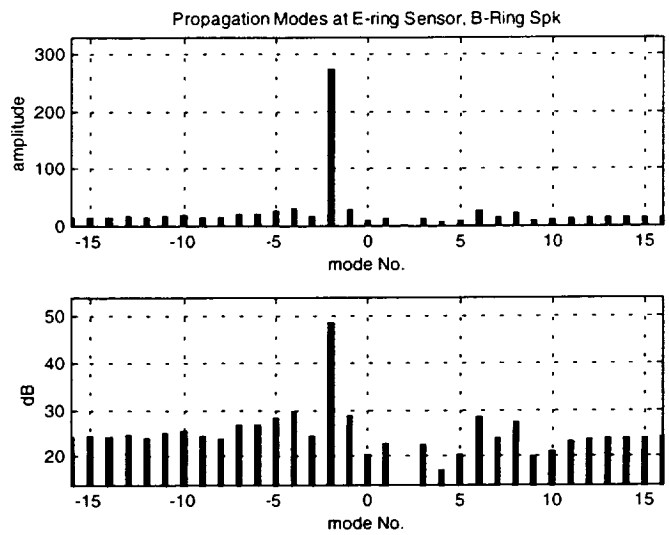

Figure 44 Circumferential modal decomposition, C-ring

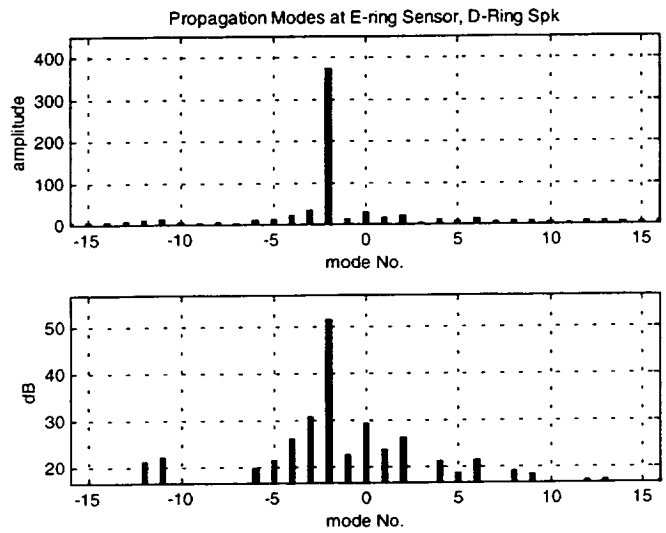

Figure 45 Circumferential modal decomposition, D-ring

Inside an engine duct, there can exist multiple radial modes at the same circumferential mode order. Each ring needs to be capable of generating all of the propagating modes with a measurable strength. The following tests demonstrate the capability of the ring actuators to generate multiple radial modes at the same circumferential mode order.

In the tests, an actuator ring was fed with controlled signal that generates the M=2 modes. Five axial positions were measured. At each axial position, a plane of grid points with 15 radial positions and 32 circumferential positions was recorded. The data were used to conduct modal decomposition by using the spatial FFT in circumferential direction and the spatial Bessel function decomposition in the radial direction.

In Figures 46 and 47, the modal decomposition results of the incident and reflection components for a 1200 Hz actuation are shown. As can be seen from figures, the M=-2 modes are dominant components. Several radial modes were excited. By examining the energy of the modes, it is seen in Figure 48 that in the first four radial modes, the energy in the M=-2 mode is at least 10 dB higher than the total energy in the rest of the circumferential modes. We have also examined the case when the actuator was excited at 1300 Hz. A similar pattern was found and is shown in Figures 49 through 51.

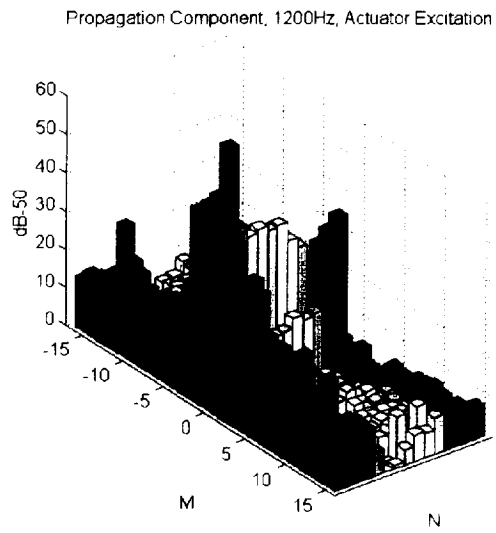

Figure 46 Modal decomposition, 1200Hz, Incident components

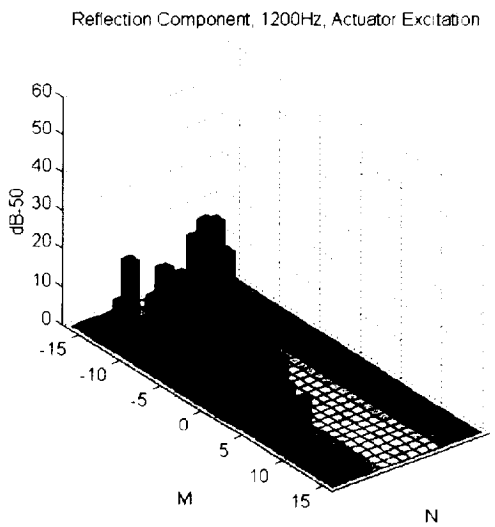

Figure 47 Modal decomposition, 1200Hz, reflection components

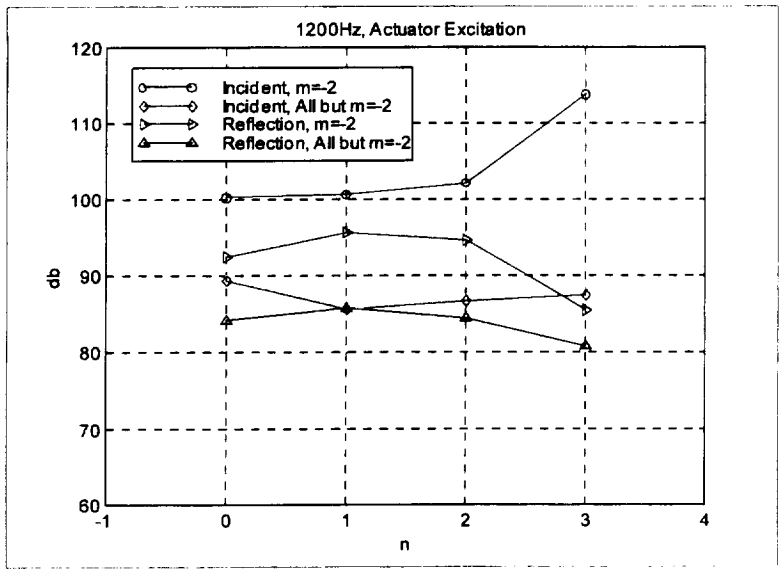

Figure 48 Modal energy distribution, 1200Hz

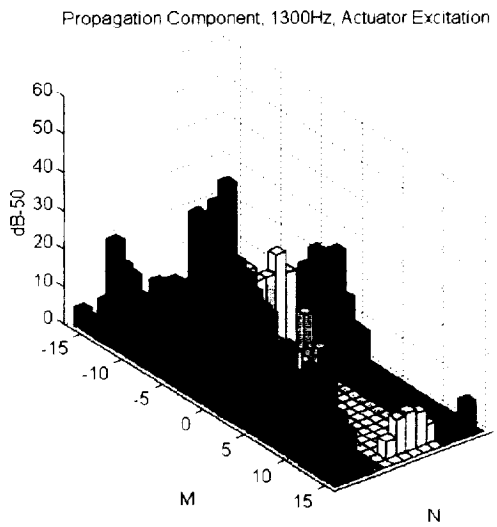

Figure 49 Modal decomposition, 1300Hz, Incident components

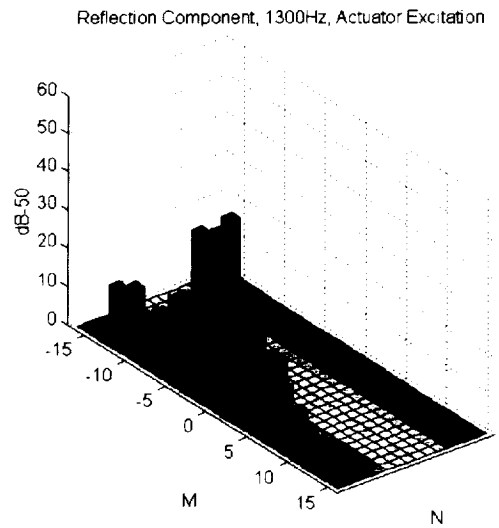

Figure 50 Modal decomposition, 1300Hz, Reflection components

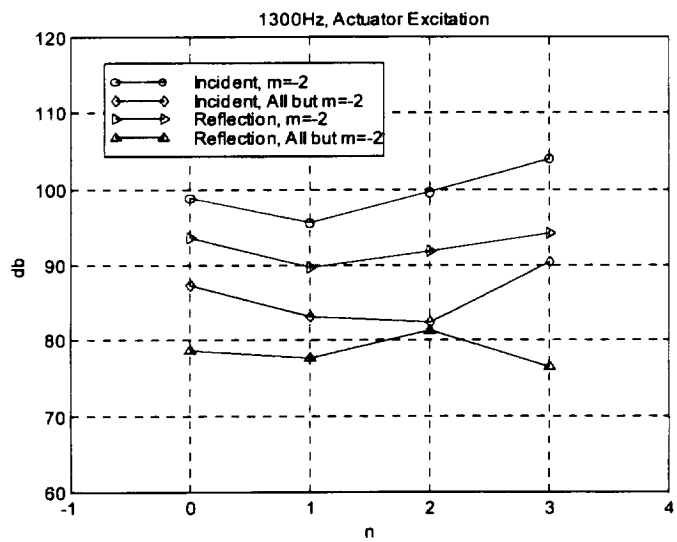

Figure 51 Modal energy distribution, 1300Hz

6.4 Wall Microphone Sensor Performance

In this test, the sensors were the microphones mounted on the duct wall. Tests conducted below were designed to verify the performance of the wall mounted microphones to pick up the control and/or source modes.

In the tests, the excitation was given by an actuator ring and the signals were picked up by five wall mounted microphone sensor rings, i.e., A-ring, B-ring, C-ring, D-ring, and E-ring (see Figure 39). The recorded data was used to perform the circumferential modal decomposition by FFT analysis.

In Figure 52, the real and imaginary parts of the SPL detected by A-ring sensor are shown. The corresponding FFT decomposition is shown in Figure 53. The modal decompositions for the B-ring through the E-ring sensors are shown in Figure 54 through Figure 57, respectively. As expected, the sensor modal decomposition is noisier than the actuator decomposition, because there are only 8 microphones in each sensor ring. Higher order modes have been folded into lower mode during the FFT analysis. Nevertheless, as seen in Figure 55 through Figure 57, more than 10 dB outstanding SPL levels are accomplished for sensor rings C-E. The outstanding values at A and B rings are less than 10 dB. This could be the additional noise from evanescent waves because these two sensor rings are to close to the actuators. When using the source excitation, which added 17 inches from A-ring sensor to the noise source, the outstanding levels were improved as shown in Figure 58 and Figure 59.

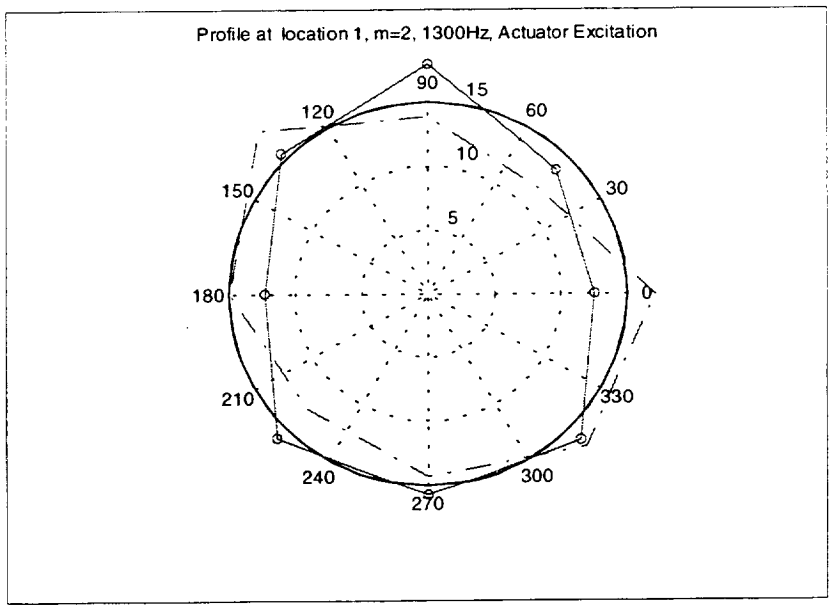

Figure 52 A-ring sensor SPL, real and imaginary parts

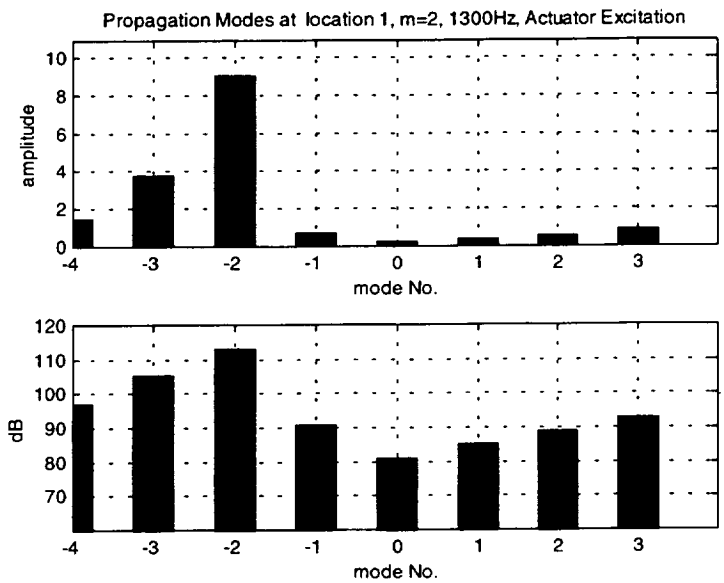

Figure 53 **A-ring sensor SPL, Circumferential modal decomposition**

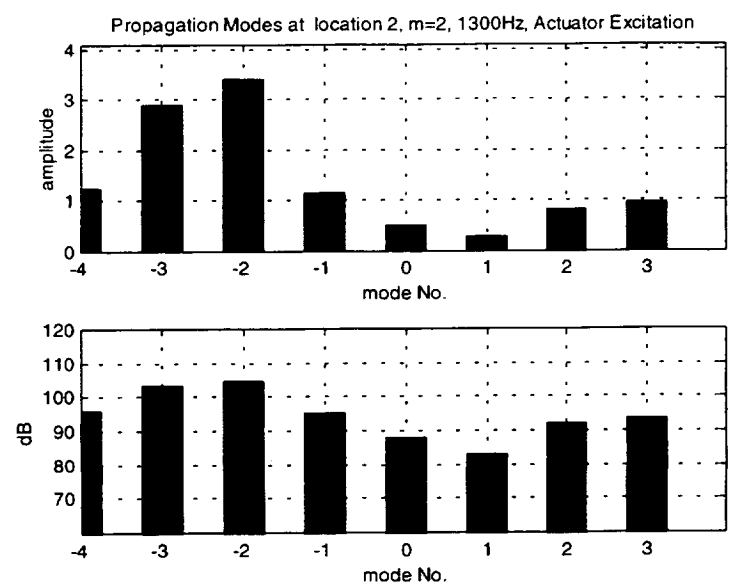

Figure 54 **B-ring sensor SPL, Circumferential modal decomposition**

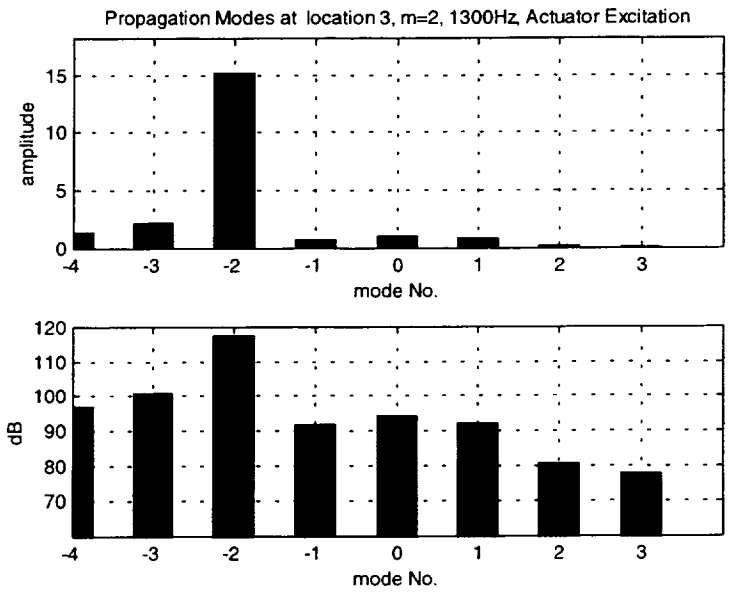

Figure 55 **C-ring sensor SPL, Circumferential modal decomposition**

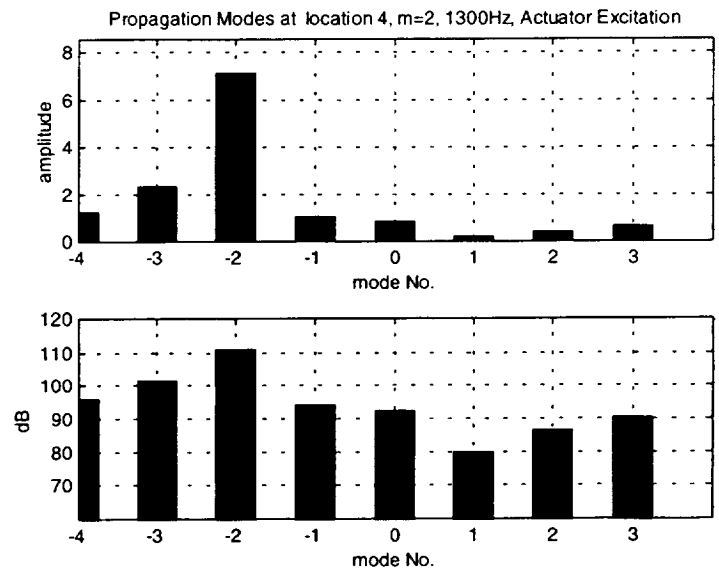

Figure 56 **D-ring sensor SPL, Circumferential modal decomposition**

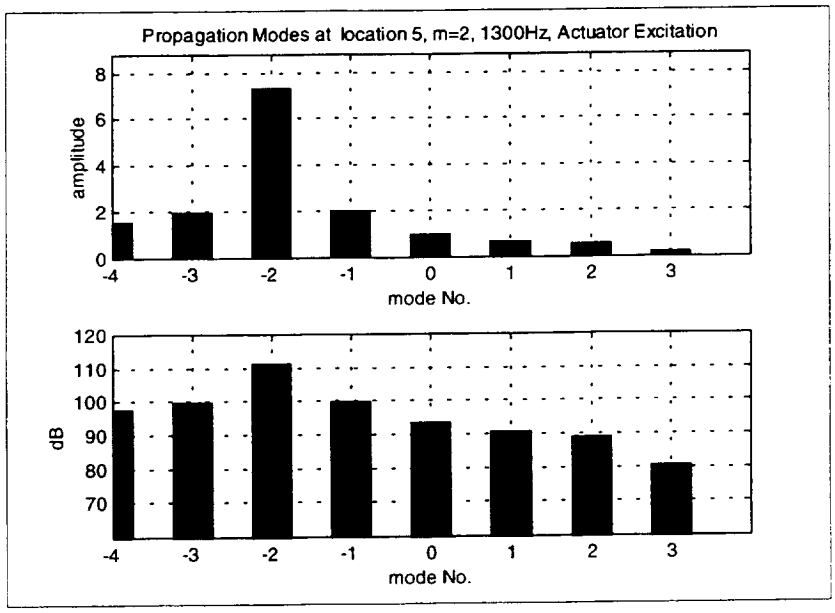

Figure 57 **E-ring sensor SPL, Circumferential modal decomposition**

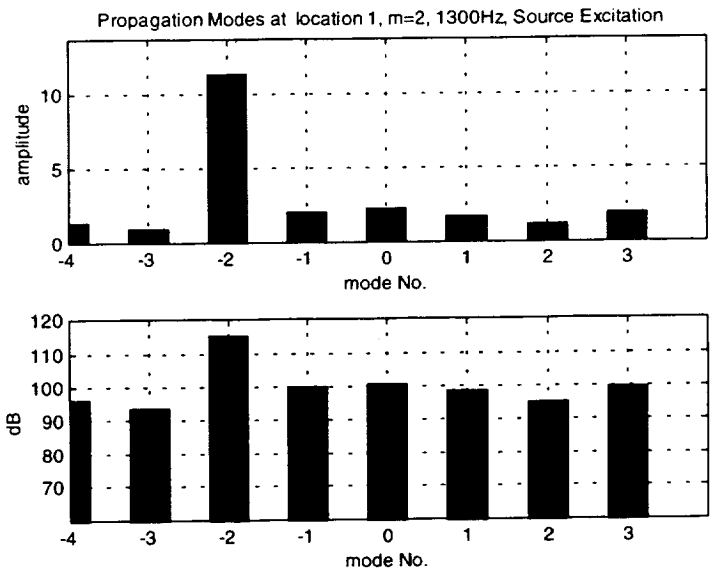

Figure 58 **A-ring sensor SPL, Circumferential modal decomposition, Source excitation**

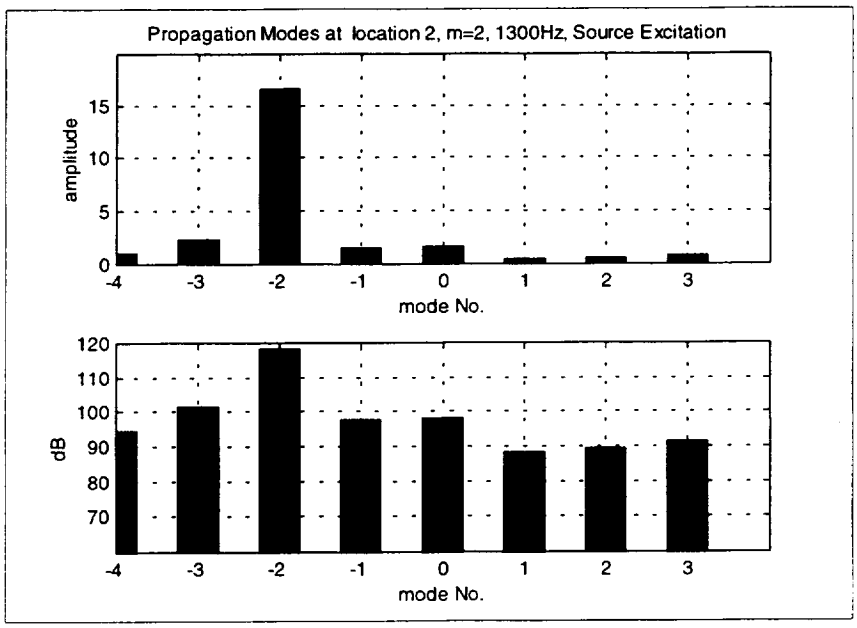

Figure 59 B-ring sensor SPL, Circumferential modal decomposition, Source excitation

6.5 Conclusions

From the inlet ANC system actuator and sensor tests, it can be concluded that:

1. The actuators selected have stable characteristics versus the ambient temperature change and running time;
2. Using back sealing, the speakers have stable characteristics under the ambient pressure. A pressure releasing hole on the speaker diaphragm has negligible affect on the speaker performance at 1 inch water pressure;
3. Sorted speakers have been used so that the speaker characteristics in an actuator ring are very similar. As a result, the mode generation of the actuator rings has more that 16 dB SNR;
4. Wall mounted microphone sensor rings detect the signal with about 10 dB modal SNR.

7 Inlet ANC Control System

7.1 Description of the BYU Controller

Based on the preliminary analysis of the control problem and discussion with the various team members, a control system was designed and developed to be able to minimize the modal response in potentially both the inlet and exhaust of the fan duct. This section describes each component of that control system and what its function is.

7.1.1 Controller Architecture

The overall operation of the control system can be shown in block diagram form, as in Figure 60. The signal, d(t), represents the uncontrolled signal that exists in the time domain at each of the sensors in the various sensor rings. The control system is based on synchronous sampling, such that each of the microphones is sampled at a frequency of four times the frequency of the signal to be controlled. In this case, the tonal at 2 BPF (blade passage frequency) for the M = 2 circumferential mode was chosen. Thus, the signals are sampled at a frequency of 8 BPF. This synchronous sampling was achieved by using a tach signal from the rotating shaft, which serves as an external trigger to the digital signal processing (DSP) board.

To perform the desired modal control, it is imperative that the error microphones be compensated to have a matched response, so that the circumferential modal decomposition produces meaningful modal amplitudes. Each microphone will have a transfer function associated with it in converting the acoustic pressure into an electric signal, designated by $C_{in,i}$ in Figure 60. The effects of these various transfer functions must be removed by multiplying each of the frequency-domain signals by the reciprocal of those transfer functions, designated by $C^{-1}_{in,i}$ in Figure 60. Before transforming the error signals to the frequency domain to do this calibration, the error signals are first time-averaged to remove unwanted background noise from the signals. This is done each time a new block of four time samples is obtained by using a sliding exponential window, such that the averaged error signal is given by

$$e_{i,ave}(t) = C \cdot e_i(t) + (1 - C) \cdot e_{i,ave}(t-1). \tag{4}$$

Here, C is a number that determines the effective length of the averaging window. This window length is given approximately by 1/C, so that if C is chosen to be 0.005, for example, the window effectively provides an average of about 200 blocks of data. Since synchronous sampling is used, the desired signal will add up coherently as each block is averaged, while the extraneous noise will tend to average out to zero.

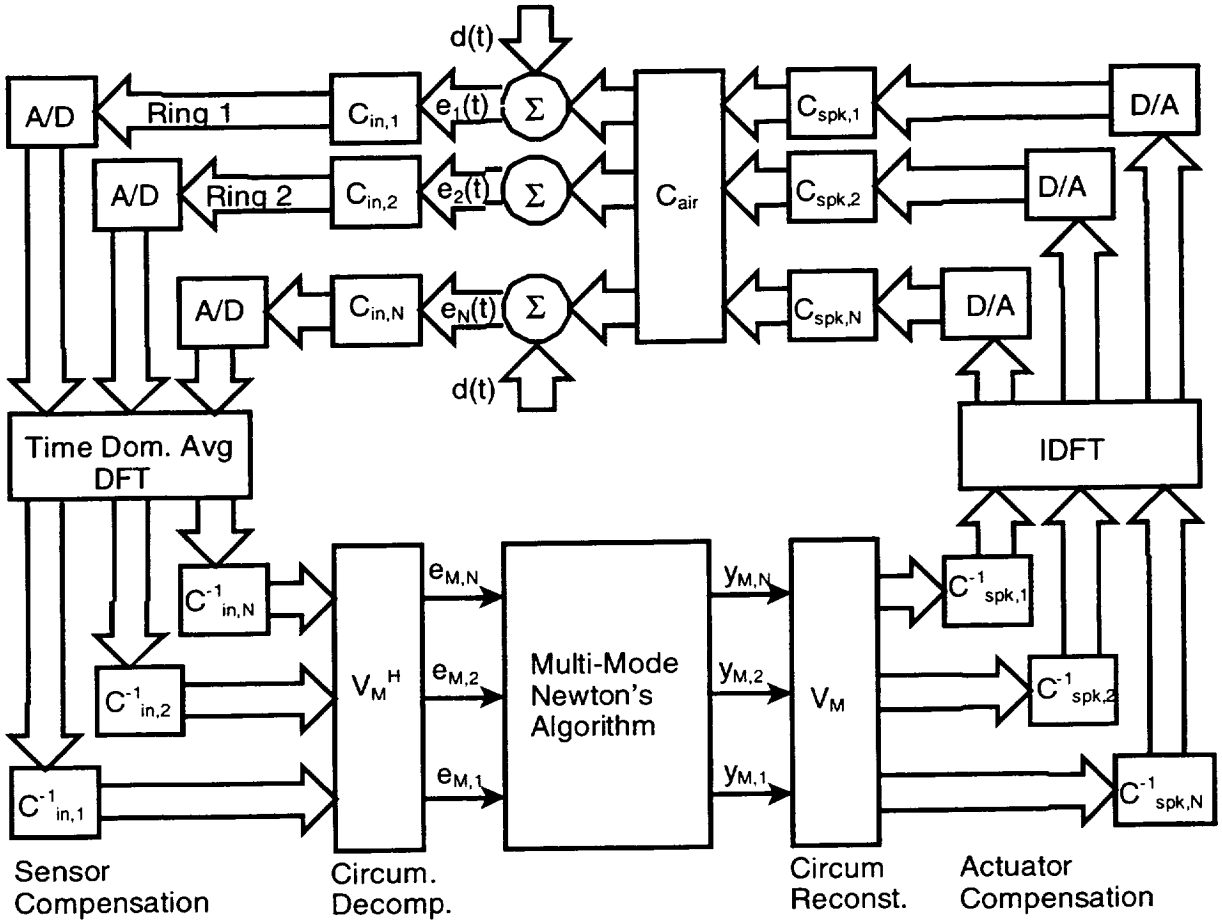

Figure 60. Block diagram of the multi-mode system.

As each new block of data (consisting of four time samples for each sensor) is obtained and time-averaged, a time-domain discrete Fourier transform (DFT) is performed that transforms the data into the frequency domain. This is a very efficient operation, since only the first bin of the DFT (which corresponds to the frequency of interest) needs to be calculated. After this operation, each of the frequency-domain error signals is then multiplied by the inverse transfer function for that error sensor, $C^{-1}_{in,i}$. This has the effect of calibrating the response of all of the error sensors. These inverse transfer functions are obtained using an a priori calibration routine. For the a priori calibration, a calibration speaker is driven by a Schroeder sine signal, which consists of a number of sinusoids that span the entire frequency range of interest. These sinusoids are phased in a manner that leads to a relatively uniform spectrum across the band of frequencies of interest. The speaker and a calibration microphone are placed in close proximity with the error microphone to be calibrated, and the responses of both the calibration microphone and the error microphone are recorded. The data is transformed to the frequency domain, and the ratio of the calibration microphone to the error microphone is then stored for each frequency component. For operation of the controller, the calibration frequency component closest to the

operating frequency is identified, and the transfer functions for that frequency are downloaded to the DSP and used by the controller for $C^{-1}_{in,i}$.

The control system then performs a circumferential modal decomposition for each ring of error sensors. The default circumferential mode number is M = 2, although the controller allows the user to specify any desired mode number, as well as the number of sensor rings and the number of sensors/ring. The modal decomposition is accomplished using a look-up table of the Fourier decomposition coefficients for the desired mode. The result of this step is that the control system has an array of error signals that represent the circumferential modal amplitudes for the desired modal index. There is one modal error signal for each ring, and this vector of modal error signals is the quantity that is minimized, in a least squares sense, by the control algorithm.

The next step for the control system is to calculate the control output, using the multi-mode Newton's algorithm, given by

$$\begin{aligned} y_M(k) = (1-\mu\lambda_1)y_M(k-1) - \mu\lambda_2(y_M(k-1) - y_M(k-2)) \\ -\mu\left[C_M^H C_M\right]^{-1} C_M^H e_M(k-1). \end{aligned} \tag{5}$$

In Equation 5, μ is a convergence parameter chosen to maintain stability of the adaptive algorithm, λ_1 is a weighting factor designed to penalize large control values at the expense of minimal attenuation of the error, and λ_2 is a weighting factor designed to penalize excessively rapid variations in the control signal that can lead to unstable behavior. As can be seen in Figure 60, $y_M(k)$ is the control output modal amplitude vector at time block k, and $e_M(k)$ is the error signal modal amplitude vector at time block k. The matrix C_M is the propagation path matrix, whose components, $C_{M,ij}$ consist of the transfer function from the jth actuator ring modal amplitude to the ith sensor ring modal amplitude. The result of Equation 5 is a vector of updated control signal modal amplitudes, where each component of the vector gives the complex modal amplitude for the corresponding actuator ring. This modal amplitude will then be converted into individual actuator signals that will be used for the next block of four time samples. The conversion from modal amplitude to individual actuator signals is accomplished with a circumferential reconstruction operation. This consists of multiplying the modal amplitude by the appropriate Fourier coefficient, such as

$$u_{n,i}(k) = y_{M,n}(k) \cdot e^{j2\pi Mi/16}, \tag{6}$$

where M is the circumferential mode index, n is the actuator ring number, i is the actuator index for each actuator in the nth ring, k is the time block number, and 16 actuators/ring has been assumed.

Each of the actuators has its own unique response, which must be corrected for to ensure that a clean modal output results from the control signals. This is accomplished through both hardware and software. For this research, the decision was made to carefully select the actuators so that the magnitude and phase matching of the speakers within a given actuator ring were within acceptable tolerances. As a result, the only calibration that the control system

accomplished in this regard was to calibrate the electronics for each of the output channels. It is also worth mentioning that it was decided to take advantage of the knowledge we have of the M = 2 mode to be able to reduce the number of output channels required. As a result, there are only four output signals from the controller for each ring at each time step, which are each shifted in phase by 45°. Since the modal pattern repeats after that, the remaining actuators were driven by wiring them either in or out of phase with the appropriate speaker from the four outputs. After the control outputs were determined, they were then calibrated by multiplying them (in the frequency domain) by the inverse transfer function of the electronic path associated with that control channel.

The final step of the control system consisted of inverse transforming (to the time domain) the output control signals to obtain the time domain control signals for each of the output channels. These four signals (for each ring) were then output from the corresponding control channel at the appropriate time step within the next time block.

7.1.2 Controller Hardware

The control system described in the previous section was implemented on a digital signal processing (DSP) system in a manner to provide the user with significant flexibility. The decision was made to implement the system using DSP boards manufactured by Spectrum Signal Processing, based on the Motorola DSP96002 DSP chip. This decision was made due to the fact that this board had been used for a previous stage of the research and had proven to work very well for that research. Given the large number of input and output channels, and also given the increased computational burden for the DSP system, it was determined that two Spectrum 96000 DSP boards would be needed, operating in parallel. These two boards were connected by means of a backplane, which allowed the boards to share data that is needed by both processors. In addition, each DSP board is equipped with a DSPLink connection, which Spectrum uses for interfacing with input/output (I/O) boards. The capability exists to connect three I/O boards to each DSP board. For this research, 32-channel input boards were used, as well as 16-channel output boards. The hardware configuration chosen for the sensor and actuator rings is based on ten microphones per sensor ring, and 16 actuators per actuator ring. As a result, the controller was designed to operate with three input boards and two output boards, which provides the capability of having nine sensor rings and eight actuator rings. Two input boards and one output board are interfaced with the first Spectrum 96000 DSP board, while one input and one output board are interfaced with the second DSP board.

7.1.3 Controller Software

The control system was implemented with software designed to run on the Spectrum 96000 DSP boards described in the previous section. The code that was designed to run on the DSP boards was programmed in assembly language, to provide maximum efficiency of operation. The DSP boards are also capable of interacting with the host PC in which the DSP boards are housed through dual-port RAM (DPRAM) memory. Given this capability, a menu-based user interface was programmed in "C" that provides the user an efficient way of interacting with the DSP boards, as well as provides real-time information that is displayed on the screen to help the user determine the effectiveness of the control system.

Upon starting the program, the user is presented with a menu-interface that provides options for carrying out the calibration steps and implementing the control system. In practice, the sensor and actuator calibration are done before the inflow control device (ICD) is installed. For the transducer calibration, the user is prompted to specify the number of transducers/ring, the number of rings, the lower and upper frequencies of interest for the calibration, the frequency step within that range, and the number of averages to include in the calibration measurement. The calibration program for either the sensors or actuators is then started, and the user is prompted as to which sensor or actuator will be calibrated. After completing the calibration for that transducer, the calibration data is displayed, and the user is allowed to choose whether to accept the data and go on, or to repeat the calibration for that transducer.

After the calibration of the transducers, but before the calibration of the propagation path to determine the matrix, C_M, the user must then run a program that measures the frequency of interest. This can either be done with the fan running, using the tach signal from the rotating shaft, or with the fan off, using an artificial tach signal at the desired frequency. The purpose of this step is to provide the control software with the information necessary to download to correct calibration data to the DSP boards for the frequency of interest. After determining the tonal frequency, the user can then run the program that does the calibration of the propagation path. This is done in the following manner. If the calibration is done with the fan on, the modal response of the acoustic field at each sensor ring location is first measured with no control sources on. This provides a measure of the modal field excited with the fan alone. The controller then excites each individual actuator ring with a control signal that corresponds to the desired circumferential mode. The user is prompted for the amplitude of this mode. This then excites the radial modes corresponding to that circumferential mode, and the response is again measured at each of the sensor rings. If the fan is running, the modal response of the fan noise is subtracted from the measured response, so that the resulting value corresponds to the circumferential modal contribution of the actuator ring alone for each of the sensor rings. These values are then stored as the components of the C_M matrix, where the ij^{th} component is given by

$$C_{M,ij} = \frac{e_{M,i} - d_{M,i}}{y_{M,j}}, \tag{7}$$

where $e_{M,i}$ is the measured response at the ith sensor ring with the actuator ring operating, $d_{M,i}$ is the measured response at the ith sensor ring with only the fan operating, and $y_{M,j}$ is the modal control signal driving the jth actuator ring. To make this measurement, the user can also specify

how many averages are used for each measurement. When the measurement has been completed, the user is shown the calibration data, and asked whether to accept the data and move to the next actuator ring, or to repeat the calibration for that ring.

After all of the actuator rings have been used as sources to provide a fully populated C_M matrix, the matrix is inverted to obtain C_M^{-1}. Since the matrix will not be square, in general, it is necessary to use the pseudo-inverse, which is given as $[C_M^H C_M]^{-1} C_M^H$. This is obtained by means of a singular-value-decomposition (SVD) routine that has been programmed into the control system. After the pseudo-inverse matrix has been obtained, the coefficients of C_M^{-1} are then stored in a data file that the control system downloads to the controller prior to starting the actual control.

After all of the previous calibration steps have been completed, the user is prepared to begin control of the fan duct noise. The user can select between manual control or automatic control. In both cases, the algorithm is triggered by the tach signals from the rotating shaft, such that the error sensors are sampled at four times the frequency of interest. At each time sample, all of the error sensors are input to the controller, and the controller then outputs the previously calculated actuator signals for that time sample. Based on which sample of the four sample block has been input, the controller then performs one of the following four tasks. When a complete block of four samples has been acquired, the controller performs a time-domain average of the signals, using an exponential time window, as discussed previously. After the next time sample has been acquired, the controller performs a DFT of all the error signals to transform the time-averaged data into the frequency domain. Following this transform, each of the error signals is then compensated, using the calibration data obtained for the error sensors. After the next time sample has been acquired, the controller performs a spatial Fourier transform using the frequency domain error signals to obtain the circumferential modal amplitudes for each of the sensor rings. If the automatic control option has been selected, the controller then calculates the output modal amplitude for each actuator ring for the next time block, using the error modal amplitudes calculated. If the manual control option has been selected, the output modal amplitudes are not changed from the values that were input by the user. It should be noted that in the manual control mode, the user does have the ability to manually change those output modal amplitudes through the on-screen menu options. After the next time sample of the block has been acquired, the controller determines the frequency-domain output signals for each individual actuator of each ring. These values are then compensated using the calibration data obtained for the speaker channels. Finally, the frequency-domain output signals are transformed back into the time domain, using a DFT, to obtain the next block of four time-domain output signals for each actuator channel.

7.2 Verification Results For the BYU Controller

A number of tests have been performed to determine if the various tasks of the BYU controller described in the previous section are working properly. This section will describe those tests and the results of the tests.

7.2.1 Error Sensor Calibration

When calibrating the error sensors, the error sensor and reference sensor signals were also input to a dual-channel FFT analyzer, from which the transfer function between the two sensors could be directly measured. The results of the calibration from the FFT analyzer were then compared with the transfer function obtained by the DSP control system. The results were found to agree very well with each other. In making the comparison, there was one difference between the two measurement systems that had to be accounted for. The DSP system was only capable of sampling four channels simultaneously. As a result, there was a small difference in the sampling time for each successive block of channels sampled (8 μs). Thus, for example, there was a 16 μs difference between the first channel sampled, and the ninth channel sampled. When this difference in sampling times was taken into account, the transfer functions measured by the DSP system and the FFT analyzer were typically in agreement to within less than 1° in phase, and 5% in magnitude (0.4 dB).

7.2.2 Actuator Channel Calibration

After the actuator channels had been calibrated, the manual control routine was run, and the signals output from the actuator channels were input to the FFT analyzer. If the calibrations were perfect, each successive output channel should have the same amplitude and a 90° phase shift, relative to the previous channel. This was checked several times, and it was found that the phase was typically within 0.1° of the desired phase, and 1% (0.1 dB) of the desired magnitude.

7.2.3 Frequency Estimate

This routine was tested by inputting a known frequency tach signal into the DSP system, and verifying that the controller was able to estimate the proper frequency. When a proper tach signal was presented to the controller, it was able to consistently estimate the proper frequency to within 1 Hz. The biggest challenge that was faced was that the tach signal obtained from the NASA test rig was not clean enough for the DSP system, such that occasional glitches occurred. After some trial and error, a method was found to obtain a tach signal that worked well with the DSP when using the tach signal corresponding to pulses at 256 BPF. There were still occasionally some problems when using a tach signal corresponding to pulses at 128 BPF. This did not affect the testing thus far, but could be an issue when simultaneously controlling both inlet and exhaust, since the slower sampling frequency would allow more processing time for the control system.

7.2.4 Propagation Path Calibration

This was the routine that was most difficult to verify proper operation, since there was no obvious independent measurement of the propagation path transfer functions that could be compared against. There were several steps taken, however, to try and verify proper operation. The error signal data measured by the DSP system was stored during the calibration process.

These signals were then independently processed in MATLAB to determine the propagation path transfer functions that should have been obtained by the DSP system. These transfer functions were then compared to those actually obtained by the DSP system, and it was found that the results agreed very well, typically agreeing to five or six significant figures. The discrepancies at that point were attributed to the difference in numerical precision between the DSP and MATLAB. As a result, it was concluded that the DSP system was calculating the propagation transfer functions properly, based on the measured input data.

The transfer function matrix is then inverted by the controller using a singular value decomposition (SVD) to obtain the pseudo-inverse matrix used for the actual control routine. This part of the process was tested by presenting many different matrices of different sizes and values to the inversion routine. The matrix inverses were also computed using MATLAB, and it was found that in all cases, the control system was obtaining the proper pseudo-inverse.

The one aspect of this calibration step that has not been able to be conclusively tested is whether the DSP system is obtaining the proper error sensor signals during this calibration phase. It is suspected that it may not be, which could lead to an inaccurate transfer function measurement, and hence suboptimal control performance. The reason for this suspicion is as follows. As this routine was designed for the tests to date, the user inputs a desired amplitude to drive the individual actuator rings with. This amplitude is the same for all actuator rings. However, it was observed that the various actuator rings responded somewhat differently, such that the resulting sound levels at the error sensors was noticeably different with some actuator rings than with others. This is particularly a problem when trying to do the calibration with the fan running, since if the level is too low for one or more actuator rings, the response to the actuator ring at the error sensor rings will be buried in the fan noise. This problem has been corrected in the current version of the control system, in that the user is allowed to specify the amplitude for each individual actuator ring. After the calibration for that actuator ring is complete, the results are displayed on the screen, giving the user the opportunity to either accept or reject the calibration data. If the calibration is rejected, the user can change the driving amplitude if desired, and the process is repeated for that actuator ring. If it is accepted, the control system moves on to the next actuator ring.

7.2.5 Control Algorithm

As mentioned previously, when implementing the DSP control, the user has the option of using manual control (no adaption) or automatic control (with adaptive updates). When running manual control, everything behaves as one would expect. The only real difference between the routine for manual control and automatic control is the section of code that updates the control output signals. The code is written in such a way that at each iteration, current and previous error signals and control signals are stored on the DSP. As a test, current and past error sensor signals and actuator output signals from a few control runs were downloaded to MATLAB. These values were then used to predict what the current control outputs should have been, using the Newton's algorithm described previously. The stored calibration data were also used to verify that the various calibration steps associated with the control routine were being calculated properly. These predicted values were then compared with the values calculated by the DSP

controller. Again, it was found that the results from the MATLAB calculations agreed with the results from the DSP controller to five or six significant figures. Thus, it was concluded that the control updates were being calculated in a proper manner.

7.3 Control Results

The previous sections indicate how each task associated with the controller was tested. The control system was used in a number of tests to assess the performance of the overall control system. In early testing, it was found that the attenuation achieved with the control system was not nearly as effective as what was hoped for. The controller did demonstrate convergence, and for most of the tests indicated that some amount of attenuation occurred. However, in many cases, the amount of attenuation indicated by the control system did not agree well at all with the results from the NASA rotating rake measurement. Considerable testing time was spent trying to determine the possible cause of this discrepancy. This section will overview some of these early test results.

Table 9 shows some of the results obtained for the inlet tests that were performed. The controller was configured to attenuate the M = 2 circumferential mode. In the table for the inlet noise, the actuator rows and sensor rows that were used are indicated by letters. There were a total of four possible actuator rows, and five sensor rows. The lettering is such that "A" represents the row closest to the rotor, while "D" (or "E" for the sensors) is the row closest to the inlet.

Table 9. Inlet Duct Tests

Test Number	Corrected RPM	Actuator Rows	Sensor Rows	Attenuation (dB)
2525	1300	A,B	D,E	16
2527	1400	A,B	D,E	11
2529	1500	A,B	D,E	18
2531	1600	A,B	D,E	14
2532	1300	A,B	B,C	16
2533	1400	A,B	B,C	4
2534	1500	A,B	B,C	14
2535	1600	A,B	B,C	14
2546	1500	A,B	D,E	10
2547	1500	A,B	A,B	21
2552	2000	A,B,C,D	A,B,C,D	4

It can be seen with these test results that the controller was able to attenuate what it measured for the sensor ring amplitudes. The difficulty that was observed is that the measurements made by the NASA rotating rake did not agree at all with the controller results, whenever sensor rings A,B, or C were used. In those cases, such as test 2535 for example, the controller would indicate that attenuation had occurred, but the rake would indicate that either amplification had occurred, or at best only minimal attenuation. However, whenever sensor rings D and E were used, which corresponded to the sensor rings mounted on the lip of the inlet, the results obtained from the controller and the rotating rake generally agreed within 1 or 2 dB. There were some cases where the control was poor, but both systems still agreed on the results.

In trying to understand how to improve the performance of the BYU controller, there have been two possible improvements that have been incorporated into the controller. As mentioned previously, it is thought that there may be a problem with getting accurate sensor input data for the propagation path calibration. The controller has been modified to give the user more control over this process, which was designed to rectify any possible problem with this step. The other possible difficulty is that the original version of the controller prompted the user for initial actuator control signal values. Since nothing is really known about the control solution, the values input by the user have a good possibility of being far from the optimal values. The control then iteratively adapts towards the solution that minimizes the sensor ring modal amplitudes.

It is quite possible that the minima that the controller is trying to identify correspond to very broad minima. This would have the effect of being able to allow the controller to be very slow in converging, and to converge to a solution that may not be the desired minimum. To overcome this possible effect, the controller has been modified so that the controller first monitors the sensor ring amplitudes and then calculates the estimated optimal control based on those signals. Those control signals are then used as the initial control signals, and the control adapts from those initial values to try and fine-tune the control solution. This procedure is incorporated into the Hersh controller, and it has been observed that the Hersh controller is generally able to zero in on the desired solution faster and more robustly than the original BYU controller. In the final testing, it was found that these changes led to improved performance. The control results obtained with these changes are outlined in Section 8.

8 ANC Test Results Measured By The NASA Lewis Rotating Rake

8.1 Test Bed

The GE ANC Modal Control System was tested installed in the NASA Lewis Research Center's (LeRC) 48" Active Noise Control Fan (ANCF)[4,5]. The ANCF uses a 16-bladed variable-pitch rotor and can be configured with stator vanes to provide specific mode generation and propagation for Active Noise Control Research. A unique feature on the ANCF is the direct attachment of the rotor centerbody to the rig support column, eliminating the need for struts, which could contaminate acoustic measurements. Additionally, an Inflow Control Device (ICD) allows for static testing. The combination of low tip speed (~520 ft/sec) and the 48" diameter produces fan tones of the same frequencies produced by full-size advanced engines. The ANCF is constructed of component spool pieces that can be replaced by ANC systems to be tested.

The primary measurement device on the ANCF is the Rotating Rake. The Rotating Rake is an implementation of a technique originally conceived by T.G. Sofrin[6] whereby a rake containing radially distributed pressure transducers rotates in the circumferential direction a precise fraction of the fan rotational speed. Since each circumferential acoustic mode is known to rotate at a unique frequency[7] in the rotor reference frame, a Doppler shift is induced in the rake reference frame. Further reduction of the data into radial modes is accomplished through a least squares curve fit[8].

The ANCF is located in the NASA LeRC's Aeroacoustic Propulsion Laboratory[9] (AAPL), a hemispherical anechoic (to 125 Hz.), test facility. A schematic of the inlet and exhaust ANC Modal Control Systems installed on the ANCF is shown in Figure 1. Descriptions of the systems are provided in Sections 2.3 (exhaust) and 5.4 (inlet).

---

4 Heidelberg, L., Hall, D.G., Bridges, J.E., and, Nallasamy, M., "A Unique Ducted Fan Test Bed for Active Noise Control and Aeroacoustics Research", NASA TM-107213, May 1996; also AIAA Paper 96-1740, May 1996.

5 Sutliff, D.L., Nallasamy, M., Heidelberg, L., and Elliott, D.M., "Baseline Acoustic Levels of the NASA Active Noise Control Fan", NASA TM-107214, May 1996; also AIAA Paper 96-1745, May 1996.

6 Cicon, D.E., Sofrin, T.G., and Mathews, D.C., "Investigation of Continuously Traversing Microphone System for Mode Measurement", NASA CR-16804, Nov. 1982.

7 Tyler J.M., and Sofrin T.G., "Axial Flow Compressor Noise Studies", SAE Transactions, Vol. 70, 1962, pp. 309-332.

8 Hall, D.G., Heidelberg, L., and Konno, K., "Acoustic Mode Measurements in the Inlet of a Model Turbofan using a Continuously Rotating Rake: Data Collection/Analysis Techniques", NASA TM-105963, Jan. 1993; also AIAA Paper 93-0599, Jan. 1993.

9 Cooper, B.A., "A Large Hemi-Anechoic Chamber Enclosure for Community-Compatible Aeroacoustic Testing of Aircraft Propulsion Systems", Journal of the Institute of Noise Control Engineering of the USA, Jan/Feb 1994.

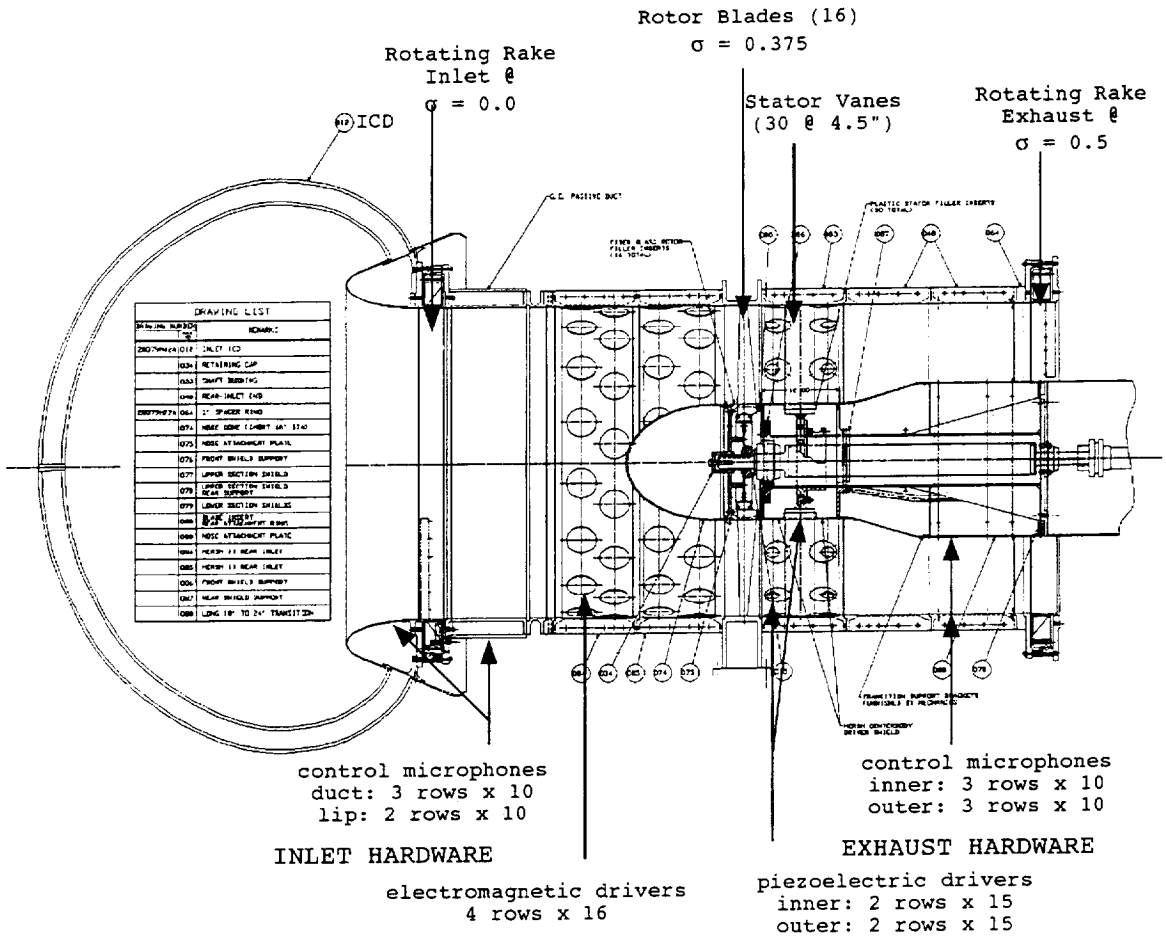

Figure 61. Schematic of active noise control system hardware installed on the active noise control fan

8.2 Test Conditions

The test of the inlet and exhaust ANC Modal Control Systems occurred over the period of June 1998 to January 1999. The performance of two controllers was tested. These are referred to as the MMNA (for the GE CRD/BYU Multi-Mode Newton Algorithm) and the AQ (for the Hersh Acoustics Adaptive Quadrature algorithm), and are described in Sections 2.3 (AQ) and 7.1 (MMNA). Each controller was tested, separately, in the inlet and the exhaust. The hardware, amplifiers, actuators, microphones and signal conditioners were kept in the respective duct locations. Only the controller and computer I/O were changed. The rotating rake measured the performance of each setup.

The ANCF configuration was 30 vanes (spaced axially at 4.5" from the rotor) with a blade pitch of 40°. The system was tested over a fan corrected (to 59°F) RPM range of 1100 to 2450. BPF is cutoff over this range with this rotor-stator configuration. The primary circumferential rotor-stator interaction mode at 2BPF is m=2. Up to 4 radial modes can propagate in the inlet,

while in the exhaust 3 radial modes can propagate at the nominal fan speed of 2300 RPM. Table 10 shows the cut-off RPM for the radial modes.

Table 10 Cut-off rpm for circumferential mode m=2

RADIAL MODE #	INLET (Radius ratio=0.0)	EXHAUST (Radius ratio=0.5)
0	509	447
1	1118	1178
2	1662	2159
3	2195	---

8.3 Rotating Rake Results

8.3.1 Modal Distortion Characteristics with Fan at Idle

The ANC systems were tested with the fan at idle to document the modal purity of the actuator arrays and signal distribution systems. Testing the system in this manner provides the modal distortion characteristics. Modal distortion is qualitative and quantitative amount of power in modes other than the desired control modes. The modal signal-to-noise ratio can be defined as the difference between the m=2 PWL and the PWL of the extraneous modes (i.e., mathematically removing the m=2 PWL from the total tone PWL). A difference of 15 dB or more is desirable. Modal distortion is generally the primary limiting factor in tone PWL reduction.

The modal purity of the MMNA controller using the inlet hardware is shown in Figure 62. Rows A, B, and D show a very strong m=2 mode 25 dB above the extraneous modes. The modal signal-to noise ratio is 13.4 to 16.3 dB for these driver rows. The MMNA control system incorporates the calibration of the actuator-to-actuator variation. This may account for the very good signal to noise ratio. The very low signal-to-noise ratio, -2.4 dB, of driver row C indicates a problem. There are significant extraneous modes at m = -10, -6, -2, 6, 10. This is a distinct pattern of extraneous modes of 2 +/-4n. The MMNA controller uses 4 output channels per row. These 4 output channels are each split into 4 signals to obtain the 16-actuator signals that are sent to the actuator amplifier. An error in this wiring split caused the signals to the actuators to be incorrectly phased ($\Delta\varphi$=45° for m=2) resulting in the spatial distortion pattern of +/-4n. The wiring was corrected. The modal character of row C was then measured by the in-duct microphone sensor rings to be the same order as those of the other rows.

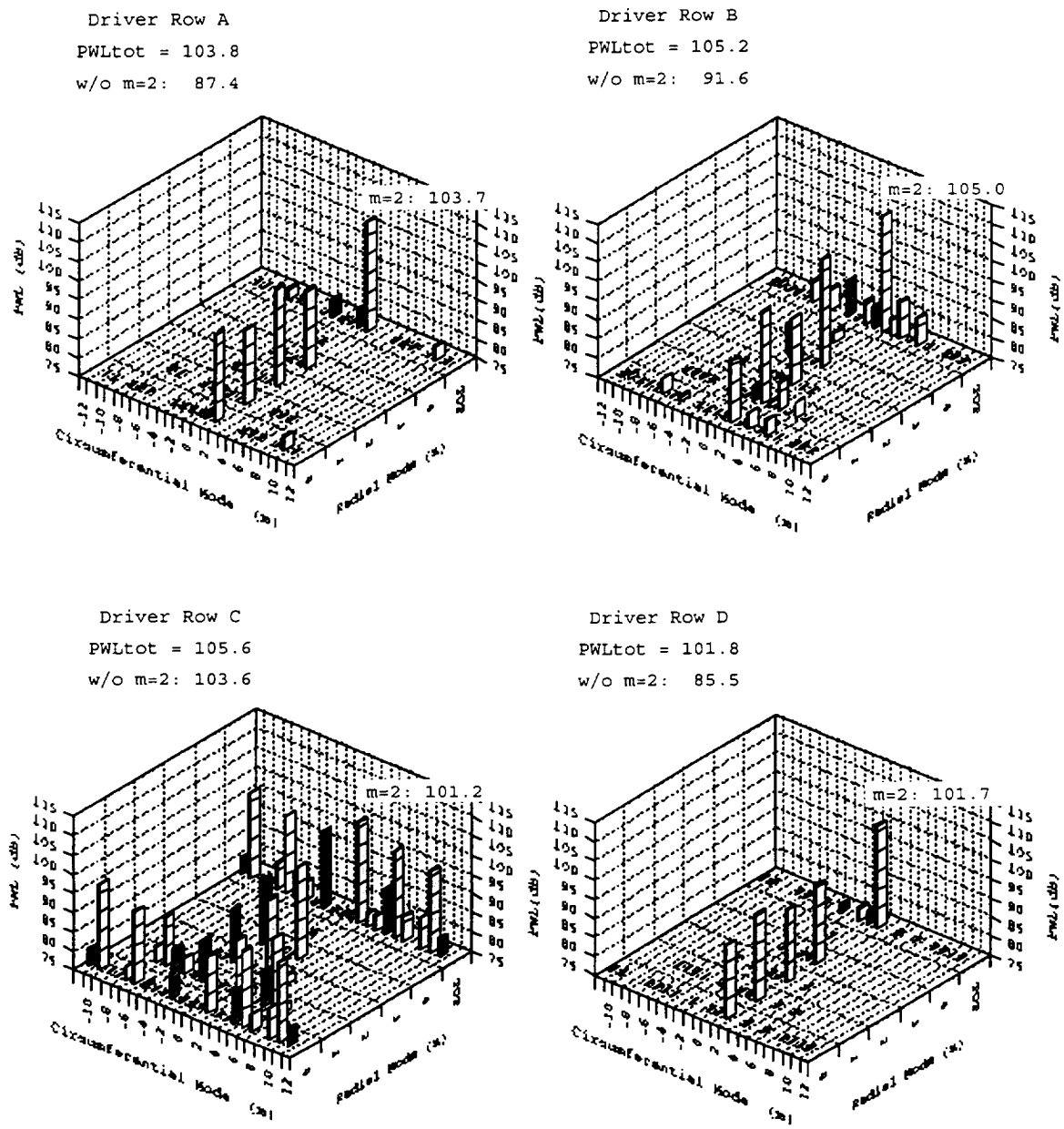

Figure 62. MMNA controller modal purity in inlet. Fan is at idle. Ω_{eq} = 2300 RPM

The modal purity of the MMNA controller coupled to the exhaust hardware is shown of Figure 63. The upstream and downstream inner driver rows have a modal signal-to-noise ratio of 11.6 and 10.5 dB, respectively, which is adequate. The modal distortions of the outer driver rows are excessive, with signal-to-noise ratios of -0.6 dB and 5.3 dB. This low signal-to-noise will still allow control and analysis of the m=2 mode, but will prevent significant noticeable reduction in tone PWL.

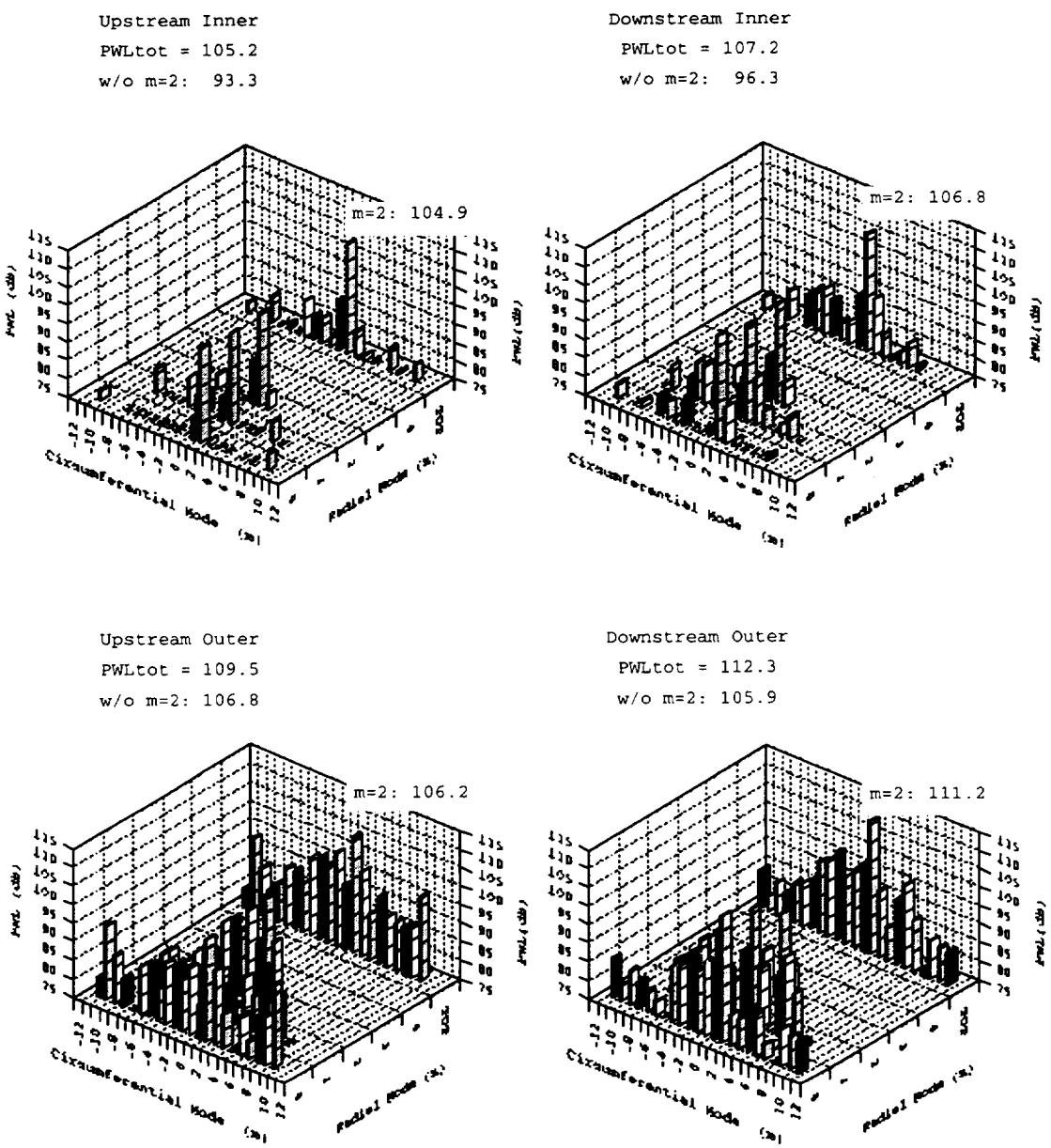

Figure 63. MMNA controller modal purity in exhaust. Fan is at idle. Ω_{eq} = 2300 RPM

The AQ controller modal purity using the inlet hardware is shown in Figure 64. The modal signal to-noise ratio is 17.0 to 19.6 dB. The AQ controller output is single independent output per row, which is split to the 16 actuator signals through the use of a Hilbert Transform (analog phase shift network). The single output may be more robust resulting in a higher signal-to-noise.

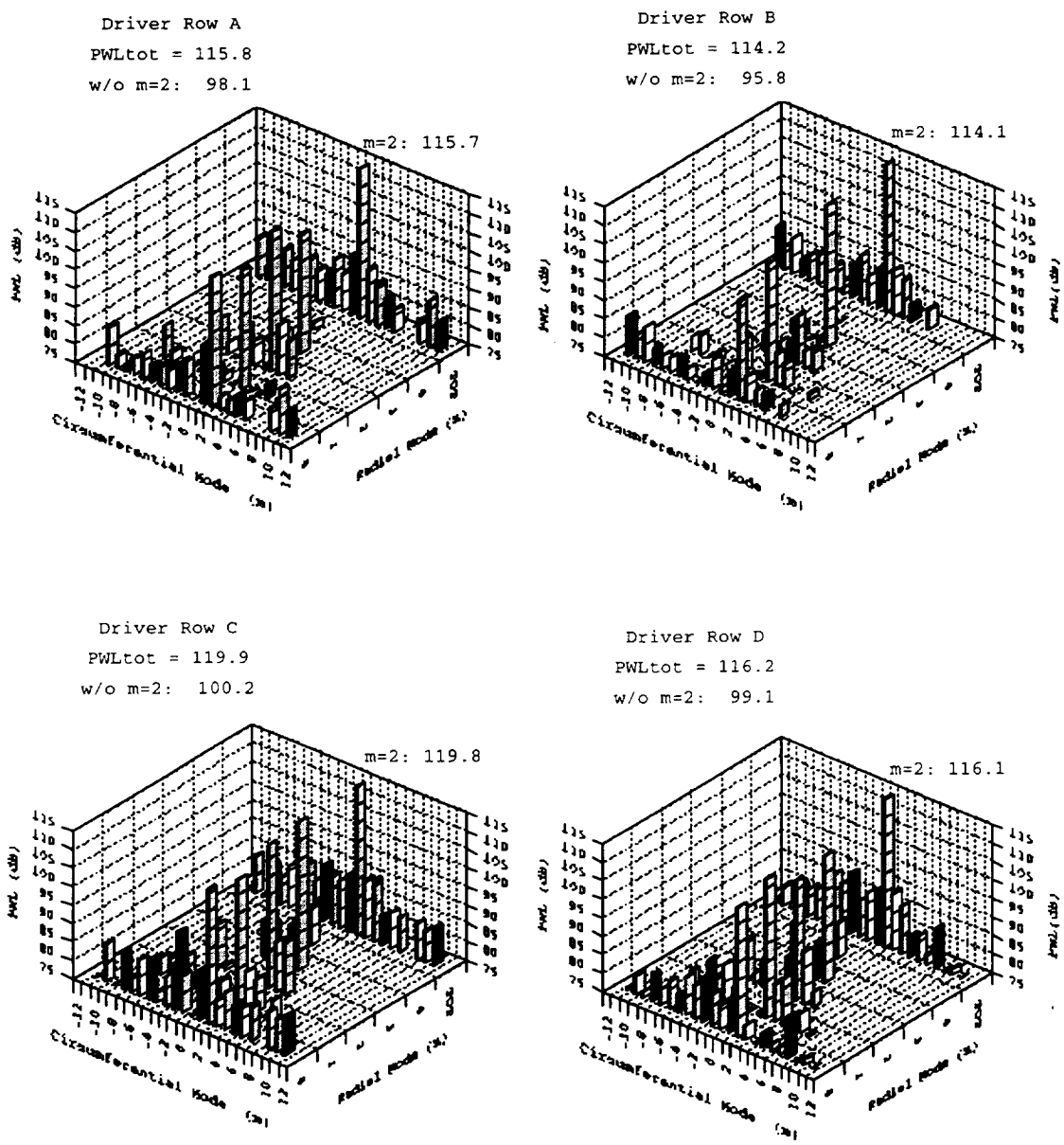

Figure 64 . AQ controller modal purity in inlet. Fan is at idle. Ω_{eq} = 2300 RPM

Figure 65 shows the modal characteristics generated by the AQ controller connected to the exhaust hardware. The extraneous modes of the upstream inner driver row are about 15-20 dB below m=2, resulting in a signal-to-noise of an acceptable 10.4 dB. The signal-to-noise of the other rows range from -1.8 to 2.8 dB.

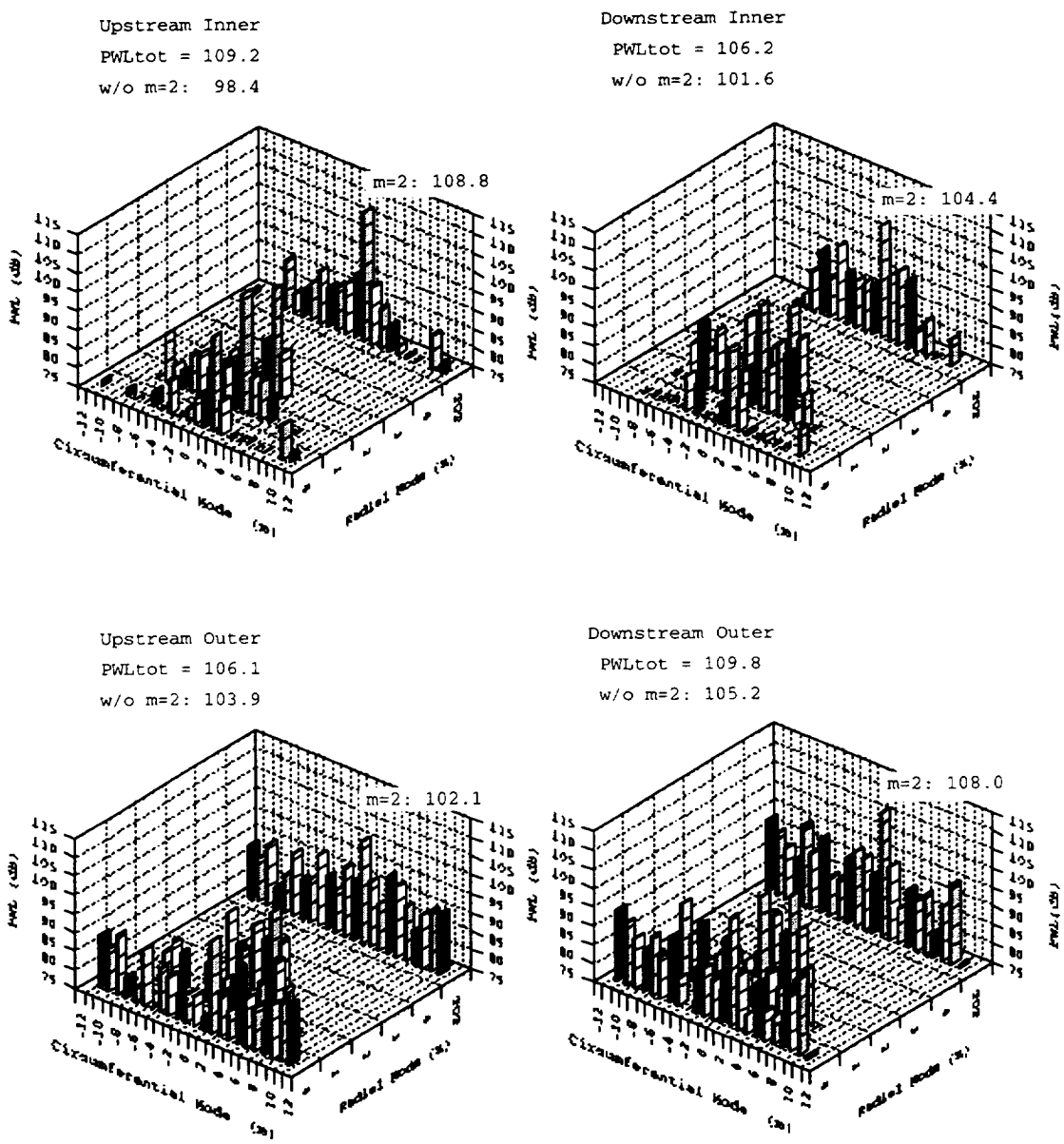

Figure 65. AQ controller modal purity in exhaust. Fan is at idle. Ω_{eq} = 2300 RPM

The modal purity of the two controllers was comparable. The larger effects were due to the type of drivers. The electromagnetic speakers in the inlet hardware system had significantly lower modal distortion than those of the piezoelectric actuators installed in the exhaust. This is partially due to the exhaust piezoelectric drivers being matched for operation below resonance, while the frequency range of this test extended though their resonance range. It is possible that some actuators were inadvertently mis-wired for this test. Follow up testing under a separate NASA program is recommended to investigate this. The electromagnetic speakers have a flatter response.

8.3.2 Mode Reduction Performance

The effectiveness in reducing the m=2 mode of the with MMNA control system/inlet hardware is shown on Figure 66 as a function of RPM. The number of control channels (input x output) varied as the number of radials increased with increasing RPM. The 2x2 control was very effective in reducing m=2 when 2 radials were present at the lower radials. About 15-25 dB reduction was achieved, nearly to the measurement floor. The effectiveness of the 2x2 control degrades at 1550 RPM and at 1600 an increase is noted. This indicates that the influence of the 3rd radial, though not cut-on, is degrading the performance. From 1800 to 2350 RPM 5x4 control was used. Moderate reduction occurred at 1800 RPM where with 3 radials the system was over specified. Throughout the range the (2,0) mode was greatly reduced. The higher radials were not as effectively controlled.

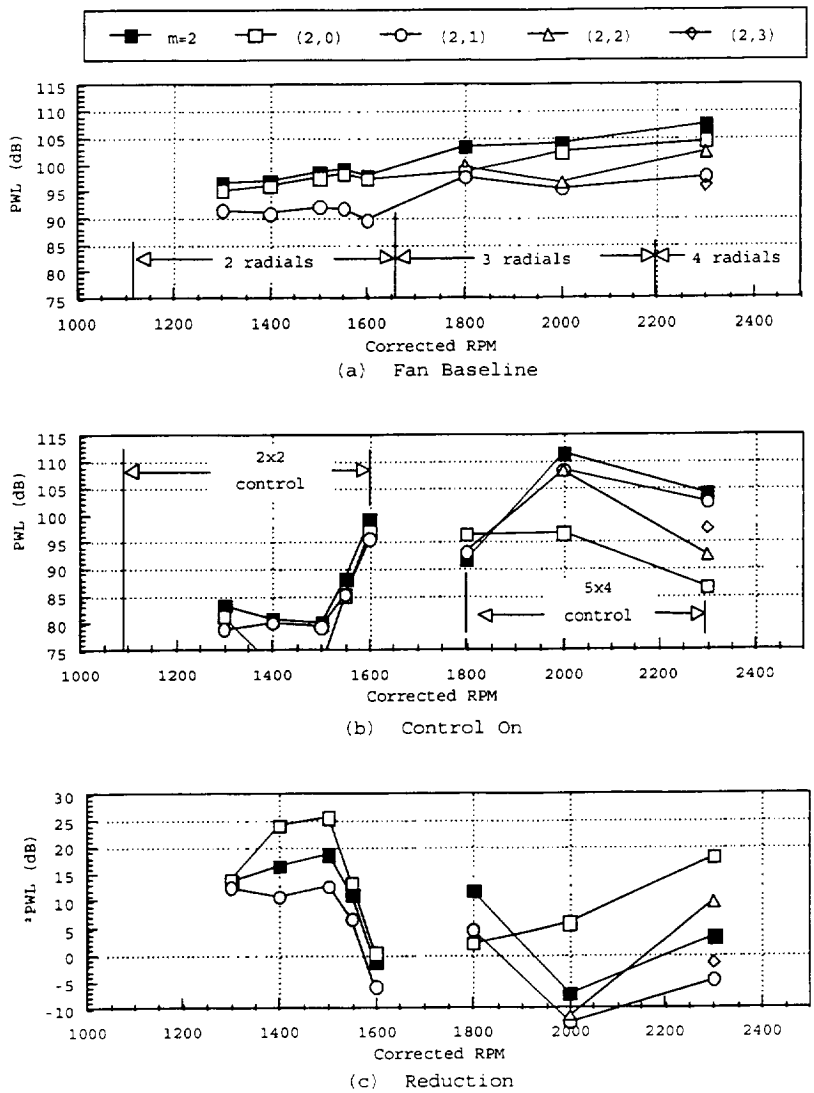

Figure 66. MMNA controller performance in inlet.

Figure 67 shows the modal performance of the MMNA control system/exhaust hardware. Three radials were controlled using 4x4 control. The m=2 mode was reduced 8 to 12 dB. All radials showed reduction.

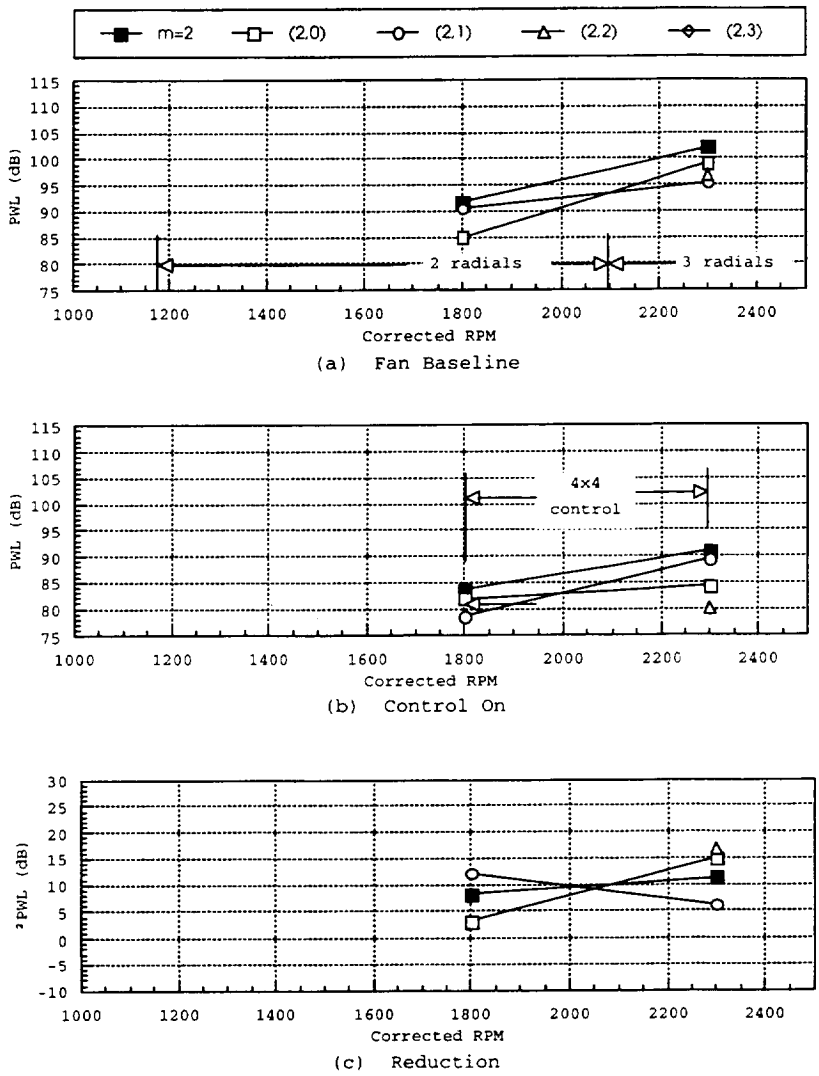

Figure 67. MMNA controller performance in exhaust.

The performance of the AQ controller coupled to the inlet hardware is shown on Figure 68. This system eliminates the 2 radials present at the lower RPM using 2x2 control. The performance tends to degrade as the cut-on RPM of the 3rd radial is approached (Ω=1662). At 1600 RPM there is essentially no reduction achieved using 2x2 control. Using 3x3 control again reduces the modes to nearly the measurement floor. This is evidence that the 3rd radial, while still cut-off is effecting the performance and indicates that control channel specification may not be limited to only the number of mathematically cut-on modes. At Ω=1800 and above 5x4

control was used. This resulted in m=2 reductions limited by the (2,1) radial. The other radials were reduced substantially, 5 to 20 dB.

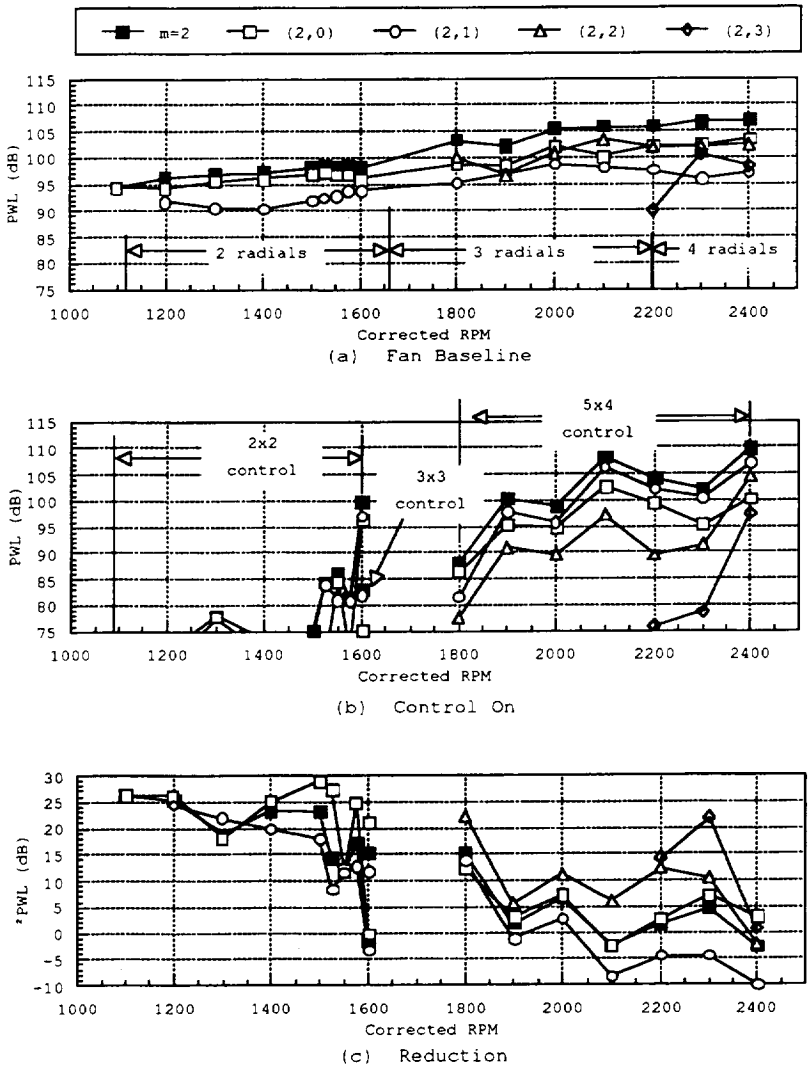

Figure 68. AQ controller performance in inlet.

Two factors may account for the lack of effectiveness in reducing the (2,1) radial. First, the n=1 is the lowest level radial of the baseline (control off). The nature of the control algorithms tends to reduce all microphone levels in a RMS sense. This may result in modes that are low in the baseline to be raised while other modes whose baseline levels are high are reduced. Second, analytical studies indicate substantial reduction in the pressure occurs at the outer duct wall where the control microphones are located. However, closer to the duct centerline the pressure increases, which couples to the (2,1). The studies indicate the first error microphone row was too close the actuators and in there field of decaying (2,4) radial mode.

Figure 69 shows the performance of the AQ controller using the exhaust hardware. The 4x4 control reduced the 3 radials 10-20 dB over the range of 1800 to 2450 RPM. The total m=2 PWL reduction was about 15 dB.

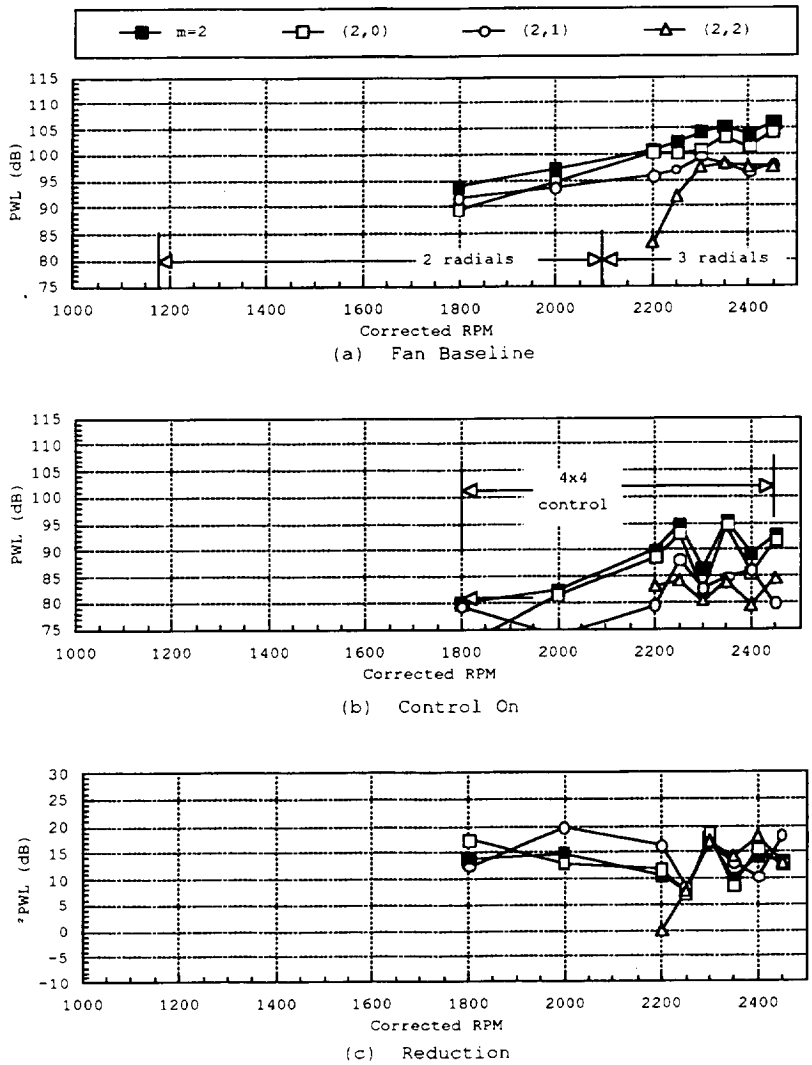

Figure 69. AQ controller performance in exhaust.

The total tone PWL reduction was limited in the inlet by the n=1 radial. In the exhaust limited in the exhaust by lower fan noise signal, and the higher actuator spillover generated by the piezoelectric drivers.

The performance, in terms of modal reduction, of the AQ controller was a few dB better than that of the MMNA controller. One possibility is for this the output amplitude of the MMNA controller was not sufficiently scaled for optimum resolution. Another possibility is the differences in the convergence method of the two controllers, discussed in Sections 2.3.4 (AQ)

and 7.1.1 (MMNA). It may be that a calculation of the inverse transfer function to determine each convergence update, as implemented by the MMNA controller, is subject to inaccuracies that limit the performance. A third possibility is the AQ controller used a 16-bit A/D converter for the error microphone input; the MMNA controller used a 12-bit A/D. Sections 3.5.2 (AQ) and 7.3 (MMNA) indicate that the error signals were driven close to the numerical floor for both systems. This may be the most likely explanation. Further investigation is needed to clarify this.

The AQ controller coupled to the exhaust hardware was used to investigate the effect of different driver/microphone row combinations. These combinations were tested at 2300 RPM, so three radials were cut-on. Figure 70 compares the reduction achieved with only 2 rows of drivers. The most effective under-specified condition was using only the inner driver rows, achieving 6.9 dB of reduction compared to the 12.4 dB achieved using all 4 actuator rows. The inner wall drivers couple efficiently to the higher order radials whose profiles peak on the inner wall.

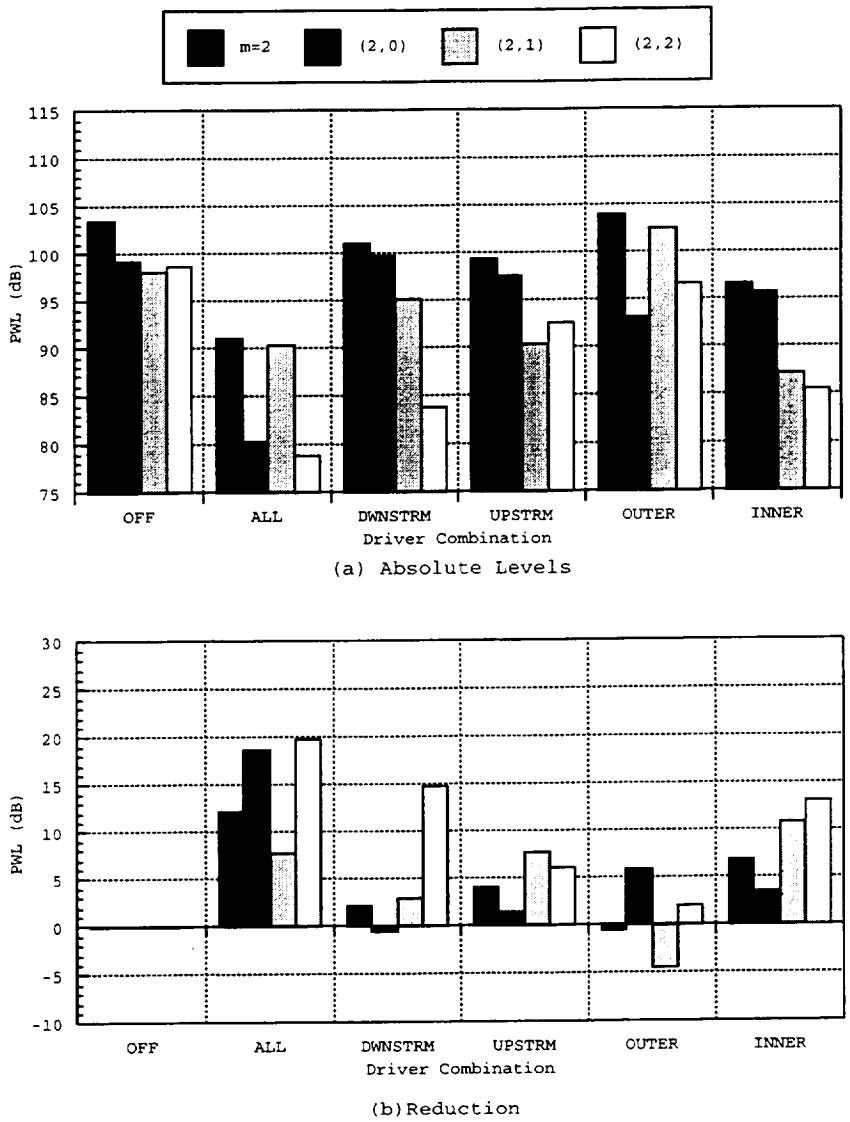

Figure 70. Effect of driver combinations/under-specification. AQ Controller Exhaust Hardware $\Omega = 2300$ RPM

Figure 71 compares the reduction achieved using various combinations of the 6 microphone rows. The most effective was using the rows: D inner, D outer, E inner, E outer; with the remaining rows electrically shorted to prevent electronic noise being read by the controller (Di, Do, Ei, Eo, Fs). Reduction was achieved for all combinations including an under-specified (2 channel) case. This may indicate that with proper analysis an under-specified system could be used to cancel high numbers of radials.

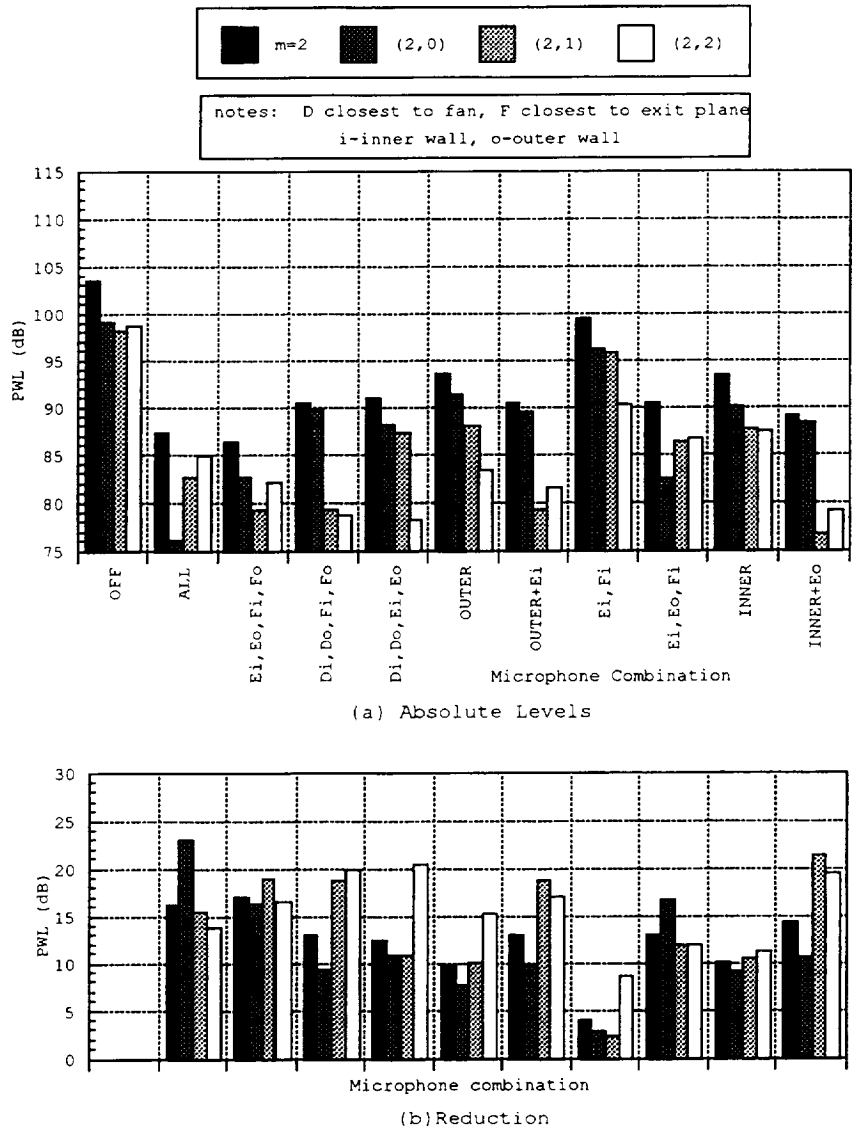

Figure 71. Effect of microphone combinations/under-specification. AQ Controller Exhaust Hardware $\Omega = 2300$ RPM

9 Evaluation of Feasibility of Application of ANC to Current Turbofan Engines

9.1 Objectives

The objective of this study was to estimate the system noise reduction potential of active noise control for application to an inlet and exhaust duct of a high bypass ratio (HBR) turbofan engine of current design. The ANC system would be designed to reduce only the blade-passing-frequency (BPF) tones and higher harmonics. The effectiveness of the ANC system will be evaluated in terms of ΔEPNdB suppression as applied to a particular aircraft at certification flight conditions.

Additional objectives were to identify the practical issues that may lead to design, implementation, or acceptance problems for ANC systems on aircraft engines. The state of readiness for a full scale engine demonstration of an ANC system is addressed, along with recommendations for potential approaches for overcoming anticipated problems.

9.2 Summary of Results

The predicted flyover noise benefits of an ANC engine applied to an aircraft such as a 767 using twin CF6 engines have been found to be minimal. The key problem is not that an ANC system would be predicted to not work as designed, but that the benefits gained from reductions of the tones from typical aircraft flyover spectra are small. When assumed installation penalties are extracted from the ANC system installation for loss of passive acoustic treatment area, the overall benefit may be negative in some cases, due to the increase in fan broadband noise. If the ANC actuators and sensors could be installed with minimal treatment loss, the installation penalties could be minimized.

A major, but not exhaustive, list of practical design issues have been identified. The installation issues in themselves may serve to render an aircraft application of ANC impractical. Extreme design ingenuity would be required to overcome the potential installation, operation, safety, and cost problems that are anticipated. A multi-disciplinary, system approach to the design will be required.

9.3 Approach

This study builds upon results that have been documented and presented previously[10,11]. The engine upon which these and the current studies are based is the GEAE CF6-80C2 HBR turbofan engine, a successful modern design high bypass ratio engine that is used currently in aircraft such as the Boeing 747, 767, MD-11, and the Airbus A300, A310, and A330. Extensive

---

[10] Kraft, R. E., Janardan, B. A., Gliebe, P. R., and Kontos, G. C., "Active Control of Fan Noise: Feasibility Study. Volume 4: Flyover System Noise Studies, Part 2", NASA Contractor Report (in review), Jul. 1996.

[11] Kraft, R. E., Janardan, B. A., Gliebe, P. R., "Estimate of Aircraft Flyover Noise Reduction by Application of Active Noise Control to Engine Fan Tones", AIAA 97-0489, Jan. 1997.

test data exists at GEAE for this engine for fully-treated configurations tested on a static engine test stand, and for data reduction both in third octave and narrowband format.

The first step is to use measured narrowband farfield data to separate the contributions of the BPF tone and its harmonics from the surrounding broadband noise spectrum. It is assumed that the effect of the ANC suppression system will be to suppress the tone content but have no effect on broadband levels. Once separated, the tonal and broadband contributions can be adjusted as desired before re-synthesizing the spectra into predicted flyover noise levels.

The analytical ANC inlet and exhaust duct simulation programs CANCSIM and AANCSIM, were used to predict the suppression of the fan tone noise for different ANC system designs. In order to apply the ANC simulation, the source radial mode content at BPF and at least the second harmonic must be given for input to the analysis. Although the number of cut-on (propagating) radial modes can be calculated, the relative (complex) modal coefficients of the modes has never been measured on the CF6-80C2, and therefore must be obtained by assumption or a separate source mode content analysis.

Rather than use an unverified assumption such equal energy per mode (which still would not provide relative phasing), it was decided to apply the NASA-developed source mode prediction program V072 to obtain modal coefficients. Even of the prediction were not accurate, the results should at least be representative. The V072 program generated forward- and backward-radiated mode content in an annular section of duct with a radius ratio given by the hub to tip ratio of the outlet guide vanes, which is where the sound is assumed to be generated. For the inlet, the forward-radiated modes in the annular section are re-expanded at the end of a short, flat bullet-nose to provide the coupling to the cylindrical inlet duct.

The CF6-80C engine has a 93 inch diameter fan with 38 rotor blades and 80 outlet guide vanes (OGV's). A cross-section of the engine is shown in Figure 72. Figure 73 shows the number of cut-on radial modes in the inlet duct for the two lowest spinning mode orders predicted by rotor alone and rotor/stator interaction over a frequency range generated in the BPF, second harmonic, and third harmonic tones over a range of operating rpm's from approach to takeoff speed.

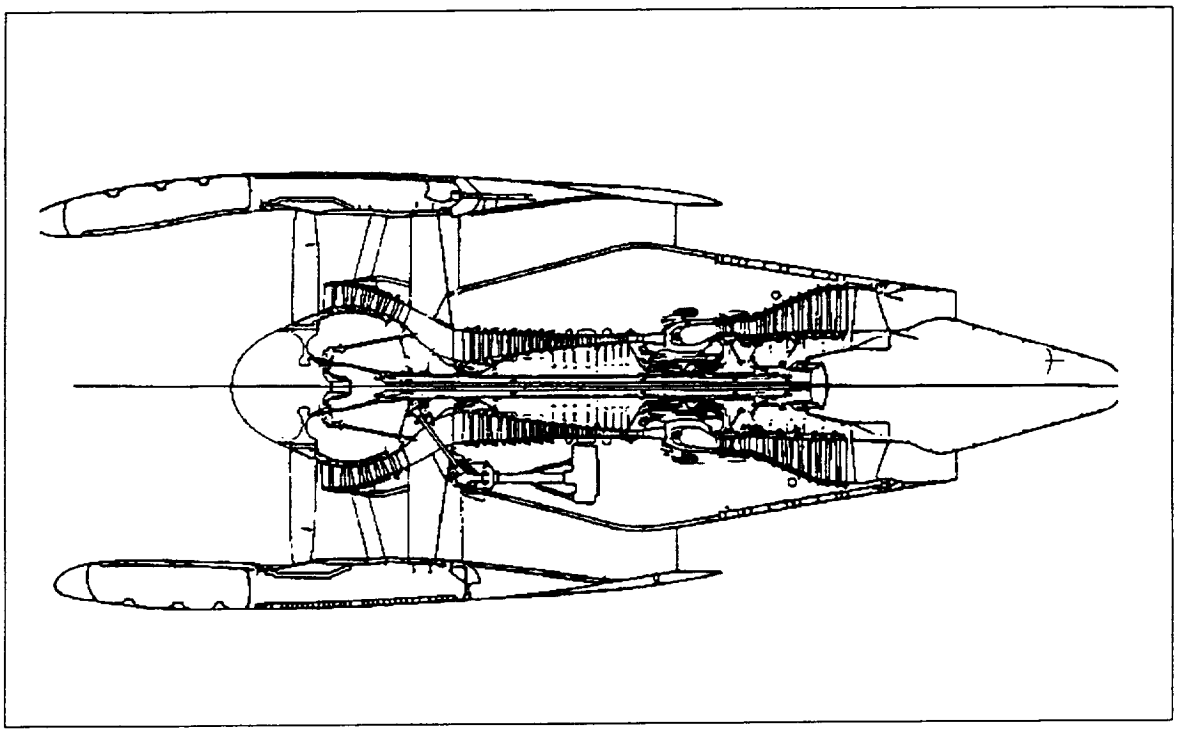

Figure 72. Cross-section of GEAE CF6-80C2 engine.

For a given spinning mode order and tone, the bottom of the heavy vertical line gives the frequency generated at approach, and the top of the heavy line gives the frequency at takeoff. The sloping lines give the cut-on points of radial modes as a function of spinning mode order for a duct Mach number of 0.4. A given radial mode is cut-on above the line. For instance, for the m = 4 spinning mode of the 2BPF tone, there are 20 radial modes cut-on at approach, and about 31 or 32 radial modes cut on at takeoff. Similarly, Figure 74 gives the number of cut-on radial modes for the BPF, 2BPF, and 3BPF tones in the exhaust duct of the CF6-80C2.

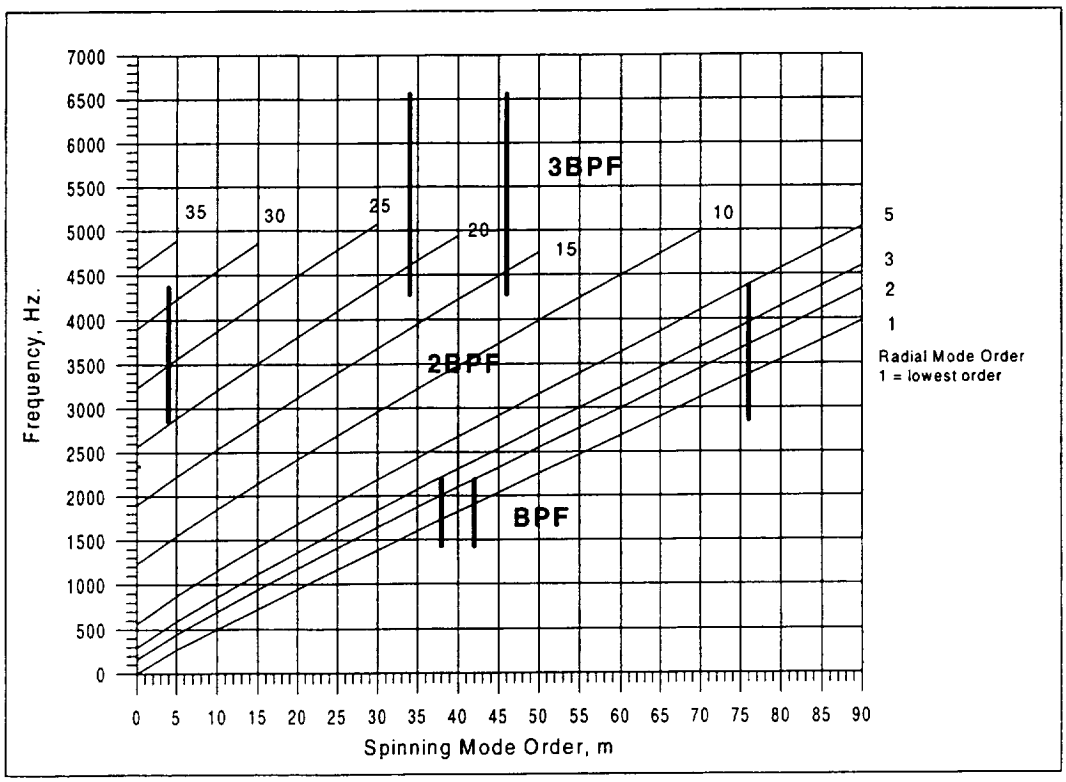

Figure 73. Cut-on frequencies for modes in the CF6-80 inlet duct. Vertical bars indicate range from approach to takeoff rpm's. Temperature = 70 degF, Mach 0.4.

From Figures 73 and 74, it is obvious that there are many more cut-on radial modes in the inlet than in the exhaust duct at other than BPF frequencies. The engine was designed such that the BPF modes are cut-off at approach speeds, but the result is a very low order spinning mode at 2BPF, and very high radial mode orders at 3BPF, even though the spinning mode order are high. The situation in the exhaust duct is slightly more hopeful than the inlet duct, since the m = 4 spinning mode at 2BPF has between about 8 and 12 radial modes cut on in the annulus.

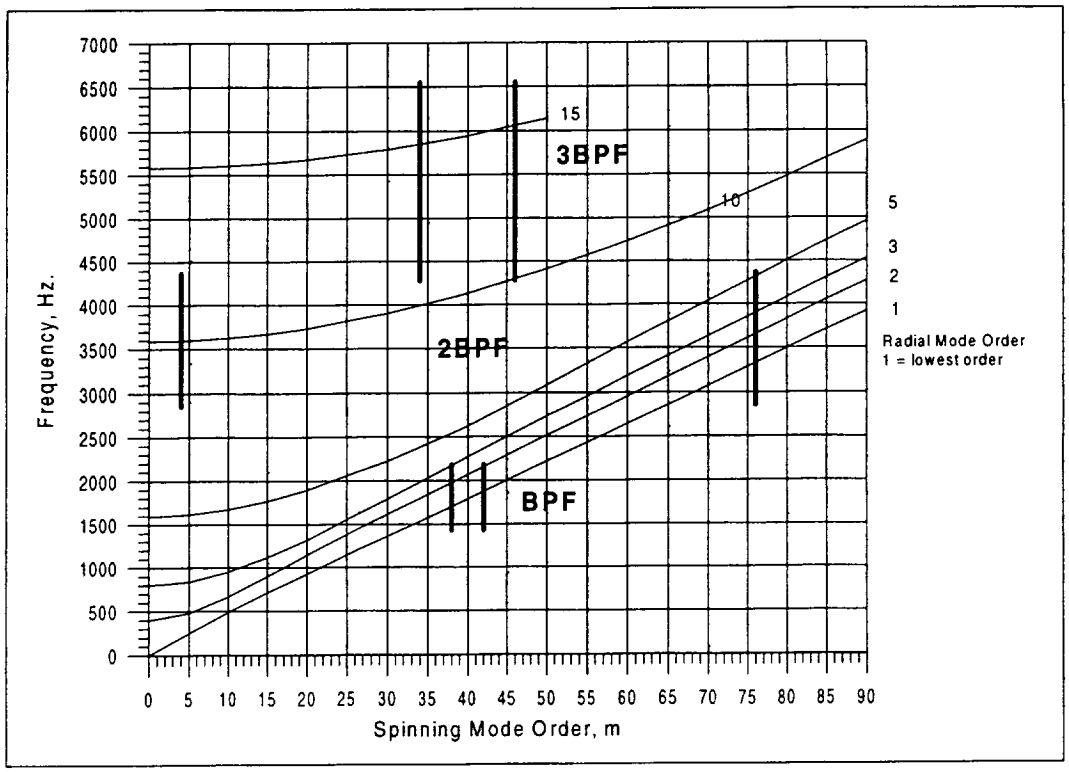

Figure 74. Cut-on frequencies for modes in the CF6-80 exhaust duct. Vertical bars indicate range from approach to takeoff rpm's. Temperature = 70 degF, Mach 0.4.

The ANC system design problem is that there must be a number of ANC system actuator rings in the inlet or exhaust duct that is equal to the number of radial modes that are desired to be suppressed. The number of actuator elements in each ring must be sufficient to generate an ANC signal that matches the target spinning mode order being suppressed. The axial spacing of the actuator rings must be sufficient to couple adequately to the axial wavelengths of the target radial modes at that spinning mode order. Thus, a substantial amount of duct wall area and duct length may have to be devoted to the ANC actuator assembly. This would imply a commensurate loss of treatment area.

We will assume a design constraint of a maximum of four actuator rings in the inlet duct, and a maximum of four pairs of outer and inner actuator rings (8 total rings) in the exhaust duct. The loss of wall treatment area due to the installation of these rings will be estimated. We will assume no penalty will be extracted for the error sensor placement upstream (inlet) or downstream(exhaust) of the actuator rings. This will be assumed even though the error sensors will be located in a hardwall segment of duct.

Figure 75 shows a conceptual drawing of where the actuator rings and sensors might be located in the nacelle of a CF6-80C2. The actuator rings shown on the outer wall of the exhaust duct, if mounted in the location shown, would have to be on the moving blocker doors of the thrust reverser, which probably would not be practical or allowed. Thus, it is assumed for the analytical studies that the exhaust duct ANC system consists of four actuator rings mounted on

the inner cowling of the duct. Actuator rings are not shown mounted in the fan case between the rotor and the OGV's, because it is unlikely that it will be possible to mount actuator hardware on the fan case in this region.

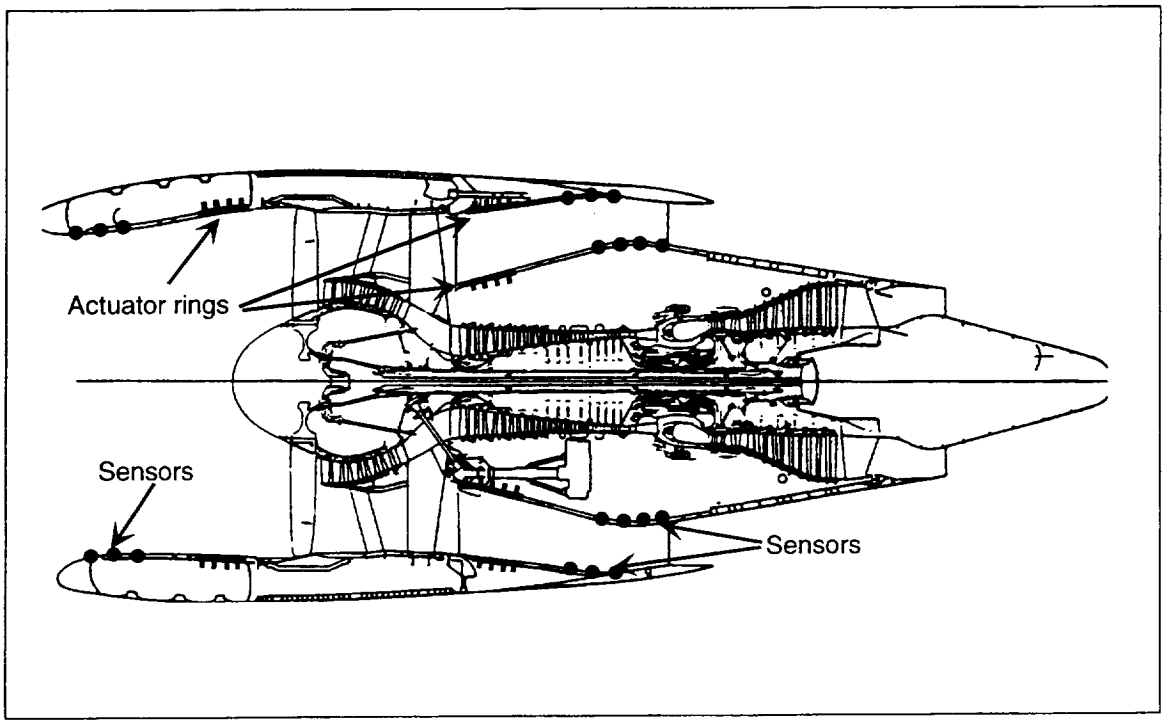

Figure 75. Conceptual view of installation of ANC actuator rings and error sensors in nacelle of CF6-80C.

The location of the error sensors in a hardwall duct segment facilitates the expansion of duct modes for the simulation of the control system operation. The error sensors could conceivably be located in a treated duct section, but this would require the additional complexity of expanding in the duct modes obtained from the finite impedance boundary condition. This could be accomplished theoretically, and is within the capability of the analytical model, but introduces enough uncertainty and complexity that it was avoided for this investigation. The effects of treated sections of duct between the actuator segments and the hardwall error sensor segment are included, as it is assumed that the ANC system would normally be used in conjunction with acoustic treatment.

The ANC effectiveness will be evaluated several ways, always comparing to the suppression obtained for the fully-treated passive treatment case:

1. An ideal CF6-80C2 case for which the tones are completely removed (to surrounding broadband noise level) in various combinations with no loss of treatment area. This will provide an upper limit to the suppression performance of any ANC system.
2. Analytical predictions of effects of tonal ANC suppression for two or four actuator rings in the CF6-80C2 inlet or pairs of rings in the exhaust, with an estimated loss of broadband

suppression due to treatment area loss. The ANC system control system design would be aimed at the two or four lowest order radial modes.

3. A hypothesized modification to the CF6-80C2 fan with reduced vane count, which would reduce the number of cut-on radial modes and, it is assumed, give a slight benefit in lowering broadband noise levels.

In all ANC system analytical cases, the V072 program was used to predict radial mode content. The system performance comparisons are made in terms of flyover noise ΔEPNL, comparing the fully-treated passive levels to the ANC system configuration levels.

9.4 Feasibility Assessments

9.4.1 Ideal Case

In order to determine what the maximum potential noise suppression of ANC applied to the CF6-80C2 mounted on a twin-engine passenger aircraft would be, an ideal calculation that completely and arbitrarily removed the full BPF and 2BPF tones was run. It was assumed that there would be no loss in passive treatment suppression. The removal of the protruding tone down to the broadband level is the best performance that could be expected from the ANC system. Further tone reduction would be over-design of the system.

The difficulty, of course, is that the tone energy is distributed among a large number of propagating modes, particularly for the 2BPF tone. The ANC system must detect and suppress a sufficient number of radial modes to affect a large proportion of the propagating energy.

The tones were removed by examining farfield narrowband data as measured on a static test stand and manually modifying the narrowband spectra at each radiation angle by lowering the tone levels until they equaled the surrounding broadband levels. The calculations were made for a fully-treated configuration of the CF6-80C2, for which test data were available. The narrowband data were then reconstituted into one-third octave bands for calculation of ΔEPNdB.

Table 11. lists the suppressions obtained under various sets of assumptions for this idealized case. Note that a negative number implies suppression, a positive number implies a noise increase. For all cases, the design number of 80 vanes was used. Both the BPF and the 2BPF tones were removed, assuming the ANC system could operate on both tones simultaneously. At approach speed, the computation was made both with and without the presence of airframe noise. No airframe noise was included in the computations at cutback and takeoff, but an arbitrary 3 dB reduction in jet noise (that is, a 3 dB decrease in level at all frequencies and angles) was included as an option, to see if the ANC performance improved if jet noise were arbitrarily lowered.

Table 11. Calculated ANC system suppression for 80-vane CF6-80C engine on twin-engine aircraft for ideal case of total BPF and 2BPF tone contribution removal, both inlet and exhaust. Negative ΔEPNdB implies suppression.

Aircraft Operating Condition	ANC Noise Reduction, ΔEPNdB
Approach, with airframe noise	-0.08
Approach, no airframe noise	-0.35
Cutback, no airframe noise	-0.70
Cutback, -3 dB jet noise	-1.00
Takeoff, no airframe noise	-0.27
Takeoff, -3 dB jet noise	-0.52

The results indicate disappointingly low potentials for ANC suppression, even for this idealized case. Apparently, the tones contribute little to the overall noise levels. A maximum suppression of 1.0 EPNdB, which would also require a 3 dB suppression in jet noise, is probably not worth the added expense and complexity of installing the ANC system. When loss of passive treatment effectiveness and the fact that the ANC system will probably not reduce the tone 100% of the way to the broadband background level are taken into account, as will be seen next, the prognosis becomes even worse.

The effects of applying ideal ANC tone suppression separately to the inlet and exhaust noise components was also considered for the 80-vane design. For the inlet case, the exhaust noise is totally neglected (assumed to be zero) and vice-versa. The ideal cases for the inlet and exhaust ducts are presented in Table 12. Again, a negative number implies suppression, a positive number implies a noise increase.

Table 12. Calculated ANC system suppression for 80-vane CF6-80C engine on twin-engine aircraft for ideal case of total BPF and 2BPF tone contribution removal, inlet and exhaust separately. Negative ΔEPNdB implies suppression.

Noise Source	Aircraft Operating Condition	ANC Noise Reduction, ΔEPNdB
Inlet	Approach, with airframe noise	-0.86
Inlet	Cutback, with airframe noise	-2.20
Inlet	Takeoff, no airframe noise	-0.28
Exhaust	Approach, with airframe noise	+0.16
Exhaust	Cutback, with airframe noise	-0.87
Exhaust	Takeoff, no airframe noise	-0.95

Note a fair reduction in inlet-radiated noise at cutback condition. This indicates a strong contribution from the inlet-radiated 2BPF tone at this condition. Note, however, that the EPNL actually increases for the exhaust-radiated noise at approach. This is an indication of the vagaries of the EPNL calculation, where a tone correction at a different frequency is contributing more when the 2BPF is removed. This is why EPNL flyover noise must be considered in the final evaluation rather than simply PWL or tone SPL reduction.

The ideal tone-removal ANC suppression cases were also considered for the hypothesized 52 vane configuration of the engine. The main difference in the reduced vane count case is that there is an assumed reduction in fan-generated broadband noise levels. As a crude approximation, the broadband noise reduction due to reduced vane count change from Vane Count #1 to Vane Count #2 is assumed to be given by

$$\Delta BB = 10\log\left[\frac{\text{Vane Count \#2}}{\text{Vane Count \#1}}\right] \quad \text{dB} \tag{8}$$

The broadband noise reduction is arbitrarily set to zero for the 1/3 octave band containing the BPF and below, is then ramped up linearly to its maximum value at the 1/3 octave band containing the 3BPF, then held constant at higher frequencies.

Calculations similar to the 80-vane ideal case were made for the 52-vane (reduced jet noise) cases. In these cases it is assumed that the BPF tone is cut-on, so that both the BPF and the 2BPF tones were removed from the spectra. The results for the combined inlet/exhaust and separate inlet and exhaust cases are shown in Table 13. One can see moderate suppression potential for the separate inlet and exhaust noise, but the overall engine noise still shows reductions of 1 dB or less. This indicates higher levels of broadband noise suppression (fan noise and jet noise) must be obtained for this engine before ANC tone reductions will become effective. The same conclusion is likely to be applicable to any current modern high bypass ratio turbofan engine.

Table 13. Calculated ANC system suppression for 52-vane CF6-80C engine on twin-engine aircraft for ideal case of total BPF and 2BPF tone contribution removal, all inlet and exhaust combinations. Negative ΔEPNdB implies suppression.

Noise Source	Aircraft Operating Condition	ANC Noise Reduction, ΔEPNdB
Inlet and Exhaust	Approach, with airframe noise	-0.44
Inlet and Exhaust	Approach, no airframe noise	-0.86
Inlet and Exhaust	Cutback, no airframe noise	-0.70
Inlet and Exhaust	Cutback, extra -3 dB jet noise	-1.09
Inlet Only	Approach, with airframe noise	-1.47
Inlet Only	Cutback, with airframe noise	-2.21
Exhaust Only	Approach, with airframe noise	-0.76
Exhaust Only	Cutback, with airframe noise	-1.11

9.4.2 Results from ANC System Simulations

The above cases made no use of the ANC analytical simulation program, but simply assumed that the rotor-generated tones could (somehow) be completely removed from the spectra. For the remaining cases, ANC suppression is calculated using the analytical simulation programs CANCSIM and AANCSIM. The analytical models include the effects of passive treatment suppression. The impedance of the acoustic treatment at the tone frequencies was determined using standard impedance models. Cases were run for the baseline CF6-80C2 engine with 34 blades and 80 vanes and for an assumed modification of the fan for which the vane number was reduced to 52.

Since the BPF tone for the baseline CF6-80C2 is near to cutoff and assumed to be highly suppressed even at high fan speeds, the ANC suppression was applied to 2BPF only. The two lowest spinning modes generated at BPF are the m = 38 (rotor alone) and m = -42 (rotor/stator). At 2BPF, the lowest spinning mode is an m = -4, with 17 cut-on radial modes.

For the baseline cases, the ANC system design for the inlet used four actuator rings mounted on the outer duct wall. In the exhaust duct, two configurations were used, one with four rings in the exhaust mounted on the inner wall only, and a second where four rings were added to the outer wall, giving a total of eight rings. The source mode content was obtained from the V072 program. In the inlet duct each ring had 25 equally-spaced actuator elements. In the exhaust duct, 24 equally-spaced actuator elements were used.

It was assumed that each actuator ring has an axial length of 1.8 inches, and that the actuator rings are separated by a 3.6 inch hardwall segment. The length of duct required for four actuator rings is thus 21.6 inches, and the length for 2 rings is 10.8 inches. These are the lengths that are assumed to be lost to acoustic treatment in the inlet and exhaust ducts for each set of actuator rings. No treatment penalty is taken for the error sensor arrays.

The cases where the rotor blade count is reduced to 34 and the vane count is reduced to 52 have the effect of cutting on the blade passing tone but greatly reducing the number of cut-on modes at the second harmonic. The vane count of 52 is considered to be a practical minimum number of vanes without extensive structural modifications to the engine. The m = -18 spinning mode generated at BPF has two cut-on modes in the inlet and three in the exhaust. At 2BPF, for m = 16, there are 11 modes cut-on in the inlet and 10 in the exhaust. Again, a loss of treatment length of 21.6 inches in each of the inlet and exhaust ducts is assumed.

Advantages given to the ANC system were:

- Random errors in actuators and sensors is ignored, set low background noise (perfect actuators and sensors).
- Assumed a pure rotor/stator interaction spinning mode, ideal modal computation (no spurious modes).

- No limitations on error sensor hardwall segment length, number of sensor rings equal to number of cut-on radial modes, no limit on sensor number. No penalty for the extra hardwall duct length required to contain sensors.
- No restrictions on computation time.
- Assumed at most four axially-spaced actuator rings could be installed.
- No power limitations on actuator output, no efficiency concerns.

Disadvantages given to the ANC system were:

- The four actuator ring system was aimed at four lowest radial modes. Higher modes were discriminated but not suppressed.
- Actuator and sensor rings were closely-spaced relative to modal axial wavelengths, leading to possible problems with mode generation, discrimination.
- Actuator area replaces treatment area. Reduces treatment suppression linearly with treatment length at all frequencies.

The error sensors could have been located in a treated segment of duct, but this would have required an ANC system modal expansion in modes of the treated duct section for ANC algorithms that are based on modal discrimination. Although the eigenvalues for the treatment impedance boundary conditions in the ideal simulation are known exactly, it is assumed that these values are not so easy to come by in the actual case, since the impedance itself may not be known very accurately.

The actuators could also have been located in treated sections, so that there would be treatment segments located circumferentially between actuators, leading to less treatment area loss. The practical objection to this is that this design will cause complications in the construction of treatment panels, which have structural weight and cost requirements. The analytical simulation is unable to handle other than a hardwall actuator ring, so this is the main reason for requiring this assumption.

The first cases considered were the baseline cases of 4 actuator rings in the inlet and 4 actuator rings in the exhaust, where the treatment lengths were reduced 21.6 inches in the inlet and 21.6 inches in the exhaust. The ANC system was designed to reduce the 2BPF tone. In these cases, with their high number of cut-on radial modes, the ANC system designs simply failed to work, that is, no 2BPF tone suppression could be obtained. This was the case for combined inlet/exhaust, inlet alone, and exhaust alone. Increasing the number of actuator rings from 4 to 8 (4 inner + 4 outer) in the exhaust was no help.

The conclusion is that an "add-on" ANC system is simply unable to cope with existing (unmodified) turbofan designs without extending the ANC system design (adding actuator rings) to far beyond the realm of practicality. If this is the case for an ideal analytical simulation of the ANC system, even more problems would be expected for an actual physical implementation on a real engine.

Predictions were made using the ANC simulations for the case where the vane count is reduced from 80 to 52 vanes, giving a reduction in fan-generated broadband noise as noted above. At approach condition, the ANC system was designed to operate on both BPF and 2BPF tones, but at cutback, only BPF was suppressed. Table 14 shows the results of these calculations, in terms of ΔEPNdB where the case with ANC suppression and reduced treatment is compared to the fully-treated passive case.

Table 14. ANC system suppression calculated using analytical simulation for 52-vane CF6-80C engine on twin-engine aircraft, all inlet and exhaust combinations. Negative ΔEPNdB implies suppression.

Noise Source	Aircraft Operating Condition	ANC Noise Reduction, ΔEPNdB
Inlet and Exhaust	Approach, with airframe noise	+1.27
Inlet and Exhaust	Approach, no airframe noise	+1.28
Inlet and Exhaust	Cutback, no airframe noise	+1.56
Inlet and Exhaust	Cutback, extra -3 dB jet noise	+1.73
Inlet Only	Approach, with airframe noise	+0.34
Inlet Only	Cutback, with airframe noise	+2.66
Exhaust Only	Approach, with airframe noise	+3.78
Exhaust Only	Cutback, with airframe noise	+2.56

It can be noted that the noise levels for the ANC configurations compared to the passive fully-treated configuration go up across the board. This is an indication that the effects of the loss in treatment are greater than the gains provided by the ANC tone reduction in all cases. The ANC system is working properly at approach speed in this case, giving close to 7 dB ΔPWL tone suppression in the inlet and about 5.5 dB ΔPWL tone suppression in the exhaust (with 2 and 3 cut-on radial modes, respectively). At 2BPF at approach, with 11 and 10 cut on modes in the inlet and exhaust, ANC system operational problems are again encountered in both the inlet and exhaust.

At cutback speed, there are 8 cut-on modes in the inlet and 9 in the exhaust. The 4 ring ANC systems in the inlet and exhaust are unable to achieve tone suppressions. A tone suppression can be achieved in the exhaust with the 4+4 ring system, but the overall effects on ΔEPNdB are still controlled by the loss in treatment.

In order to further investigate the trade-off between treatment length and ANC system effectiveness, a 2 actuator ring case (2 rings in both inlet and exhaust) for which the treatment loss was reduced to 10.8 inches was run. The two actuator rings provided 6.9 dB PWL tone suppression in the inlet and 6.2 dB PWL tone suppression in the exhaust, so that the ANC system is definitely working as it is supposed to. Table 15 shows the results for this case.

Table 15. ANC system suppression calculated using analytical simulation for 52-vane CF6-80C engine on twin-engine aircraft, all inlet and exhaust combinations, 2-ring actuator case. Negative ΔEPNdB implies suppression.

Noise Source	Aircraft Operating Condition	ANC Noise Reduction, ΔEPNdB
Inlet and Exhaust	Approach, with airframe noise	+0.15
Inlet and Exhaust	Approach, no airframe noise	+0.18
Inlet and Exhaust	Cutback, no airframe noise	+0.93
Inlet and Exhaust	Cutback, extra -3 dB jet noise	+0.95
Inlet Only	Approach, with airframe noise	-0.26
Inlet Only	Cutback, with airframe noise	+0.99
Exhaust Only	Approach, with airframe noise	+1.15
Exhaust Only	Cutback, with airframe noise	+1.49

Note that the noise levels still increase, with the exception of the inlet at approach, but that the increases are smaller (the ANC performance is better) than in the 4 actuator case. The gain in performance, however, can be attributed to the smaller loss in treatment area. The ANC tone reduction still makes a very small contribution to the total.

The results of the simulation study are commensurate with the ideal tone removal studies presented earlier. In effect, the gains from the ANC tone suppression cannot compensate for the losses in reduced treatment area, even with benefits in broadband noise reduction gained from fan stator count design changes.

This indicates that ANC will be useful only for engines that are specifically designed such that the EPNL for the passively treated engine is controlled by protruding tones. In addition, those tones must be composed of a limited higher order radial mode content that is susceptible to ANC suppression by a practical number of ANC actuator rings. This is pointing toward engines designed with high levels of cut-on BPF tones and lower levels of higher harmonics (possibly by reducing the spacing between rotor and stator). This is counter to the design philosophy that has led to the current generation of low noise turbofan engines.

Simultaneously, methods must be incorporated that lower the amount of broadband noise generated by the fan and the jet (possibly the core, as well) to allow the tones to control the EPNL. Thus, the ANC-treated engine must be designed from the preliminary design stage to be dependent on the ANC system as an integral part of the suppression package. Given the other problems to be encountered, as presented below, it becomes questionable whether such an approach will be safe, operationally efficient, practical, and cost-effective.

9.5 Other Practical Issues

Since the effectiveness evaluation of the ANC system performance for turbofan engines was so lacking in promise, only a very limited effort was made to identify potential design and installation problems that might be encountered in designing an ANC system that could practically be used on an engine to be mounted on an aircraft. Numerous potential problems were identified, however, any of which is likely to present significant design challenges to the implementation of a practical and acceptable ANC system.

A proposed list of issues that will have to be addressed in the design of a practical ANC system for installation on an aircraft engine is the following:

1. EPNL Payoff
2. Installation area and volume limitations
3. Cost
4. Engine design modification requirements
5. Weight
6. Safety
7. Operability/Reliability/Survivability
8. Noise Certification/Flight Departure
9. Power limitations - type and amount needed
10. Actuator technology
11. Control system technology
12. System design tools - accuracy and validity
13. Error sensor technology

This list is in a preliminary and arguable order of priority and is probably not comprehensive. Problems in each area will have to be overcome before an ANC system becomes operational.

Assuming an ANC system could be designed that would provide an acceptable EPNL payoff, the next issues are almost certain to be cost and weight. It is almost impossible to provide guidelines as to what would be an acceptable cost and weight penalty, as this will depend upon the magnitude of the noise problem that needs to be solved, and a comparison with alternative noise reduction solutions. The acceptable cost of an ANC system from the buyer viewpoint may be much less than that desirable for a profit-oriented ANC system vendor.

There must be sufficient area and volume available in the engine nacelle to accept the ANC system hardware. Examination of a typical installed engine casing indicates that much of the surface is covered with pipes, valves, mechanisms, etc., that would preclude the installation of an actuator of a few inches in dimension, much less an evenly-spaced circular array of actuators. There may be more room in the engine nacelle, but even here flanges and stiffeners

will make locating additional hardware difficult. The nacelle will have depth limitations. The outer wall of the exhaust duct is usually devoted to the thrust reverser mechanism, and it is difficult to get passive treatment in this region, much less ANC actuators.

Generally there are only small amounts of spare electrical power available on an aircraft. Even though the ANC system would be operating during a very limited time during takeoff and approach, there must be sufficient electrical power available for all requirements, thus, there may be additional cost associated with providing the power, if necessary. The efficiency of transforming electrical power into acoustic output will definitely be a design consideration for the actuator, along with its weight.

An effort will be required to determine how the ANC system integrates with the rest of the aircraft control system. Certain signals such as an engine 1/rev blip may be required by the ANC system for operation. The control that turns the ANC system on and off will have to be automated and integrated with other controls.

Another issue will arise if the ANC system is dispatch critical. If the system is not working, can the airplane take off? What will the effectiveness be if (or, more properly, when) certain sensors or actuators fail? What sort of cockpit display or warning is required? Is redundancy, which will add to weight and cost, necessary? Is an on-line diagnostic fault analysis system necessary? When part of the ANC system fails, what is the ease of replacement, can it be done at the gate?

Maintainability is another issue. The life-expectancy of the ANC system must be commensurate with that of the engine, and periodic maintenance or parts replacement must be easy and cheap. Along the same lines are questions of system survivability. Aircraft engines are subject to ingestion of objects such as birds, hail, sand, etc., that cause damage and wear to surfaces and parts. ANC actuators mounted on or near the outlet guide vanes will be particularly susceptible to foreign object impact damage. Survivability under icing conditions, lightening strikes, or EMI is also an issue.

Clearly, the ANC system must be part of the noise certification procedure. If it is to be useful, the ANC system must be critical to achieving desired noise suppression, that is, without the system, the noise should increase to above the limit level. Otherwise the ANC system is not necessary. Guidelines will have to be established with national and international regulating authorities regarding procedures to be followed if the system should fail (either in flight or on the ground). This sort of instant system noise suppression performance failure does not exist for passive treatment systems. What are the airport noise penalties going to be for flight operation without the ANC system?

It would be assumed that the ANC system, in itself, would have little effect on flight safety. This assumes it would fail gracefully, and not take other systems with it. In its absence, the aircraft must be able to perform all flight requirements without safety impact.

The ANC system must be able to react swiftly to transient situations. Engine operating conditions are continuously changing during takeoff and approach, and ANC system difficulties

may be encountered that require re-calibration of the ANC control algorithm in order to maintain suppression performance, depending on how long the re-calibration takes.

Finally, the ANC system should have no effect on engine operating efficiency. The number one issue here is weight, which must be minimized. Secondary considerations are effects of actuator interfaces with the duct surfaces on duct flow, both when operating and when turned off. Performance losses could be expected if the actuators had a significant effect on flow boundary layers. Additionally, if the actuator operation induced some sort of periodic disturbance in the flow, they may give rise to an additional acoustic source.

Each of the above issues, and probably others, will have to be addressed by a comprehensive design team during preliminary stages of the system design of an aircraft engine that will feature ANC noise suppression. Many of the issues will arise even for the development of an ANC system for a static engine ground demonstration of ANC capabilities.

9.6 Conclusions and Recommendations

For at least the particular engine selected for study, the effect of assumed treatment area loss on EPNL is greater than the gain from ANC tone removal. The problem is loss of suppression at non-ANC broadband frequencies due to treatment area displaced by the ANC system installation requirements. It is expected that the same results would hold for all typical engines of by-pass ratio between 4 and 6, and very possibly higher. This indicates the importance of designing the ANC actuators and sensors to be installed with minimal treatment loss.

The analytical simulation studies show that you do get the desired ANC suppression when number of actuator rings is equal or close to the number of cut on radial modes, depending on the energy distribution among radial modes. Even with treatment loss, it is possible to exceed the full passive treatment suppression at the tone.

The error sensor array can be optimized for number of sensors, but the required length of the error sensor array may be a problem. Wall-mounted sensors couple differently to the duct than the fan source, thus require multiple degrees-of-freedom to match mode patterns. Fewer than all cut-on modes can be suppressed with a limited number of actuator rings (get N modes with N rings), but error sensors must discriminate *all* cut-on modes to be able to cancel the selected modes.

Successful design and application of an ANC system will require accurate knowledge of fan modal source characteristics, both circumferential and radial. Selective directivity ANC schemes based on axial wavelength may work if the tone source is a single, very clean, spinning mode order. Sufficient axial length will still be required for actuator arrays to generate selective axial wavelengths, and the ANC generated signal must be phased properly with the fan-source-generated spinning mode, otherwise the ANC system may generate unwanted circumferential lobes at the desired radiation angle. The non-modal approach may work with farfield error

sensors, but the problem of getting it to work with in-duct sensors is as complex as the modal global control strategy.

Getting more effective results from the pure tone ANC system will require a fan where EPNL is more influenced by tone levels, and the number of radial modes in those tones is limited in number. Low radial mode orders at the expense of high spinning mode orders will require large numbers of actuators in each ring. Most typical modern turbofans are not designed to have reasonably low spinning mode orders with few cut-on radial modes at BPF at the current time.

For successful ANC application, fan rotor and/or stator may require redesign to lower the number of cut-on radial modes. At the same time the amount of broadband noise generated by the fan and the jet will probably also need to be lowered. The feasibility of ANC is not promising for a by-pass ratio 4-6 fan application, based on the CF6-80C2-80 results. There is little potential for ANC application as a "hush kit".

It is recommended tha effort continue in the development of ANC component technologies, such as actuator, sensor, and control algorithms.

10 Appendix 1 - ANC System Analytical Simulations

10.1 Introduction

Analytical simulations of an active noise control system coupled to a cylindrical duct representing a turbofan inlet and an annular duct representing a turbofan exhaust were developed to provide guidance to the development of the test ANC system hardware and software. The ANC simulations are based on cylindrical and annular duct modal propagation programs that were developed or used under NASA contracts in the past[12,13]. Figure 76 is an illustration of the inlet duct geometry for the cylindrical duct modal analysis.

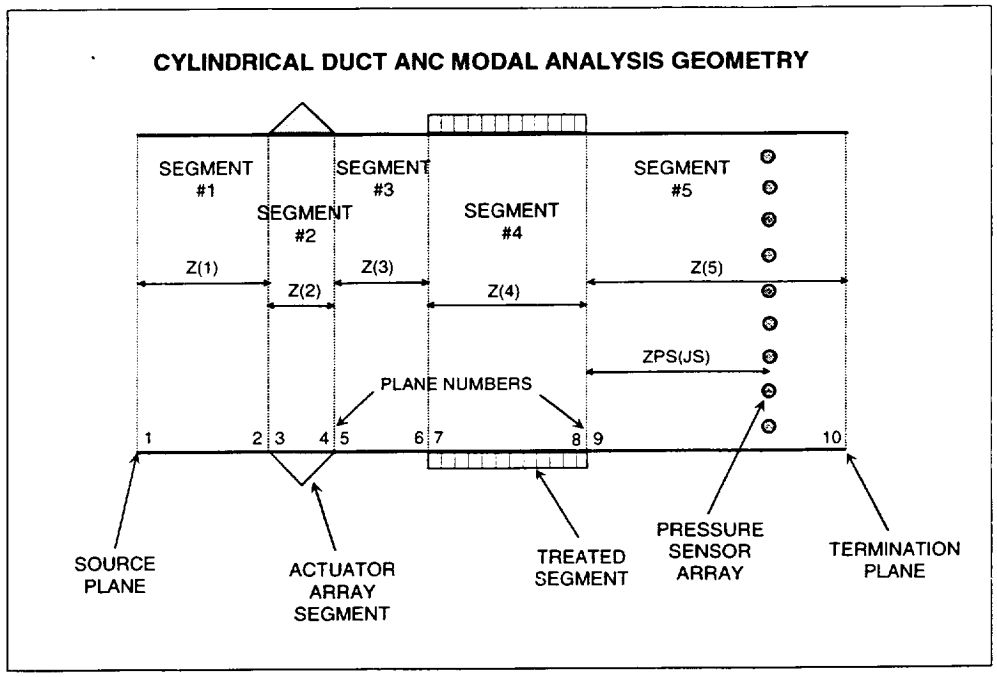

Figure 76 Cylindrical duct ANC modal analysis geometry

The ANC simulation was adapted to the duct modal propagation programs by coupling rings of piston-driven acoustic actuators to the walls of the duct, obtaining pressure "measurements" at selected pressure sensor points on the walls of the duct, and incorporating a feedback-loop ANC algorithm that takes the pressure sensor measurements, performs the ANC algorithm calculations, and then generates the driving signals for the piston actuators. The ANC simulation model was initially developed using GEAE internal research funding[14].

---

12 Motsinger, R. E., Kraft, R. E., Paas, J. E., and Gahn, B. M., "Analytical and Experimental Studies of Acoustic Performance of Segmented Liners in a Compressor Inlet", NASA CR-2882, Sept. 1977.

13 Joshi, M. C., Kraft, R. E., Son, S. Y., "Analysis of Sound Propagation in Annular Ducts with Segmented Treatment and Sheared Flow", AIAA-82-0123, Jan. 1982.

14 Kraft, R. E. and Kontos, K. B., "Theory of Active Noise Control in Aircraft Engine Ducts Using Loudspeakers", GE TM 92-484, Sept. 1993.

The cylindrical and annular duct modal analysis programs are idealized in that they require a uniform axial distribution of duct cross section, and ignore the modal reflections at the exit to the duct. A turbofan engine source of arbitrary spinning mode order and distribution in radial modes can be located at the entrance to the duct. No interaction between the turbofan and ANC sources is assumed. The models allow for the presence of passive treatment segments of arbitrary impedance (on inner and/or outer walls for the annulus). Each case is run at a single frequency.

The ANC source actuators are coupled to the duct using an analysis that transforms the non-homogeneous boundary condition to a non-homogeneous differential equation. Each actuator can be driven at a different amplitude and phase. The actuators are assumed to be of rectangular shape and are equally-spaced. Originally, the actuators were assumed to move as a rigid piston, but an analysis was developed to allow the actuator surface to move in the shape of a half sine wave in the circumferential direction (uniform top-hat function shape axially).

Two computer codes were written in FORTRAN, CANCSIM for the cylindrical duct analysis and AANCSIM for the annular duct analysis. The latest versions of the codes and accompanying Users' Guides have been supplied to NASA and all Subcontractors for use in the development of the test ANC systems. A brief description of the codes follows, but more detailed description of their use will be found in the Users' Guides.

10.2 Application to Turbofan Inlet Duct

10.2.1 Introduction to CANCSIM

The computer program CANCSIM2 simulates the installation of a system of active noise control (ANC) actuators in a cylindrical duct that is representative of an aircraft engine fan inlet. Up to six actuator rings can be installed at arbitrary axial locations in the duct, and each ring may have up to 50 actuator elements.

The computer program is based on the classical modal analysis for a multi-segment cylindrical duct. The computation is done for a single, discrete frequency, which is the frequency of the tone to be suppressed. The fan noise source is specified at the source plane in terms of its mode coefficients (in pressure units) for a set of radial modes of a given spinning mode order. The spinning mode is given index m, the radial modes are given index j (starting from j = 1 as the lowest radial mode). One spinning mode order is chosen as the target mode for ANC suppression, but additional spinning mode order source contributions can be included to determine the effect of additional noise components on the operation of the ANC system.

The control system that drives the actuator elements is simulated through a program subroutine that can be modified to reflect different control system designs. Up to 100 pressure sensors (the ANC error feedback signals) may be located in a specified hardwall segment of duct. A subroutine is provided to convert the pressure "measurements" into component modes at the entrance of the measurement section, and the mode coefficients can be used as input to the feedback control system algorithm.

The program has the capability of including treated segments in the duct, for which the wall impedance must be specified. The duct radius remains constant for the entire length. The maximum number of duct segments is set at 10, and the segments must be allocated as follows:

One hardwall entrance segment. By making this a hardwall segment, it is assured that the source is equivalent for each run (the modes depend on the segment eigenvalue). This segment can be arbitrarily short in length.

One segment allotted for each actuator ring in the ANC system. The length of the segment is the axial length of the actuators in the ring. The length can be different for different segments. The wall impedance for these segments is specified as hardwall (infinite impedance, zero admittance).

One segment for each type of treatment, specified in terms of impedance at the given frequency and segment length. Note the convention that admittance is specified in terms of the $e^{-i\omega t}$ convention, while impedance is specified in terms of the $e^{+i\omega t}$ convention.

One hardwall segment to contain all the pressure sensors. The sensors are all located on the wall (at the duct radius), but can be given arbitrary angular and axial positions in the segment. The "measured" pressures are obtained by expanding the modal solution at each sensor location.

One hardwall segment at the duct exit. This should be hardwall so that the mode reflection coefficients can be determined in terms of hardwall modes. This segment could be the same as the pressure sensor segment.

The maximum size of the problem is determined by settings for program array dimensions, and these can be increased arbitrarily, at the expense of increased storage requirements. Several of the maximum dimensions are related. For instance, the maximum spinning mode order in the problem should be less than the maximum number of actuator elements per ring (to prevent spatial mode aliasing, the maximum spinning mode order should be less than half the number of actuator elements). The maximum number of radial modes to be suppressed by the ANC system at the target spinning mode order should be less than or equal to the maximum number of actuator rings, and must, of course, be less than the maximum number of radial modes in the modal analysis. The number of modes to be expanded by modal analysis from the pressure sensor measurements should be less than the number of pressure sensors.

An option to include measurement errors in the pressure sensors was incorporated. The measurement errors are entered for each sensor in terms of standard deviation of pressure magnitude (in dB units) and standard deviation of pressure phase (in degrees).

A Gauss-Newton iteration control algorithm that operates in the frequency/modal domain was incorporated. The algorithm coefficients are part of the input. This simulates (approximately) the algorithm used in the prior GE ANC test in the NASA 4 ft. ANC Fan Rig. The algorithm is discussed in more detail in a separate section below.

The program allows more than one axially-spaced ring of ANC actuators. This required a fairly extensive change in the architecture of how the ANC algorithm was implemented, as well as an extension of the ANC algorithm to multi-dimensional (matrix) form. The multi-ring algorithm, which is a multi-dimensional form of the Gauss-Newton algorithm, is described below.

For the multiple actuator ring case, it is necessary to determine the modal transfer functions for each actuator ring individually, in addition to determining the fan source modes alone. This means that the first NANC+1 iterations (where NANC is the number of actuator rings) are used for the system setup, and the first ANC iteration with all rings functioning doesn't occur until iteration number NANC+2.

Since it has been determined that, with sensor and actuator errors, the ANC algorithm convergence parameters may need to be set to give many iteration steps, it was desirable to automate the iteration procedure rather than manually request one more step. The program was modified to perform the first NANC+2 iterations automatically, and automatically end the program based on the ANC convergence criteria, proceeding at least two steps past the calibration. The user can follow the results of the computation of these iteration steps on the screen.

It was found that although certain combinations of convergence parameters gave reasonable suppression values, the suppression would reach a "floor", around which the values would oscillate with greater magnitude than the dB suppression convergence tolerance. Coding was included such that, upon reaching a negative suppression value, if the suppression goes up (becomes more positive) by more than twice the tolerance, the iteration stops. A minimum of 10 iteration steps, including the calibration steps, will always be done. Additionally, the iteration-ending process also checks for divergence, where the suppression levels are positive (amplification) and increasing above +20 dB or in steps greater than +2 dB (taking at least 10 steps).

An error sensor (microphone) noise floor capability is included as an option. As part of the input, the user specifies the broadband noise floor level for each sensor. It is assumed that the background level is the same at each sensor.

The background level is added as noise to the "measured" pressure signal at each sensor at the frequency of the calculation. The background SPL is interpreted as the narrowband noise level in the frequency bin that contains the ANC tone. First, the SPL level specified in the input is converted to a peak amplitude "noise" pressure value, and a randomly determined phase (uniformly distributed between 0 and 2π) is applied to give the complex "noise" pressure signal added to the pressure mode sum signal.

One must be careful in the interpretation of this background noise level. First, the broadband level must be assigned a narrowband bin width that is appropriate to the measurement process that will be used in a practical experiment. Second, the data acquisition will normally not be a simple acoustic pressure autospectrum at each sensor location, but will be some form of

cross-spectrum with respect to a reference signal (reference microphone or trigger). Since it is assumed that the background noise is not correlated with the pressure signal, this means that the "effective" background noise level may be much lower than that which would be measured as the noise autospectrum alone, that is, the desired pressure signal is extracted from the noise. The signal-to-noise-ratio may even be negative. The SPL level assigned to the noise should account for the signal-to-noise-ratio of the data acquisition process.

Additional actuator and sensor error capabilities were incorporated. These include

- Sensor random and calibration errors
- Actuator random and calibration errors
- Actuator elements that "go out" (fail) during a run

The capability of incorporating pressure sensor or ANC actuator is included as an option. The possible sources of error are of three types:

1. Random errors with given standard deviation of magnitude and phase for sensor input or actuator output. Error varies for each sensor or actuator with each iteration with a normal distribution about the calculated mean.
2. Calibration errors that are determined randomly with given magnitude and phase standard deviation one time, at the start of a run. The initial calibration error is determined randomly from a normal distribution, but then the errors for each actuator or sensor are stored and the same values are reapplied at each subsequent iteration step.
3. Actuator-failure capability is provided. At a predetermined iteration step, an arbitrary number of actuator elements in any ring can become "defective", that is, the output is reduced 20 dB and the phase is randomized for those designated actuator elements.

It should be noted that the actuator-failure case has the possibility of generating strong spurious spinning modes that are not specified as one of the spinning modes in the input variables. CANCSIM2 will not identify these spurious modes following the loss of the actuator elements. A computer program was written to determine the spinning modes generated by the defective actuator system to use for determining whether additional spinning modes should be included in the CANCSIM2 input list.

10.2.2 ANC Control System Implementation

10.2.2.1 Discussion of Gauss-Newton ANC Algorithm

The simulation for the active control system algorithm is based on the control system used in the 1995 ANC test in the NASA 4 ft. diameter ANC Fan Rig under NASA Contract NAS3-26617, Task Order 5. The ANC system uses a modal-based algorithm that cancels a single mode of a given spinning mode order, m, at a single frequency. For this test condition,

only a single radial mode was cut-on for the fan rotor-stator interaction at twice blade-passing-frequency with m = 6, so that the ANC system aimed at a single mode was very effective.

The Modal Control Routine is described in detail in the GEAE Contractor Final Report[15]. An outline of the steps in the Modal Control Routine follows:

1. The error signals in the form of pressure sensor measurements from a ring of 16 microphones are acquired.
2. Time-domain averaging is performed for each sensor synchronized by a trigger obtained from rotor rpm. This enhances the signal at the tone frequency.
3. A Discrete Fourier Transform is used to determine the pressure spectral Fourier component at the tone frequency at each sensor.
4. An *a priori* calibration is applied to the pressure signal for each sensor.
5. A spinning mode decomposition is applied to the 16 pressure Fourier coefficients to determine the m-mode complex coefficient at the tone.
6. The control signal to the actuators is updated according to a Gauss-Newton method control algorithm, which is based on the measured pressure mode coefficient for the previous step and two previous actuator velocity driving signal output values.
7. The control algorithm output is converted to a time-domain driving signal to each actuator to produce the desired spinning mode output in the duct.
8. The actuator control signals are adjusted based on *a priori* actuator calibrations.
9. The control signals are converted to the time-domain and sent as output to drive the actuator elements.
10. The process is repeated to update the control system.

Although this method was used as the basis for the computer program, some modifications were made to make the method more appropriate for the computer simulation. The algorithm was implemented entirely in the frequency domain as described below.

In the implementation of the simulation of this control system in computer code, it was first assumed that the time domain data acquisition and analysis for Steps 1. through 3. can be replaced by the frequency-domain "measurement" of the pressure at each sensor position obtained from the expansion in modes in the analytical solution. It is assumed that no calibration adjustment per Step 4 is required to the analytically-determined pressures, but the capability of applying a random error to the measurement at each sensor has been included.

The modal decomposition of the complex pressures in Step 5 is accomplished in the computer program using a least squares fit of the data to a specified set of modes. This is not exactly the same method that was used in the NASA test algorithm, but it should give similar

---

[15] Pla, F. G., Hu, Z., and Sutliff, D. L., "Active Control of Fan Noise: Feasibility Study Volume 3: Active Fan Noise Cancellation in the NASA Lewis Active Noise Control Fan Facility", to be issued.

results, and has the advantage of being able to include sensors at different axial positions. This allows inclusion of multiple radial modes and separation of forward and backward-travelling modes.

The spinning mode decomposition used in the test method was computationally more efficient than the least squares method in the analytical model, but the computer simulation does not attempt to model the process in real time. If it is desired to simulate performance of the modal decomposition used in a specific algorithm under evaluation, this step in the computer program can be replaced by one with more fidelity.

The control signal is generated in Step 6 using the Gauss-Newton method, from the formula

$$V_n = (1-\mu\lambda_1)V_{n-1} - \mu\lambda_2(V_{n-1} - V_{n-2}) - \mu C_M^{-1} A_{n-1} \tag{9}$$

where

$n =$	iteration number
$V_n =$	n^{th} iteration of the actuator driver output velocity control signal
$A_n =$	n^{th} iteration of measured target pressure mode coefficient (error signal)
$C_M^{-1} =$	Inverse of transfer function relating V_n and A_n, ie.,

$$A_n = C_M V_n \tag{10}$$

This iteration will attempt to drive A_n to zero.

The coefficient μ is the step size in the iteration. The coefficient λ_1 is the weighting coefficient for the control signals. It prevents small reductions at the error sensors at the expense of large control signals. The coefficient λ_2 is the weighting coefficient that penalizes large changes in control variables that could destabilize the iteration.

This is the algorithm implemented in the computer simulation. The velocity vector V_n and the modal coefficient A_n are stored at each iteration step. Note that the control algorithm is one-dimensional, so that there is one complex driver velocity control signal resulting from one complex modal coefficient error signal.

In the test program, the transfer function C_M was obtained with sensors and actuators mounted in the fan rig with the fan not running and the control system turned on, such that on the zeroth iteration we have

$$C_M^{-1} = \frac{V_0}{A_0} \tag{11}$$

where A_0 is the measured mode coefficient for an arbitrary input signal V_0. The transfer function then remains constant for the remainder of the run. This procedure is likely to be valid for the NASA fan in which the Mach number under operating conditions remains very small.

For the computer simulation, slightly different procedure is adopted. It is assumed that in many cases, the transfer function will be quite different with the fan operating at speed than it is with the fan off (airplane on the ground). Thus, the transfer function will probably need to be determined with the fan running. A procedure to do this is the following.

First, the fan source is characterized by measuring the mode coefficient with the fan running and the ANC system turned off. This provides the zeroth iteration to obtain the coefficient A_0^{FAN}. We first assume that A_0^{FAN} is due to steady-state operation of the fan, so that it remains constant throughout operation of the ANC system (we will see how this restriction can be relaxed below).

With both the fan running and the ANC on (using an arbitrary value of V_0), we have a measured mode coefficient from the first iteration that is the sum of the fan source and the ANC:

$$A_1 = A_1^{ANC} + A_0^{FAN} \tag{12}$$

We assume that V_1 is chosen to be large enough that the pressure due to the ANC system A_0^{ANC} is of similar amplitude to that from the fan, but V_1 is otherwise arbitrary, such that no suppression may be achieved in this step (the overall signal may increase).

Using the definition of the transfer function, we can derive the expression

$$C_M^{-1} = \frac{V_1}{A_1 - A_0^{FAN}} \tag{13}$$

in terms of A-values measured with fan alone and with fan plus ANC. This is the form used to compute the transfer function in the computer simulation implementation.

Since A_0^{FAN} will depend on the SPL of the fan source input modes, an initial guess at the ANC calibration velocity coefficient V_1 is made part of the program input. If a value of V_1 is used that is too low, the algorithm will require additional steps in the iteration to make the adjustment. There may be sufficiently low values of V_1 for which the ANC algorithm will not converge.

The algorithm can be made to continually update the system transfer function by defining it as

$$C_M^{-1} = \frac{V_{n-1}}{A_{n-1}} \tag{14}$$

Then the transfer function is calculated from

$$C_M^{-1} = \frac{V_{n-1}}{A_{n-1} - A_0^{FAN}} \tag{15}$$

and is replaced at each step of the iteration. There is an input option in the program to use either the constant or the continual upgrade of the transfer function.

It is still assumed that the fan source remains steady in time, although this could be relaxed by periodically turning off the ANC and re-calibrating A_0^{FAN}. This would cause a sudden noise increase for the brief time period required to reacquire the fan source signal.

Step 7 is implemented to determine the velocity magnitude and phase of each actuator element for the desired spinning mode given the driving signal output velocity V_n in a manner nearly equivalent to the NASA test algorithm. Since perfect actuators are assumed, it is not necessary to apply the actuator calibration in Step 8. Since the simulation analysis operates in the frequency domain, it is not necessary to convert the actuator element driving signals back to the time domain as in Step 9, the actuators are simply given a known velocity magnitude and phase at the calculation frequency.

At this point, the subroutine that couples the actuator motion to the duct is invoked. First, the spinning mode content of the actuators is determined, and the actuator source mode coupling is distributed in amplitude among the desired spinning mode and any spurious spinning modes generated. If any of these spurious modes are included in the propagation calculation, their amplitudes are stored.

Next, the radial modes coefficients for the spinning modes in the ANC source are determined at the end of the actuator ring segment away from the forward direction of propagation (toward the duct exit). In this version of the program, the modes propagating back toward the fan source are ignored, although they can easily be included in more advanced versions of the program that include mode reflections.

This leads to Step 10, in which a new set of pressure sensor (ANC system error) measurements are acquired, and the next ANC control system iteration is accomplished.

10.2.2.2 Upgrade for Multiple ANC Actuator Rings

The extension to the Gauss-Newton method for multiple actuator rings and multiple radial modes is given by the matrix form of Equation (16)

$$\{\mathbf{V}\}_n = (1-\lambda_1\mu)\{\mathbf{V}\}_{n-1} - \mu\lambda_2(\{\mathbf{V}\}_{n-1} - \{\mathbf{V}\}_{n-2}) - \mu[\mathbf{C}]^{-1}\{\mathbf{A}\}_{n-1} \tag{16}$$

where

n = ANC iteration number

$\{\mathbf{V}\}_n =$ the vector of actuator driver output velocity control signals for the nth iteration

$\mathbf{A} =$ the vector of radial mode coefficients for the measured target m-order modes for the nth iteration

$[\mathbf{C}] =$ matrix of transmission coefficients for i^{th} radial mode as generated by j^{th} actuator ring

The control coefficients μ, λ_1 and λ_2 are scalars defined in the same manner as previously. The elements of the transfer function coefficient matrix C_{ij} are obtained from

$$C_{ij} = \frac{A_j^{(i)} - A_j^{(S)}}{V_i} \tag{17}$$

where, for the target spinning mode order, m,

$A_j^{(i)} =$ j^{th} radial mode coefficient (measured) as generated by i^{th} actuator ring and the fan source operating simultaneously

$A_j^{(S)} =$ j^{th} radial mode coefficient (measured) as generated by fan source alone

$V_i =$ actuator driver control signal for i^{th} actuator ring operating alone (with fan source but no other actuator rings)

The transfer function coefficients must be obtained by a initializing procedure at the start of the ANC run. First, the fan source is operated alone, and the $A_j^{(S)}$ are obtained. Then, leaving the fan source "operating", the actuator rings are "turned on" one at a time to obtain the $A_j^{(i)}$ for each ring i. Note that in order to invert matrix [C], it is necessary that it be a square matrix. This implies that the number of radial modes at the target mode order is equal to the number of actuator rings. It would be possible to have an over-determined system in which there were more actuator rings than target radial modes, but some sort of least mean squares solution method would have to be applied to the Gauss-Newton equation in order to solve for the next velocity iteration. The desire for minimum system size would seem to dictate that one would never use more actuator rings than radial modes being suppressed, as long as suppression goals could be reached with the equality of rings and modes.

The algorithm is implemented in the computer program by direct inversion of the [C] matrix and matrix multiplication. This is probably not the most efficient manner to implement the algorithm in the actual engine control system, which may require a much faster implementation to be effective. It nevertheless does demonstrate the effectiveness of the multiple dimension algorithm in cancelling multiple radial modes.

A sample three cut-on mode case with three actuator rings produced nearly total cancellation of the three modes. The actual amount of suppression obtained appears to be

sensitive to the placement (axial spacing) of the error sensor rings, a phenomenon that warrants further investigation. In the case where there are more cut-on radial modes than rings, various interesting phenomena were observed for the limited number of sample cases attempted. In one case with three rings and six cut-on radial modes, the three (lowest order) target radial modes were obliterated, but the total energy flux was increased by energy picked up by the 4, 5, and 6 order radial modes from actuator coupling to these modes. Would these higher order modes be more susceptible to suppression from passive treatment?

In a final development, an updated version of the cylindrical duct ANC simulation was developed using an algorithm that allows operation where the number of radial modes to be suppressed can be less than the number of actuator rings. The objective was to see how the Gauss-Newton algorithm would work when only a limited number of the total number of cut-on modes was targeted for suppression. This requires the solution of an over-determined set of equations to determine actuator driver output. A singular value decomposition subroutine was incorporated into the program to accomplish this task.

10.2.3 Examples of Control System Operation Simulation

10.2.3.1 Single Actuator Ring Control System Operation

Several simple test runs were made to check operation of the revised control system algorithm. The output for a more complete test case is included at the end of this report and described below. For these preliminary cases, the NASA fan 4 ft. diameter inlet is modeled, and a frequency of 960 Hz. was chosen with spinning mode order m = 6 such that only a single radial mode is propagating unattenuated.

First, various combinations of the control system parameters μ, (computer variable CMU) λ_1, (computer variable CLAM1) and λ_2 (computer variable CLAM2) were used and convergence rates and overall suppression were noted. Figure 77 shows the effect of coefficient μ on convergence, with λ_1 and λ_2 both set to zero.

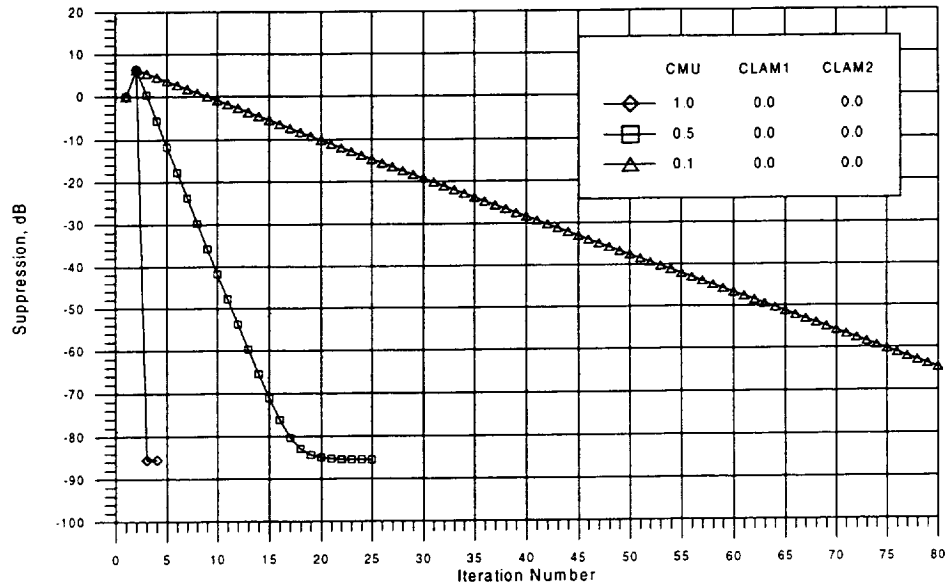

Figure 77. Control system iteration showing effects of μ.

Note that the mode is totally canceled in 2 steps when $\mu = 1.0$. As μ is increased, the rate of convergence slows down, but the maximum suppression of -85.5 dB will be achieved in all cases (the iteration was cut off after 80 steps for $\mu = 0.1$, but should eventually reach the same suppression). The suppression is so high because there are no unsuppressed additional modes to limit the suppression and there is no noise floor. It is suspected that the suppression limit is due to computer numerical accuracy limitations.

Figure 78 shows the effects of λ_1 and λ_2 on the iteration. Note that the effect of λ_2 (when λ_1 is zero) is to slow the convergence rate, but the maximum suppression of -85.5 dB is obtained The effect of λ_1 , however, appears to be to limit the maximum suppression achievable. The closer λ_1 is to 1.0, the lower the suppression. The author is unsure of the explanation of this behavior, other than the possibility that the implementation of the algorithm is in error. Comments will be appreciated.

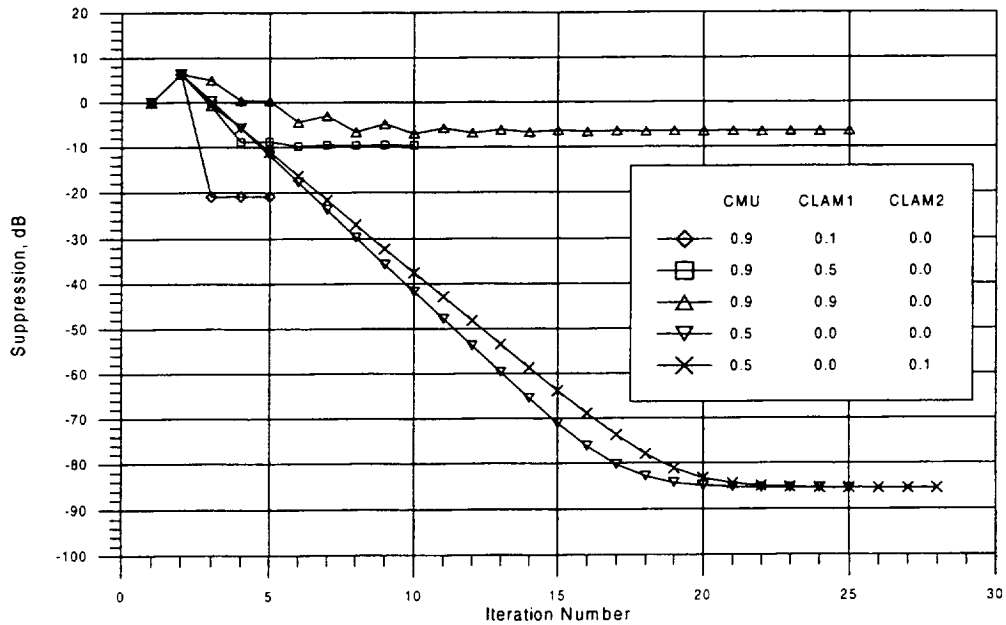

Figure 78 Control system iteration showing effects of λ_1 and λ_2.

The next case shows the effects of pressure measurement errors on the control system iteration. Figure 79 shows the iteration with $\mu = 1$ and both λ -values equal to zero, for two different magnitudes of measurement error. In the first run, there is no measurement error. In the second run, the standard deviation of SPL is set at 1.0 dB and the standard deviation of phase is set at 5.0 degrees. These values of standard deviation are doubled for the third run.

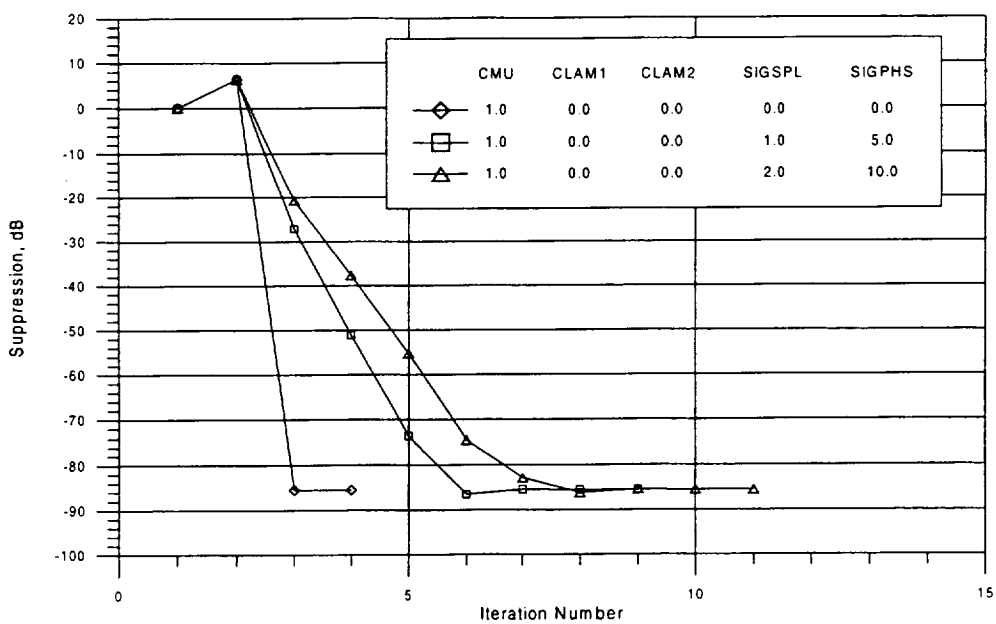

Figure 79 Control system iteration showing effects of measurement error.

Note that the presence of measurement error has not prevented the algorithm from reaching the maximum suppression of -85.5 dB for any pressure measurement error magnitude. Only the rate of supp7ression convergence has been slowed. This interesting behavior warrants further investigation—either a normally-distributed measurement error is not realistic or is not a concern to the ANC control system.

10.2.3.2 Effects of Simulated Random Errors in Sensors and Actuators

Two illustrative cases were run to predict the effects of random sensor input errors and random actuator output errors on the convergence of the ANC algorithm. In one case, random error were applied to the error sensors and the actuators had no applied errors. In the second case, the random errors were applied to the actuators, and the error sensors were assumed to be perfect.

The sample cases have three actuator rings aimed at suppressing three radial modes for $m = 6$, at 1500 Hz. in a four foot diameter duct. Only three radial modes are cut-on at this condition, so that ideally the system should give very high suppressions. When there are no random errors, to that the simulation is completely determinate, a suppression of 29.7 dB is obtained in just two iteration steps with $\mu = 1$, $\lambda_1 = 0$, and $\lambda_2 = 0$.

In the first case, a random sensor input error was applied to all 48 sensors, with pressure magnitude standard deviation of 0.2 db and pressure phase standard deviation of 2.0 degrees. In this case, there were no actuator output errors. The ANC suppression convergence tolerance was set to 0.05 dB. In a second case, the sensor error was set to zero and a random actuator output error was applied with velocity magnitude error standard deviation of 2.0% relative to each actuator ring input velocity and phase error of 2.0 degrees. For the actuator error case, the suppression tolerance was set to 0.1 dB.

For both cases, the control parameters were set at $\mu = 0.15$, $\lambda_1 = 0.9$, and $\lambda_2 = 0.9$. The results of the computation are shown in Figure 80. In the pressure sensor error case, with a convergence tolerance of 0.05 dB, it is noted that the convergence is relatively slow, but decreases monotonically. With a tighter tolerance, it would be expected to achieve a lower final value. In the actuator error case, there is a more rapid initial increase, but the suppression value begins to wander up and down after it reaches about -6 dB. It is expected that increasing the step size in the pressure sensor error case would increase the decrement rate but destabilize the convergence, and vice-versa in the actuator error case. The effects of calibration errors in sensors and actuators, the effects of combined errors, and the effects of disabled sensors or actuators need further investigation.

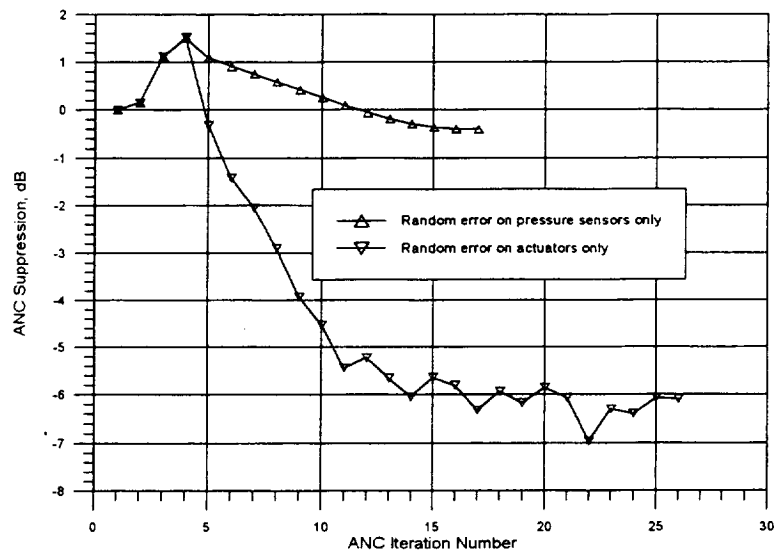

Figure 80. Convergence of 3-ring case with random errors either on sensors or actuators.

Observations were made by computer program users that the sensitivity to sensor error levels appeared to be higher than would be expected, based on actual previous test experience. A brief parametric study was conducted to look at effects of variations in sensor error standard deviation magnitudes.

First, the single actuator ring with one cut-on radial mode case was considered. This case was run for the 4-ft diameter inlet duct at 960 Hz., m = 6. The convergence tolerance was set at 0.02 dB, no background noise floor was used, and the convergence parameters were set at $\mu = 0.05$, $\lambda_1 = \lambda_2 = 0.98$. Table 2 below shows the results:

Table 16 Effects of variation of sensor standard deviation on convergence – single actuator ring

Case	Sensor Magnitude σ, dB	Sensor Phase σ, degrees	ANC Suppression Achieved, dB	Number of Iteration Steps
1	0	0	-5.995	43
2	0.1	1	-5.894	42
3	0.2	2	-5.851	42
4	0.5	5	-5.663	39
5	1.0	10	-5.450	39

Note that the suppression achieved does not vary much with error magnitude. It is suspected that the suppression achieved, in this case, depends more on the values of λ_1 and λ_2 than on the sensor errors. Adjusting the convergence parameters to give higher suppression

values, however, would come at the expense of convergence stability. Optimizing the parameters was not attempted.

A three actuator ring, three cut-on mode case was also tried. The convergence tolerance, background noise (none), and ANC algorithm parameters were kept the same as the previous single ring case. The results are given in Table 1:

Table 17 Effects of variation of sensor standard deviation on convergence – three ring actuator

Case	Sensor Magnitude σ, dB	Sensor Phase σ, degrees	ANC Suppression Achieved, dB	Number of Iteration Steps
1	0	0	-5.776	51
2	0.1	1	-4.451	51
3	0.2	2	-1.517	38
4	0.5	5	-0.798	32
5	1.0	10	-1.065	34

Note that the behavior is quite different from the single ring case. The suppression decreases in magnitude rapidly as the error increases. No explanation is offered at this time for the increased sensitivity of suppression to sensor error levels in the multiple ring case. Possibly the suppression could be increased while maintaining stability for any given case by adjusting the convergence parameters, but this was not tried. Note also the apparent anomaly for the highest error magnitude case.

A few cases run with background noise levels indicate that behavior is about as expected, that is, the error sensors hit a floor at the input noise floor values. The effect on the algorithm is to cause the iteration to oscillate around some suppression level that is higher than that achieved with no noise floor. Further characterization of the effects is needed.

10.2.4 Observations

The following are observations from results obtained from a very limited number of checkout runs of the program. Each observation requires further investigation and verification and should not be taken as a generalization.

1. The use of N actuator rings apparently will effectively suppress N radial modes as long as all N radials are discriminated accurately by the sensor array. If there are more than N radial modes cut-on, the sensor array must be capable of discriminating all cut-on modes to be certain that the first N are determined accurately, even though those above N may not be suppressed. It is possible to suppress, say, the first 3 radial modes with 5 modes cut-on with 3 actuator rings (with 5 rings of sensors). The remaining unsuppressed cut-on modes may increase (or decrease) in level from their initial values, but there is no control over these

modes. Whether one obtains an overall suppression depends on the initial mode weighting (all this assumes no passive suppression).

2. Based on one case, the ANC algorithm appears to be relatively insensitive to sensor or actuator *calibration* errors.
3. Based on one case, the ANC algorithm does seem to be quite sensitive to actuator random errors, slightly less so to sensor random errors.
4. The sensitivity to sensor random errors appears to be a function of both error level and choice of ANC algorithm convergence stability parameters. Multiple actuator ring configurations appear to be more sensitive than single ring configurations. Further investigation is warranted.
5. The ANC algorithm appears to be sensitive to the loss of an array element, particularly since the transmission coefficient matrix is not re-determined following the loss (this invites investigation). For the case run with two elements out in the second of three rings, suppression was obtained, but the algorithm bounced around and did not converge (in this case the algorithm coefficients were $\mu = 1$, $\lambda_1 = .0.0$, and $\lambda_2 = .0.0$, which may explain the lack of convergence).
6. The inclusion of an error sensor noise floor appears to provide the expected behavior, but one must be careful about the correct interpretation of the noise floor input levels.

10.3 Application to Turbofan Exhaust Duct

10.3.1 Introduction

The annular duct modal analysis propagation program has been modified to incorporate the simulation of active noise control actuator ring sources at arbitrary axial stations on the inner and outer walls of the annular duct. Pressure "measurement" points can be located at arbitrary positions on the inner and outer walls of a designated segment of hardwall duct to simulate the error sensors for the ANC feedback system. Active control system algorithms are incorporated that use the measured pressure error signals to drive the piston-type actuators. This version of the program allows up to 12 rings of actuators located on either inner or outer walls of the annulus. Figure 81 illustrates the analysis geometry of the annular duct.

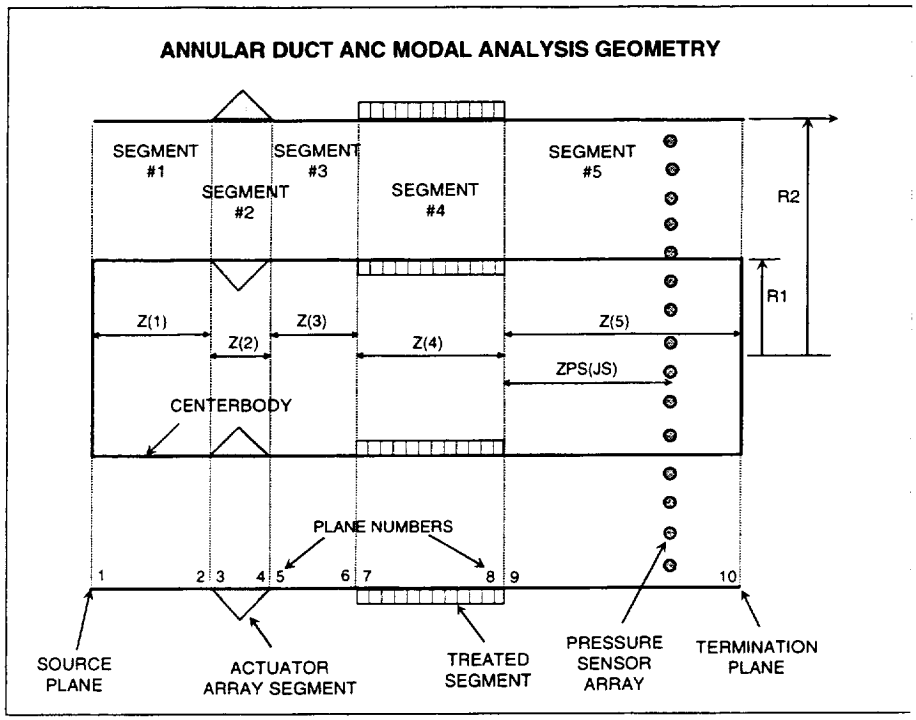

Figure 81. Annular duct ANC system geometry.

The development of the annular duct control system software followed and was based extensively on that developed for the cylindrical duct. The control system algorithm is essentially equivalent, and the reader is referred to the write-up in the cylindrical duct ANC algorithm section, above. The key addition was an analysis to couple both inner and outer rings of actuators to the duct.

Some assumptions and restrictions that apply to this version of the program are:

1. The propagation model includes the effects of mean flow with boundary layers. The boundary layer effect assumes a thin boundary layer, and has not yet been thoroughly checked out. The user is advised to use the uniform flow assumption with continuity of particle displacement to start out.
2. The model allows actuators to be mounted on both the inner and outer walls in the actuator segment. If an inner and outer ring are located at the same axial plane, they may operate either independently or may both be driven by the same feedback signal (equal response at inner and outer).
3. Pressure sensor positions can have different and arbitrary axial values within the sensor segment, which is assumed to be hardwall.
4. The number of targeted radial modes at the targeted spinning mode order should be equal to the number of independent actuator rings.

At the present time, the program has been checked with only a very limited set of test cases.

The ANC iteration has been automated. The program continues iterating until a convergence tolerance that is part of the input is satisfied, a divergence criterion is exceeded, the solution begins to oscillate, or 91 iterations have been exceeded.

The ANC algorithm is a multi-mode version of the Newton-Gauss algorithm similar to the one currently in use in the cylindrical duct program. The primary difference is the addition of additional channels due to the actuator rings on the inner wall.

Random errors for calibration and operation of the actuators and sensors have been incorporated in the same manner as for the cylindrical duct version.

10.3.2 Accommodation of Internal Noise Sources

An updated version of the AANCSIM program was developed such the fan noise source could be located at an arbitrary plane in the duct, rather than only at the duct entrance plane ($z = 0$). Both forward and backward radiating modes can be inserted at arbitrary planes.

10.3.3 Upgrade to Include Backward Modes Radiated from ANC Actuators

The updated version of the program inserts backward-radiating modes for each actuator ring. It is assumed that the backward modes have the same mode coefficients (amplitude and phase) as the forward ANC mode coefficients, but that they originate from the upstream end of the actuator segment, while the forward ANC modes originate from the downstream end. All information about the forward-radiated mode energy is available in the run output.

10.3.4 Removal of Automated Iteration Procedure

The inclusion of internal sources radiating in both directions made the logic for automatically determining the ANC control system convergence extremely difficult. In the updated program version, the automatic comparison to an input tolerance has been removed and replaced with the manual procedure of requesting another iteration or ending the program. There is a new input variable that allows the iteration to run for a set number of iterations before requesting whether to continue or end.

This gives the disadvantage of more attention and time from the operator, but gives the advantage of letting the iteration continue as long as desired to observe divergence or oscillatory behavior that the automatic routine cut off. The automation could be reinstated for the exhaust suppression only with an appropriate algorithm, but probably doesn't make sense unless the system is upgraded to have both upstream and downstream control systems.

11 Appendix 2 - Application Of The Green's Function Technique To The Prediction Of Acoustic Fields Generated By Active Noise Control Drivers

Charles E. Mitchell
Department of Mechanical Engineering
Colorado State University

11.1 Introduction

The Green's function method has been used successfully by the author and his students at Colorado State University to model several problems associated with combustion instability in rocket engines. This research has included predicting the damping effects of acoustic liners and slots of many different designs on the oscillations in these devices. Non-uniform mean flow, baffles, and convergent nozzles have also been treated in these modeling efforts. A summary of much of this research is available in the literature[16]. The goal of the work described here was to apply the Green's function approach to the problem of active noise control in fan inlets and exhaust ducts. Two specific problems were treated during the course of this project. The first of these was the description of the acoustic field generated by a single ring of evenly spaced active control drivers located on the inner surface of a cylindrical duct with mean flow. The second extended the model to treat annular exhaust ducts with driver rings located on both the inner and outer surfaces of the duct at a single axial location.

In this report a brief description of the analytical approach will be presented first. This will be followed by a discussion of the application of the technique to the two duct models of interest. Finally, the resulting computer codes, along with example inputs and outputs, will be described.

11.2 Analytical Approach

The essence of the technique is the transformation of a linear wave equation into an integral equation. This is accomplished by development of an appropriate Green's function and subsequent application of Green's Theorem. The wave equation may be non-homogeneous (for example, if the mean flow varies axially or radially). The dependent variable chosen is the velocity potential, ϕ', defined by $\mathbf{v}' = \nabla\phi'$. Pressure can then be found directly from ϕ' using the momentum equation. If it is assumed that $\phi' = \phi\, e^{i\omega t}$, then the form of the resulting integral equation for ϕ is as follows:

$$\phi(\bar{r}) = \iint G(\bar{r}/\bar{r}_0)v_W(\bar{r}_0)dS_0 + \iiint G(\bar{r}/\bar{r}_0)F(\phi)dV_0 - \iint \phi(\bar{r}_0)\nabla G \bullet \bar{n}dS_0 \qquad (18)$$

[16] "Analytical Models for Combustion Instability", by Charles E. Mitchell, AIAA Prog. In Aero/Astro., Vol. 169, pp. 403-430, 1995.

The associated relationship for p ($p' = pe^{i\omega t}$) is

$$p = \gamma\left[i\omega\phi + M\frac{\partial\phi}{\partial z}\right]$$ where M is the mean flow Mach number.

In this equation G is the Green's function, found by solving the time-independent wave equation with the non-homogeneous part replaced by the Dirac delta function and subject to the homogeneous boundary condition, $\nabla G \bullet \mathbf{n} = 0$, on bounding surfaces. The Green's function is defined for a simple geometry (cylindrical or annular) and is represented through an expansion in the normal acoustic modes for that geometry in the radial and azimuthal directions. The integrals in the equation above are taken over the actual duct geometry, which need not be simply cylindrical or annular (but should be fairly close to these in some sense). The first integral on the right hand side includes the effects of both active drivers and absorbing walls: the normal velocity at the wall, v_w, is non-zero for both. The volume integral includes the function F, which comes directly from the non-homogeneous part of the wave equation and thus can include variable mean flows in the axial direction (due to changes in cross-sectional area) and in the radial direction (due to shear layers). The last integral accounts for variations in the duct geometry away from a simple annulus or cylinder. For the duct models treated in this work the last two integrals are zero.

Formally, evaluation of the integrals gives ϕ (and therefore p) at all locations in the duct. Since the Green's function is represented as an expansion in normal acoustic modes, then so also will be ϕ and p. In practice, then, carrying out the required integrations specifies the coefficients of this expansion. If v_w, F, and the geometry are sufficiently simple in form, then these integrals may be evaluated analytically. In most other cases numerical integration is required. Moreover, since v_w can depend on ϕ, then in general all three integrals may depend on ϕ and solutions for ϕ must be found by iteration or successive approximation. For example, a reasonable first approximation would be the ϕ generated from the first surface integral for a known v_w (active driver velocity) distribution on the walls. Using this ϕ, the absorbing wall, mean flow and area change integrals can be approximated and an improved ϕ can be calculated, etc. For the duct models treated in this work, v_w was taken to be independent of ϕ and no iteration was required. If absorbing walls were to be considered, however, iteration would be necessary.

11.3 Cylindrical Inlet Duct Model

The first model to be treated using the Green's function technique was a cylindrical inlet duct with a uniform mean flow and a single ring of active noise control actuators. A sketch of the duct is presented in Figure 82 below.

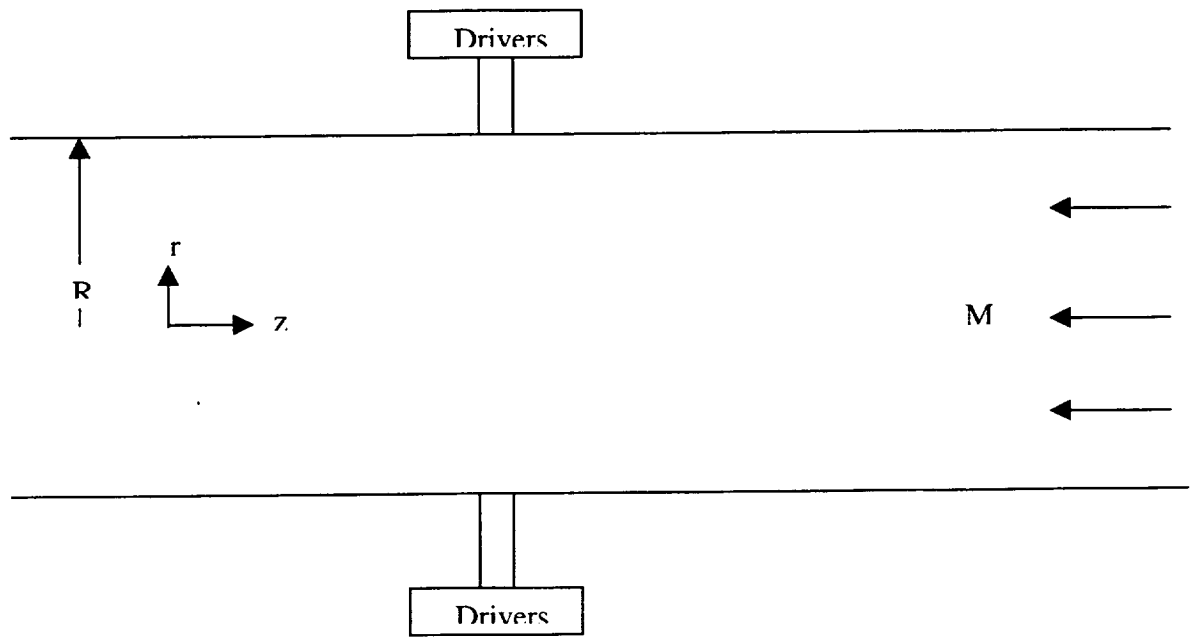

Figure 82. Schematic of Cylindrical Inlet Duct

The driver ring is located at an arbitrary axial location $z = L_a$, and consists of 15 equally spaced identical top hat drivers. At all wall locations except for the drivers the wall is taken to be acoustically hard. Because the drivers are identical and evenly spaced, only a single mode in the azimuthal direction (θ direction, out of the paper, not shown in the sketch) is driven. However, in order to anticipate situations in which multiple modes in the azimuthal direction may be of importance, such as slightly asymmetric duct geometry or variable wall absorption, azimuthal symmetry is **not** assumed in this analysis. Consequently, a three dimensional expression in terms of the normal acoustic modes was required. The impact of asymmetry on pressure predictions was tested in calculations by blanking out one of the drivers.

For this duct model, the relationship for ϕ can be written as follows (in non-dimensional form):

$$\phi(\bar{r}) = -\iint_{A_D} G(\bar{r} / \bar{r}_0) v_w(\bar{r}_0) dS_0 \tag{19}$$

where the integral extends over the actuator ring. v_w is equal to the top hat velocity magnitude on the driver surfaces and is zero otherwise. The appropriate Green's function is

$$G(\bar{r} / \bar{r}_0) = \sum_m \sum_l A_{m,l} \Omega_{m,l}(\bar{r}) \Omega_{m,l}(\bar{r}_0) e^{iB_{l,2}(z-z_0)} \tag{20}$$

where

$$\Omega_{m,l}(\bar{r}) = J_m(\lambda_{ml} r)e^{im\theta} \tag{21}$$

$$\Omega_{m,l}(\bar{r}_0) = J_m(\lambda_{ml} r_0)e^{-im\theta_0} \tag{22}$$

and λ_{ml} are roots of $\frac{dJ_m(\lambda_{ml} r)}{dr} = 0$, at r=1. The constants $A_{m,l}$ and $B_{1,2}$ depend only on $M, \omega, \lambda_{m,l}$ and normalization constants. Carrying out the integration and use of the relationship between p and ϕ presented earlier gives the following expression for p (dimensional- in Pa):

$$p(r,\theta,z) = \sum_m \sum_l p_{m,l}\Omega_{m,l}(r/R,\theta)e^{iB_{m,l}|z-L_a|} \tag{23}$$

Values for $p_{m,l}$ and $B_{m,l}$ are determined through the integration over the actuator ring and depend on v_w. These parameters are calculated and output from the computer code ANC2F. For the cylindrical model v_w was not specified directly. Instead, it was required that the sound pressure level at the wall produced by the actuators for a particular mode be specified. This, in turn, determined the required value of v_w. The values of $p_{m,l}$ and $B_{m,l}$ are slightly different for $z \geq L_a$ and for $z < L_a$ because of mean flow effects. Only values for $z \geq L_a$ are printed out from the computer code. (The other coefficients are computed but not printed). $B_{m,l}$ is the propagation coefficient. If its imaginary part is positive the mode is cut-off. For equally spaced identical drivers only one term in the m summation has $p_{m,l}$ values different from zero. If one of the drivers is blanked out (shut off) however, this is not so and many terms in the m summation contribute. Even when only one term in the m summation is present, it is usual that several terms in the l summation are of significant size, and also that more than one mode is cut-on.

11.3.1 Results of Typical Calculations

The computer code ANC2F has been run for only a few sets of input data, since the goal of this project was to demonstrate the applicability of the Green's function technique rather than to investigate a large spectrum of design possibilities. Results for one of these data sets will be presented next. Relevant input parameters:

- 15 drivers each with a diameter of 2 inches
- duct diameter of 48 inches
- mean duct sound speed of 1128 ft/s
- mean inlet Mach number of 0.10
- frequency of oscillation 1250 Hz

For this geometry, frequency and sound speed, the cut-on acoustic mode having a characteristic frequency closest to the applied frequency is the m=2, l=4 mode with a cut-off frequency of 1182 Hz. In order to set v_w for the drivers, it was required that the sound pressure level for this mode at the drivers be 110 db (corresponding to a pressure amplitude of 6.32 Pa). In the discussion which follows the m=2, l=4 mode will be called the "main mode". Code ANC2F was then run for these inputs.

The driver velocity amplitude required was predicted to be 1.268 ft/s, with a corresponding driver displacement amplitude of .01937 in. Since the drivers were identical and evenly spaced, pressure coefficients $p_{m,l}$ were non-zero only when m=2. Results for $p_{m,l}$ ("pressure coeff."), $B_{m,l}$ ("prop. Coeff.") and the cut-off frequency ("c. o. freq.") are shown in matrix form for m=2 below. (Taken directly from the computer output.)

THIS MATRIX IS FOR THE BASIC SPINNING MODE, M = 2

L	PRESSURE COEFF. (Pa)		PROP. COEFF.(PER FT)		C.O. FREQ (HZ)
1	7.708049	.000000	7.566877	.000000	274.2
2	-8.337461	.000000	6.876443	.000000	602.0
3	12.181790	.000000	5.639467	.000000	894.9
4	-28.633240	.000000	3.082705	.000000	1182.2
5	.000000	-17.762200	.703308	4.245116	1467.4
6	.000000	12.013140	.703308	6.832695	1751.5
7	.000000	-9.849725	.703308	8.962918	2035.1
8	.000000	8.626330	.703308	10.907160	2318.2

For this calculation only 8 values of l ("L" in the output) were considered, though the code permits the calculation of up to 10 values. It can be seen that there are four cut-on modes and that all four have significant amplitudes. The main mode with l=4 is dominant, but the other three cut-on modes have amplitudes that are at least 25% of the main mode. All the cut-on modes are in phase with each other and with the driver motion. The cut-off modes also have amplitudes that are significant, but they are 90 degrees out of phase with the cut-on modes. The cut-off modes also have large positive imaginary parts of their propagation coefficients ($B_{m,l}$) and should therefore decay rapidly in the axial direction away from the drivers.

By summing the contributions of the individual modes, complex pressure can be found for all values of r, θ and z. In the code such calculations are made at $z=L_a$ (driver ring axial location) and at $z=L_a+R$ (one radius upstream of the driver ring), for $\theta=0$. These pressure predictions are output in matrix form. Examples are given later when the computer codes are discussed. A plot of the results at $z=L_a$ is shown in Figure 83 below.

It is apparent that the contributions of the modes other than the main mode are quite significant, particularly near r=R, that is, at the drivers. This is not surprising since the summed contribution of all modes must satisfy the non-homogeneous wall boundary condition imposed by the drivers, while the single main mode cannot. It is also true that the cut-off modes contribute significantly to the pressure at $z=L_a$. One radius upstream (2 feet in this calculation) the picture is quite different, as can be seen in Figure 84. The contributions of the cut-on modes other than the main mode are still important and change the qualitative and quantitative pressure distribution very significantly.

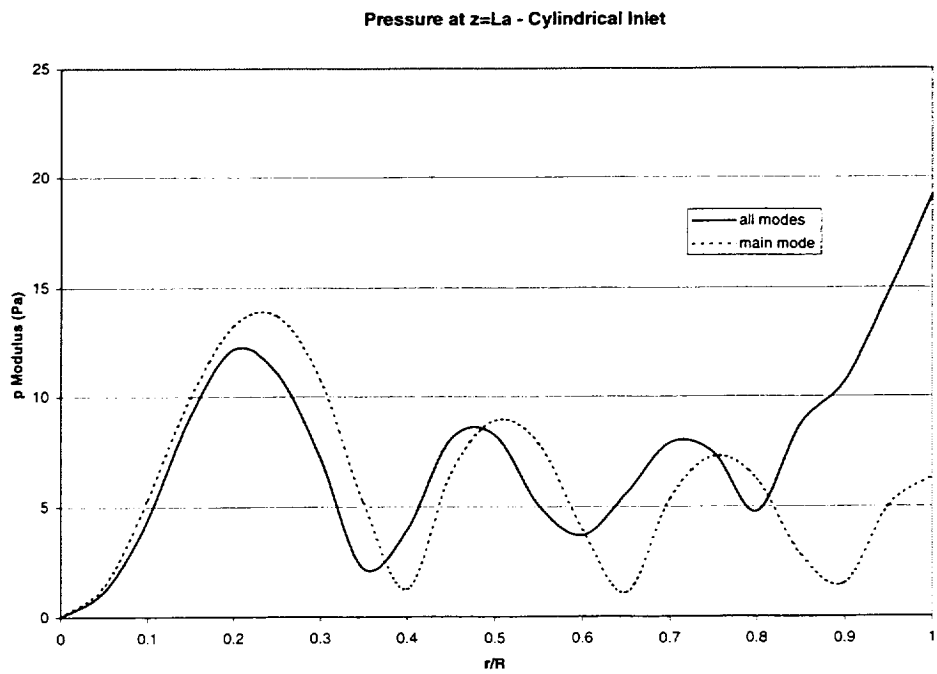

Figure 83. Radial pressure modal expansion at driver plane in cylindrical inlet.

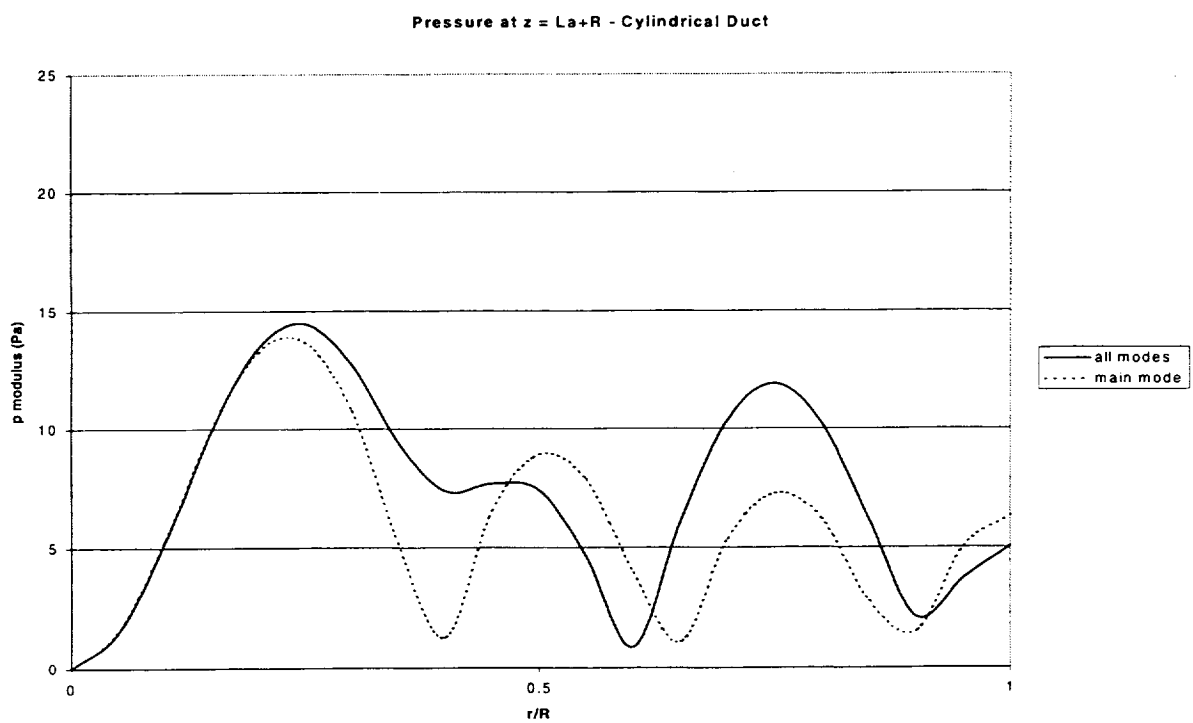

Figure 84. Radial pressure modal expansion at one diameter upstream from driver plane in cylindrical inlet.

11.4 Annular Exhaust Duct Model

The annular exhaust duct model differs from the inlet duct model primarily because of the presence of a center body. A sketch of the basic geometry is given in Figure 85.

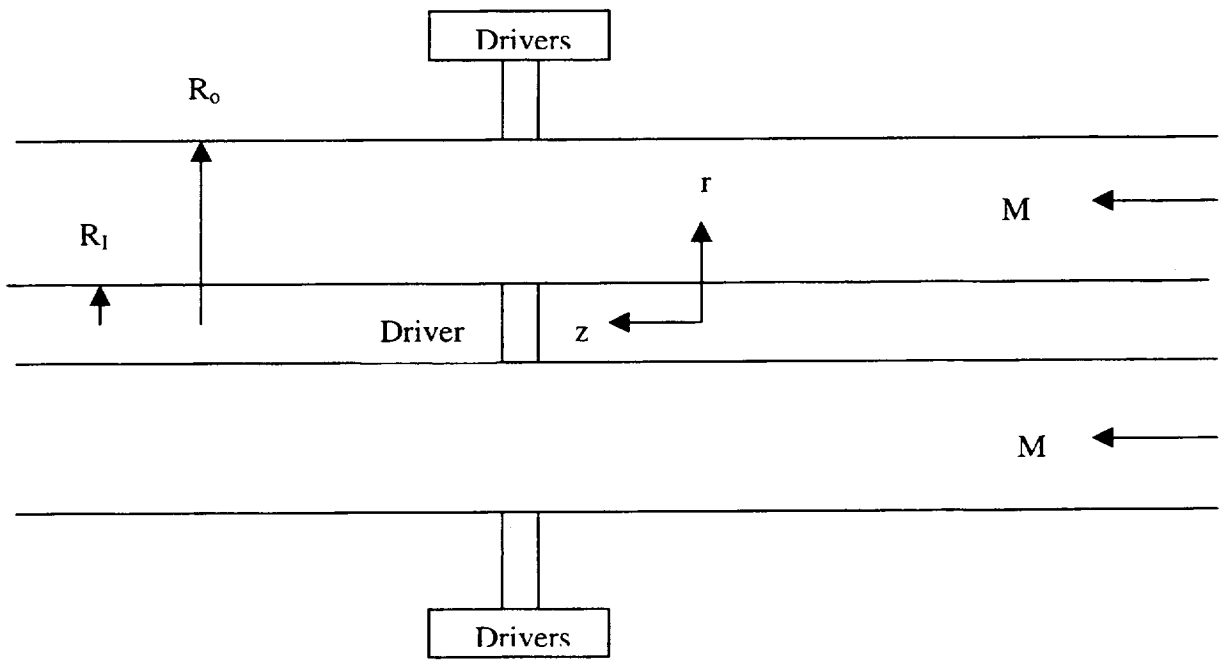

Figure 85. Schematic of annular exhaust duct model

The outer wall radius is R_o , the inner body radius is R_I. In this model there is both an outer driver ring and an inner driver ring. The actuators on both the outer and inner rings are evenly spaced top-hat drivers. The size of the individual actuators on the outer and inner rings can be different. Both actuator rings are located at the same axial location, L_a. As was done for the cylindrical model multiple modes in the azimuthal direction are included in the analysis and computer code in order to treat possible asymmetries in that coordinate direction. Here again this type of asymmetry was effected in calculations by blanking out one of the drivers. The analysis and computer codes are similar in general form to those already discussed for the cylindrical inlet duct. However, the annular geometry requires the use of Bessel functions of the second kind in order to describe the motion in the radial direction. Our previous work in rocket engines dealt with cylindrical geometry and methods and algorithms for the evaluation of Bessel functions of the first kind and their appropriate roots were already available from that work. This was not the case for the annular geometry. New subprograms had to be developed and checked out for the evaluation of both values and roots of Bessel functions of the second kind.

The basic equation for ϕ is formally the same as for the cylindrical model:

$$\phi(\bar{r}) = -\iint_{A_D} G(\bar{r}/\bar{r}_0) v_w(\bar{r}_0) dS_0 \tag{24}$$

In this case, however, the integral extends over both the outer and inner rings. Values for v_w must be specified for both rings.

Similarly, the expression for the appropriate Green's function can be written in the same form as for the cylindrical model:

$$G(\bar{r}/\bar{r}_0) = \sum_m \sum_l A_{m,l} \Omega_{m,l}(\bar{r}) \Omega_{m,l}(\bar{r}_0) e^{iB_{1,2}(z-z_0)} \tag{25}$$

here, however,

$$\Omega_{m,l}(\bar{r}) = \psi_{m,l}(\lambda_{ml} r) e^{im\theta} \tag{26}$$

$$\Omega_{m,l}(\bar{r}_0) = \psi_{m,l}(\lambda_{ml} r_0) e^{-im\theta_0} \tag{27}$$

$$\psi_{m,l}(\lambda_{m,l} r) = J_m(\lambda_{m,l} r) + B_{m,l} Y_m(\lambda_{m,l} r) \tag{28}$$

$$B_{m,l} = -\left[\frac{J'_m(\lambda_{m,l} r)}{Y'_{m,l}(\lambda_{m,l} r)} \right]_{r=1} \tag{29}$$

The parameters $\lambda_{m,l}$ are roots of

$$J'_m(\lambda_{m,l} r) + B_{m,l} Y'_{m,l}(\lambda_{m,l} r) = 0 \quad \text{for } r = R_1 \tag{30}$$

The constants $A_{m,l}$ and $B_{1,2}$ depend only on $M, \omega, \lambda_{m,l}$ and normalization constants. Carrying out the integration and use of the relationship between p and ϕ presented earlier gives the following expression for p (dimensional- in Pa):

$$p(r,\theta,z) = \sum_m \sum_l p_{m,l} \Omega_{m,l}(r/R,\theta) e^{iB_{m,l}|z-L_a|} \tag{31}$$

Values for $p_{m,l}$ and $B_{m,l}$ are determined through the integration over the actuator rings and depend on the v_w values for both inner and outer rings. These v_w values must be specified as inputs to the computer code ANN2F. The parameters $p_{m,l}$ and $B_{m,l}$ are calculated and output from the same code. The values of $p_{m,l}$ and $B_{m,l}$ are slightly different for $z \geq L_a$ and for $z < L_a$ because of mean flow effects. Only values for $z \geq L_a$ are printed out from the computer code. (The other coefficients are computed but not printed). $B_{m,l}$ is the propagation coefficient. If its imaginary

part is positive the mode is cut off. For equally spaced identical drivers only one term in the m summation has $p_{m,l}$ values different from zero. If one of the drivers is blanked out (shut off) however, this is not so and many terms in the m summation contribute. Even when only one term in the m summation is present, it is usual that several terms in the l summation are of significant size, and also that more than one mode is cut-on.

11.4.1 Results of Typical Calculations

The computer code ANN2F has been run for only a few sets of input data, since the goal of this project was to demonstrate the applicability of the Green's function technique rather than to investigate a large spectrum of design possibilities. Results for one of these data sets will be presented next. Relevant input parameters:

- 15 outer ring drivers each with a diameter of 2 inches
- 15 inner ring drivers each with a diameter of 1.5 inches
- outer actuator velocity amplitude, v_w, 1.0 ft/s
- inner actuator velocity amplitude, v_w, 1.0 ft/s
- outer duct radius, R_o, 24 inches
- inner duct radius, R_I, 7.375 inches
- frequency 1000 Hz
- mean flow Mach number 0.10
- mode number of primary mode, m=4

Execution of the code resulted in predictions for pressure coefficients and propagation coefficients. Since the drivers were identical and evenly spaced, pressure coefficients $p_{m,l}$ were non-zero only when m=4. Results for $p_{m,l}$ ("pressure coeff."), $B_{m,l}$ ("prop. Coeff.") and the cut-off frequency ("c. o. freq.") are shown in matrix form for m=4 below. (Taken directly from the computer output.)

THIS MATRIX IS FOR THE BASIC SPINNING MODE, M = 4

L	PRESSURE COEFF. (Pa)		PROP. COEFF.(PER FT)		C.O. FREQ (HZ)
1	11.316370	.000000	4.447573	.000000	472.2
2	-5.678955	.000000	2.780585	.000000	811.9
3	.000000	-35.056900	-.568187	2.335014	1086.6
4	.000000	-1.824272	-.568187	5.475510	1395.8
5	.000000	-16.308470	-.568187	8.094716	1749.4
6	.000000	-.066112	-.568187	10.578330	2124.0
7	.000000	11.982910	-.568187	12.994120	2508.6
8	.000000	.253964	-.568187	15.370800	2898.7
9	.000000	-4.033561	-.568187	17.722980	3292.1
10	.000000	-.201269	-.568187	20.058860	3687.7

For this calculation the maximum number of ten terms permitted by the code in the radial direction (designated by "L" in the output, and by l in this report) were kept. Only two modes were cut-on, m=4, l=1; and m=4, l=2. The second of these has a cut-off frequency closest to the driver frequency of 1000 Hz. However, the other cut-on mode is predicted to have a larger pressure coefficient, even though its cut-off frequency is less than half of the driver frequency. The pressure coefficients of the cut-off modes with odd values for l are also fairly large. With the exception of the l =3 mode, all the cut-off modes have propagation coefficients with large enough positive imaginary parts so that they decay very rapidly away from $z=L_a$.

By summing the contributions of the individual modes, complex pressure can be found for all values of r, θ and z. In the code such calculations are made at $z=L_a$ (driver ring axial location) and at $z=L_a+\Delta z$., for $\theta=0$, with r/R varying from its value at the inner body (.370) to 1.0. The parameter Δz is an arbitrary location downstream of the actuator rings, selected by the user. For this calculation Δz was taken to be 2 feet. The pressure predictions are given in matrix form in the output from the code. Examples are given later when the computer codes are discussed. In order to assess the relative importance of the inner and outer driver rings, calculations of pressure profiles were made with both drivers on, with only the inner drivers on and with only the outer drivers on. In all cases the driver velocity amplitude was 1.0 ft/s. A plot of the results at $z=L_a$ is shown in Figure 86.

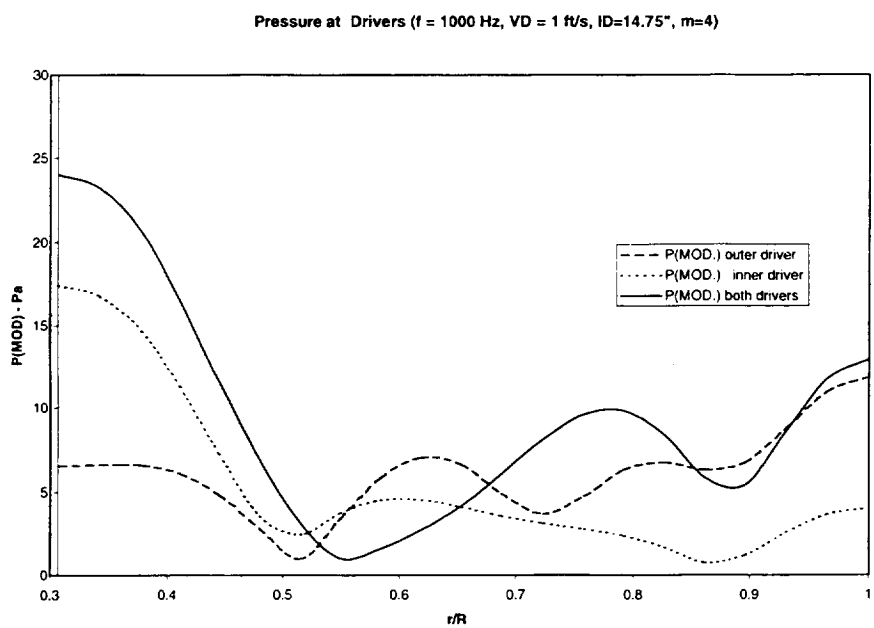

Figure 86. Radial pressure modal expansion at duct driver plane.

The impact of the inner driver is large near the inner drivers, that of the outer drivers large near the outer drivers, as would be expected. The distortion of the pressure profile compared with a pure m=4 mode is also apparent. Maximum amplitude occurs at the inner body. Predictions at $z=L_a+2$ ft. are quite different as can be seen on Figure 87.

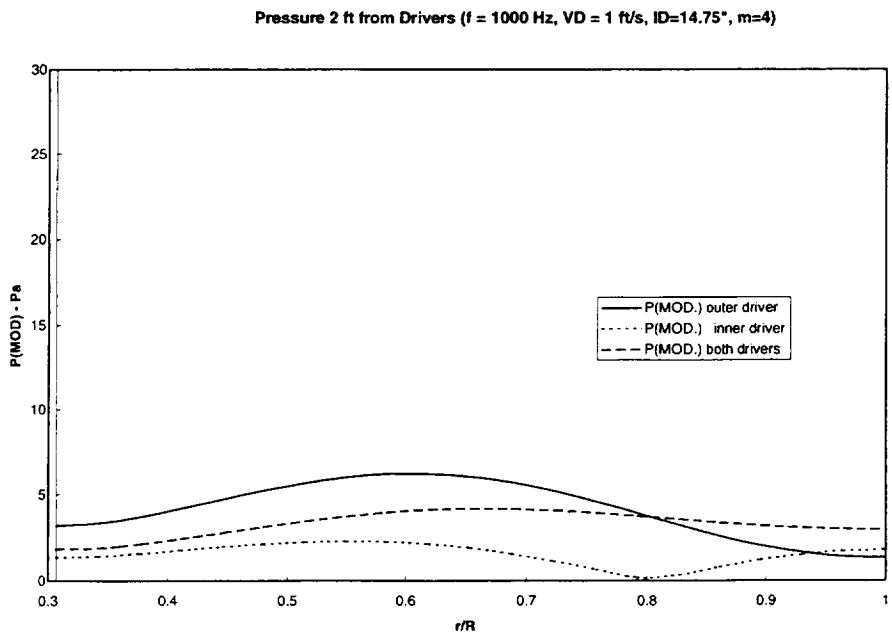

Figure 87. Radial pressure modal expansion two feet downstream of duct driver plane.

A most dramatic decrease in the amplitudes can be observed. In addition, all semblance of an m=4 type oscillation is gone. Part of the explanation must be the decay of the cut-off modes in the downstream direction. As well, some wave type behavior of the cut-on modes in the z direction must be present.

11.5 Description Of Computer Codes

1. **General Features.** Two computer codes were developed during the course of this work. The first of these (ANC2F) was designed to apply the Green's function technique to the analysis of a cylindrical inlet duct with one ring of active control drivers. The second code (ANN2F) treats annular exhaust ducts with one outer ring of drivers and one inner ring of drivers, both at the same axial location. ANN2F is also based on the use of the Green's function method. Both codes share a similar structure and include several common features. These include:

   - An arbitrary (user supplied) mean flow Mach number.
   - Evenly spaced (in the azimuthal direction) circular drivers producing "top hat" velocity profiles. The number and diameter of these drivers are supplied by the user.
   - Driver amplitude determined by supplying either a desired outer wall sound pressure level at the driver ring location (ANC2F), or separate velocity amplitudes for both outer and inner driver ring actuators (ANN2F).
   - Frequency and primary radial mode number, m, supplied by the user

- Prediction of the pressure field generated. Pressure is represented by computing amplitude coefficients for up to 170 acoustic modes in the radial and azimuthal directions. Cut-off frequencies and propagation coefficients for these modes are also calculated and given as output. Pressure amplitude and phase as a function of radius for two different axial locations are computed by summing the modal contributions.
- Symmetry in the azimuthal (θ) direction is **not** assumed. One or more of the drivers can be shut off, simulating a non-uniform driver distribution.

Executable copies of both codes are included on a diskette that accompanies this report. The codes were developed using Fortran Power Station software in standard F77 format. Execution time on a personal computer running at 266 MHz was approximately one second for all of the examples run during the course of the work.

2. **Input for ANC2F** All necessary input data is read from file ANIN2. A list of the required inputs follows:

LINE 1:

AREF- MEAN SONIC SPEED (FT/S)
MACH- MEAN FLOW MACH NUMBER
RDUCT- DUCT RADIUS (FT)

LINE 2:

NAD- NUMBER OF DRIVERS
DADIN- DIA. OF DRIVERS (IN.)
PDB-REQUIRED PRESSURE AMPLITUDE AT DRIVER (DB)
IBLANK- SET EQUAL TO 1 TO SHUT OFF DRIVER #2

LINE 3:

FREQ- FREQUENCY (HZ)
MHAT- AZIMUTHAL MODE NUMBER OF PRIMARY MODE (1=< MHAT <=8)
LHAT- RADIAL MODE NUMBER OF PRIMARY MODE (1=< LHAT <=10)
MTS- MODE NUMBER OF HIGHEST AZIMUTHAL MODE TO BE CONSIDERED (<= 8)
LTS- MODE NUMBER OF HIGHEST RADIAL MODE TO BE CONSIDERED (<= 10)

Note that a primary mode must be identified by making choices for m and l (called MHAT and LHAT). This is typically the cut-on mode closest to the specified frequency. IBLANK should be set equal to zero unless asymmetric driving, effected by shutting off driver#2 is desired. An example of input file ANIN2 is shown below. This example file is included on the diskette with the executable codes. The resulting output is given in the next section.

<u>ANIN2:</u>

1128,.1,2.
15,2.,110,0
1250,2,4,4,8

3. **Output for ANC2F** Output for ANC2F for the example input given above is placed in file AN2OUT. A printout of this file follows. Pressure and propagation coefficients are defined in the description of the analytical method given previously. In the example case the pressure coefficients are all zero (as they should be) except for the primary azimuthal mode, m=2. If one of drivers were blanked out (shut off) by setting IBLANK equal to 1 in ANIN2, then the driving would no longer be symmetric in the azimuthal direction and coefficients for all m values would be non-zero in general. The complex pressure and modulus of the pressure (summed for all modes) is given at the driver location (Z = LA) and at a location one radius upstream. For reference the pressure and modulus of the pressure for the primary mode (m=2, l=4) alone is also printed for the same locations.

```
 PROGRAM ANC2F

 CONSIDERS 15 DRIVERS WITH 2.00 IN. DIA.
 SONIC SPEED = 1128. FT/S, DUCT RADIUS = 2.00 FT.

INPUT DATA:

 FREQUENCY = 1250. HZ
 WALL SPL FOR PRIMARY MODE = 110. DB (OR 6.324555 Pa)
 MACH NUMBER = .10
 PRIMARY SPINNING MODE (MHAT) =  2
 PRIMARY RADIAL MODE NUMBER (LHAT) =  4

 RESULTS OF CALCULATIONS:

 REQUIRED ACTUATOR VELOCITY MAGNITUDE =   1.2677    FT/S
 CORRESPONDING DISPLACEMENT MAGNITUDE =   .19370E-02 IN.


 THIS MATRIX IS FOR M = -4

    L   PRESSURE COEFF. (Pa)     PROP. COEFF.(PER FT)     C.O. FREQ (HZ)

    1    -.000001    .000001    7.208977    .000000        477.3
    2     .000001   -.000001    5.966949    .000000        833.2
    3    -.000003    .000002    3.678267    .000000       1138.4
    4    -.000001   -.000002     .703308   3.859084       1433.0
    5     .000001    .000001     .703308   6.602135       1723.1
    6    -.000001   -.000001     .703308   8.789455       2010.8
    7     .000001    .000001     .703308  10.765610       2297.0
    8    -.000001   -.000001     .703308  12.630230       2582.3

 THIS MATRIX IS FOR M = -3

    L   PRESSURE COEFF. (Pa)     PROP. COEFF.(PER FT)     C.O. FREQ (HZ)
```

1	.000001	.000000	7.412045	.000000	377.1
2	-.000001	.000000	6.468808	.000000	719.5
3	.000002	.000000	4.821153	.000000	1018.4
4	-.000001	.000004	.703308	2.063918	1309.3
5	.000000	-.000002	.703308	5.517676	1596.8
6	.000000	.000001	.703308	7.849057	1882.6
7	.000000	-.000001	.703308	9.886959	2167.3
8	.000000	.000001	.703308	11.784690	2451.4

THIS MATRIX IS FOR M = -2

L	PRESSURE COEFF. (Pa)		PROP. COEFF.(PER FT)		C.O. FREQ (HZ)
1	.000000	.000000	7.566877	.000000	274.2
2	.000000	.000000	6.876443	.000000	602.0
3	.000000	.000000	5.639467	.000000	894.9
4	-.000001	.000000	3.082705	.000000	1182.2
5	.000000	.000000	.703308	4.245116	1467.4
6	.000000	.000000	.703308	6.832695	1751.5
7	.000000	.000000	.703308	8.962918	2035.1
8	.000000	.000000	.703308	10.907160	2318.2

THIS MATRIX IS FOR M = -1

L	PRESSURE COEFF. (Pa)		PROP. COEFF.(PER FT)		C.O. FREQ (HZ)
1	.000000	.000000	7.675264	.000000	165.3
2	.000000	.000000	7.206106	.000000	478.6
3	.000001	.000000	6.276731	.000000	766.2
4	-.000001	.000001	4.558246	.000000	1050.8
5	-.000001	-.000002	.703308	2.515002	1334.2
6	.000001	.000001	.703308	5.700454	1617.1
7	.000000	-.000001	.703308	7.978066	1899.8
8	.000000	.000001	.703308	9.989417	2182.3

THIS MATRIX IS FOR M = 0

L	PRESSURE COEFF. (Pa)		PROP. COEFF.(PER FT)		C.O. FREQ (HZ)
1	.000000	.000000	7.736389	.000000	.0
2	.000000	.000000	7.467675	.000000	343.9
3	.000000	.000000	6.788973	.000000	629.7
4	.000000	.000000	5.533215	.000000	913.2
5	.000001	.000001	2.856386	.000000	1196.0
6	.000000	.000000	.703308	4.363628	1478.5
7	.000000	.000000	.703308	6.906730	1760.8
8	.000000	.000000	.703308	9.019382	2043.0

THIS MATRIX IS FOR M = 1

L	PRESSURE COEFF. (Pa)		PROP. COEFF.(PER FT)		C.O. FREQ (HZ)
1	.000000	.000000	7.675264	.000000	165.3
2	.000000	.000000	7.206106	.000000	478.6
3	.000000	.000000	6.276731	.000000	766.2
4	.000000	.000000	4.558246	.000000	1050.8
5	.000000	.000000	.703308	2.515002	1334.2

6	.000000	.000000	.703308	5.700454	1617.1
7	.000000	.000000	.703308	7.978066	1899.8
8	.000000	.000000	.703308	9.989417	2182.3

THIS MATRIX IS FOR THE BASIC SPINNING MODE, M = 2

L	PRESSURE COEFF. (Pa)		PROP. COEFF.(PER FT)		C.O. FREQ (HZ)
1	7.708049	.000000	7.566877	.000000	274.2
2	-8.337461	.000000	6.876443	.000000	602.0
3	12.181790	.000000	5.639467	.000000	894.9
4	-28.633240	.000000	3.082705	.000000	1182.2
5	.000000	-17.762200	.703308	4.245116	1467.4
6	.000000	12.013140	.703308	6.832695	1751.5
7	.000000	-9.849725	.703308	8.962918	2035.1
8	.000000	8.626330	.703308	10.907160	2318.2

THIS MATRIX IS FOR M = 3

L	PRESSURE COEFF. (Pa)		PROP. COEFF.(PER FT)		C.O. FREQ (HZ)
1	.000000	.000000	7.412045	.000000	377.1
2	.000000	.000000	6.468808	.000000	719.5
3	.000000	.000000	4.821153	.000000	1018.4
4	.000000	.000000	.703308	2.063918	1309.3
5	.000000	.000000	.703308	5.517676	1596.8
6	.000000	.000000	.703308	7.849057	1882.6
7	.000000	.000000	.703308	9.886959	2167.3
8	.000000	.000000	.703308	11.784690	2451.4

THIS MATRIX IS FOR M = 4

L	PRESSURE COEFF. (Pa)		PROP. COEFF.(PER FT)		C.O. FREQ (HZ)
1	.000000	.000000	7.208977	.000000	477.3
2	.000000	.000000	5.966949	.000000	833.2
3	.000000	-.000001	3.678267	.000000	1138.4
4	.000001	.000000	.703308	3.859084	1433.0
5	.000000	.000000	.703308	6.602135	1723.1
6	.000000	.000000	.703308	8.789455	2010.8
7	.000000	.000000	.703308	10.765610	2297.0
8	.000000	.000000	.703308	12.630230	2582.3

PRESSURE DATA AT Z=LA, THETA = 0

R	PRESSURE (Pa)		MAIN MODE PRES. (Pa)		P(MOD.)	MODE(MOD.)
.00	.0000	.0000	.0000	.0000	.0000	.0000
.05	-1.2198	.0583	-1.4968	.0000	1.2212	1.4968
.10	-4.3285	-.6881	-5.3582	.0000	4.3828	5.3582
.15	-7.9014	-3.2118	-9.9451	.0000	8.5293	9.9451
.20	-10.2320	-5.9944	-13.2529	.0000	11.8586	13.2529
.25	-10.0471	-6.0047	-13.7020	.0000	11.7047	13.7020
.30	-7.0565	-2.4061	-10.7662	.0000	7.4555	10.7662
.35	-2.1098	2.0441	-5.1925	.0000	2.9376	5.1925

.40	3.1083	4.0415	1.2694	.0000	5.0985	1.2694
.45	6.7283	3.2437	6.5244	.0000	7.4693	6.5244
.50	7.4382	1.6798	8.9173	.0000	7.6255	8.9173
.55	5.0222	.3739	7.8449	.0000	5.0361	7.8449
.60	.4794	-1.6082	3.9602	.0000	1.6781	3.9602
.65	-4.3304	-4.3166	-1.1021	.0000	6.1143	1.1021
.70	-7.3809	-5.0078	-5.3656	.0000	8.9194	5.3656
.75	-7.2495	-1.0944	-7.2647	.0000	7.3316	7.2647
.80	-3.6658	5.3261	-6.2164	.0000	6.4657	6.2164
.85	2.3712	8.1055	-2.7985	.0000	8.4452	2.7985
.90	8.9515	3.5473	1.5251	.0000	9.6287	1.5251
.95	13.9498	-4.6690	5.0103	.0000	14.7104	5.0103
1.00	15.7918	-8.6995	6.3246	.0000	18.0295	6.3246

PRESSURE DATA AT Z=LA+R, THETA = 0

R	PRESSURE (Pa)		MAIN MODE PRES. (Pa)		P(MOD.)	MODE(MOD.)
.00	.0000	.0000	.0000	.0000	.0000	.0000
.05	-1.4448	-.2754	-1.4864	.1759	1.4709	1.4968
.10	-5.1751	-1.0770	-5.3211	.6296	5.2859	5.3582
.15	-9.6180	-2.3227	-9.8762	1.1686	9.8945	9.9451
.20	-12.8581	-3.8562	-13.1611	1.5573	13.4239	13.2529
.25	-13.4020	-5.4370	-13.6071	1.6100	14.4629	13.7020
.30	-10.7802	-6.7568	-10.6916	1.2651	12.7227	10.7662
.35	-5.7498	-7.4895	-5.1566	.6101	9.4421	5.1925
.40	-.0166	-7.3711	1.2606	-.1492	7.3711	1.2694
.45	4.4141	-6.2841	6.4792	-.7666	7.6794	6.5244
.50	6.0048	-4.3178	8.8556	-1.0478	7.3960	8.9173
.55	4.2723	-1.7765	7.7906	-.9218	4.6269	7.8449
.60	-.0327	.8786	3.9328	-.4653	.8792	3.9602
.65	-5.2205	3.1415	-1.0944	.1295	6.0929	1.1021
.70	-9.3132	4.5982	-5.3285	.6305	10.3865	5.3656
.75	-10.7957	5.0442	-7.2143	.8536	11.9160	7.2647
.80	-9.1776	4.5444	-6.1733	.7304	10.2411	6.2164
.85	-5.1518	3.4117	-2.7791	.3288	6.1791	2.7985
.90	-.2986	2.1095	1.5145	-.1792	2.1306	1.5251
.95	3.5424	1.1075	4.9756	-.5887	3.7115	5.0103
1.00	4.9805	.7375	6.2807	-.7432	5.0348	6.3246

4. **Input for ANN2F** The input file ANNIN2 for the annular exit duct program is similar to that for the cylindrical code. A listing of required input follows:

LINE 1:

AREF- MEAN SONIC SPEED (FT/S)
MACH- MEAN FLOW MACH NUMBER
RDUCT- OUTER DUCT RADIUS (FT)
RDUCTI- INNER DUCT RADIUS (FT)

LINE 2:

NAD- NUMBER OF OUTER DRIVERS
NADI- NUMBER OF INNER DRIVERS
DAD- DIA. OF OUTER DRIVERS (IN.)
DADI- DIA. OF INNER DRIVERS (IN.)
KWD- OUTER DRIVER VELOCITY AMPLITUDE (FT/S)
KWID- INNER DRIVER VELOCITY AMPLITUDE (FT/S)
IBLANK- SET EQUAL TO 1 TO SHUT OFF DRIVER #2

LINE 3:

FREQ- FREQUENCY (HZ)
MHAT- AZIMUTHAL MODE NUMBER OF PRIMARY MODE (1=< MHAT <=8)
MTS- MODE NUMBER OF HIGHEST AZIMUTHAL MODE TO BE CONSIDERED (<= 8)
LTS- MODE NUMBER OF HIGHEST RADIAL MODE TO BE CONSIDERED (<= 10)
MST- MODE NUMBER OF LOWEST AZIMUTHAL MODE TO BE CONSIDERED (>= -MTS)
LST- MODE NUMBER OF LOWEST RADIAL MODE TO BE CONSIDERED (>= 1)
DELZD- DISTANCE DOWNSTREAM OF DRIVER PLANE AT WHICH ADDITIONAL PRESSURE PROFILE IS TO BE EVALUATED (FT)

For ANN2F the inner and outer driver amplitudes instead of a sound pressure level at the wall must be specified. Either the inner drivers, the outer drivers or both can be activated by selecting driver velocity magnitudes appropriately. In the example given below , both driver rings are active with equal velocity amplitudes. Only the primary azimuthal mode must be identified (i.e. its m value called MHAT must be given). For the case of drivers symmetric in the azimuthal direction (drivers identical and evenly spaced) only the pressure coefficients for m = MHAT will be non-zero, and to reduce output MST and MTS can both be set equal to MHAT. This is done for the example input file which follows. Note that an arbitrary axial location must be specified at which a pressure profile is to be calculated in addition to the profile at the plane of the drivers (which is always computed). Setting IBLANK equal to 1 gives asymmetrical driving in the azimuthal direction as was the case with ANC2F. When this is done non-zero pressure coefficients for m values other than MHAT will result and MTS and MST should be set different from MHAT. The example file ANNIN2 that follows is included on the diskette. The corresponding output is given in the next section.

<u>ANNIN2:</u>

```
1117,.1,2,.61458333
15,15,2,1.5,1,1,0
1000,4,4,10,4,1,2
```

5. **Output for ANN2F** Output for ANN2F for the example input given above is placed in file ANN2OUT. A printout of this file follows. Pressure and propagation coefficients are defined in the description of the analytical method given previously. The modulus and phase angle of the complex pressure as well as the complex pressure itself (summed for all modes) as a function of the radius (starting at the inner body of the annulus) are given at the driver location (Z = LA) and at a location two feet downstream of the actuator rings (Z = LA + 2 FT).

```
 PROGRAM ANN2F

 CONSIDERS 15 OUTER DRIVERS WITH 2.00 IN. DIA. AND 15 INNER DRIVERS
WITH 1.50 IN. DIA.
 SONIC SPEED =1117. FT/S
 OUTER DUCT RADIUS = 2.00 FT., INNER DUCT RADIUS =  .614583 FT.

 INPUT DATA:

 FREQUENCY = 1000. HZ
 MACH NUMBER = .10
 PRIMARY SPINNING MODE (MHAT) =  4

 OUTER ACTUATOR VELOCITY MAGNITUDE =   1.0000    FT/S
 CORRESPONDING DISPLACEMENT MAGNITUDE =   .19099E-02 IN.
 INNER ACTUATOR VELOCITY MAGNITUDE =   1.0000    FT/S
 CORRESPONDING DISPLACEMENT MAGNITUDE =   .19099E-02 IN.


 RESULTS OF CALCULATIONS:



 THIS MATRIX IS FOR THE BASIC SPINNING MODE, M =  4

    L   PRESSURE COEFF. (Pa)     PROP. COEFF.(PER FT)     C.O. FREQ (HZ)

    1   11.316370     .000000    4.447573     .000000        472.2
    2   -5.678955     .000000    2.780585     .000000        811.9
    3     .000000 -35.056900     -.568187    2.335014       1086.6
    4     .000000  -1.824272     -.568187    5.475510       1395.8
    5     .000000 -16.308470     -.568187    8.094716       1749.4
    6     .000000   -.066112     -.568187   10.578330       2124.0
    7     .000000  11.982910     -.568187   12.994120       2508.6
    8     .000000    .253964     -.568187   15.370800       2898.7
    9     .000000  -4.033561     -.568187   17.722980       3292.1
   10     .000000   -.201269     -.568187   20.058860       3687.7

 PRESSURE DATA AT Z=LA, THETA = 0

    R       PRESSURE (Pa)        P(MOD.)    PHASE(DEG)

  .307   -1.03902 -32.38399   32.40065   -91.8377
  .342   -1.07160 -28.26276   28.28307   -92.1714
  .377   -1.14100 -19.29484   19.32855   -93.3842
  .411   -1.21201 -12.07107   12.13176   -95.7336
```

.446	-1.25451	-9.43413	9.51717	-97.5745
.480	-1.24136	-8.67002	8.75844	-98.1482
.515	-1.14864	-6.15723	6.26346	-100.5672
.550	-.95692	-1.84595	2.07924	-117.4018
.584	-.65288	1.75453	1.87206	110.4109
.619	-.23082	3.59010	3.59751	93.6787
.654	.30621	5.13384	5.14296	86.5866
.688	.94589	7.53034	7.58951	82.8406
.723	1.66678	9.52391	9.66866	80.0732
.792	3.22756	7.32629	8.00573	66.2243
.827	3.99137	5.65240	6.91959	54.7727
.861	4.68933	4.58825	6.56063	44.3758
.896	5.28168	1.71210	5.55224	17.9606
.931	5.73334	-4.68664	7.40512	-39.2638
.965	6.01658	-12.12527	13.53593	-63.6093
1.000	6.11322	-15.46682	16.63112	-68.4337

PRESSURE DATA AT Z = LA + 2.000 FT., THETA = 0

R	PRESSURE (Pa)		P(MOD.)	PHASE(DEG)
.307	-1.54059	1.05791	1.86885	145.5230
.342	-1.61205	1.11257	1.95871	145.3881
.377	-1.78680	1.24881	2.17995	145.0498
.411	-2.02187	1.43605	2.47996	144.6154
.446	-2.28625	1.65089	2.81999	144.1672
.480	-2.55505	1.87271	3.16786	143.7606
.515	-2.80770	2.08247	3.49569	143.4357
.550	-3.02768	2.26282	3.77984	143.2264
.584	-3.20283	2.39902	4.00167	143.1656
.619	-3.32573	2.47998	4.14859	143.2882
.654	-3.39382	2.49929	4.21480	143.6312
.688	-3.40924	2.45590	4.20171	144.2324
.723	-3.37828	2.35439	4.11776	145.1266
.758	-3.31056	2.20473	3.97752	146.3377
.792	-3.21797	2.02141	3.80019	147.8645
.827	-3.11348	1.82216	3.60750	149.6618
.861	-3.00988	1.62616	3.42107	151.6188
.896	-2.91859	1.45214	3.25989	153.5475
.931	-2.84864	1.31637	3.13809	155.1981
.965	-2.80577	1.23089	3.06389	156.3129
1.000	-2.79178	1.20206	3.03957	156.7046

REPORT DOCUMENTATION PAGE

Form Approved
OMB No. 0704-0188

Public reporting burden for this collection of information is estimated to average 1 hour per response, including the time for reviewing instructions, searching existing data sources, gathering and maintaining the data needed, and completing and reviewing the collection of information. Send comments regarding this burden estimate or any other aspect of this collection of information, including suggestions for reducing this burden, to Washington Headquarters Services, Directorate for Information Operations and Reports, 1215 Jefferson Davis Highway, Suite 1204, Arlington, VA 22202-4302, and to the Office of Management and Budget, Paperwork Reduction Project (0704-0188), Washington, DC 20503.

1. AGENCY USE ONLY (*Leave blank*)

2. REPORT DATE
September 2000

3. REPORT TYPE AND DATES COVERED
Final Contractor Report

4. TITLE AND SUBTITLE
Development and Demonstration of Active Noise Control Concepts

5. FUNDING NUMBERS
WU-522-81-11-00
NAS3-27720

6. AUTHOR(S)
R. Kraft, Z. Hu, S. Sommerfeldt, B. Walker, A. Hersh, H. Luo,
M. Spencer, D. Hallman, C. Mitchell, and D. Sutliff

7. PERFORMING ORGANIZATION NAME(S) AND ADDRESS(ES)
GE Aircraft Engines
One Neumann Way, MD B-5
Cincinnati, Ohio 45125-1988

8. PERFORMING ORGANIZATION REPORT NUMBER
E-12235

9. SPONSORING/MONITORING AGENCY NAME(S) AND ADDRESS(ES)
National Aeronautics and Space Administration
Washington, DC 20546-0001

10. SPONSORING/MONITORING AGENCY REPORT NUMBER
NASA CR—2000-210037

11. SUPPLEMENTARY NOTES
R. Kraft, GE Aircraft Engines, One Neumann Way, MD B-5, Cincinnati, Ohio 45125-1988; Z. Hu, H. Luo, and D. Hallman, GE CR&D, Schenectady, New York; S. Sommerfeldt, Brigham Young University, Provo, Utah 84602; B. Walker and A. Hersh, Hersh Acoustical Engineering, Westlake Village, California; M. Spencer, Signal Processing Solutions, Redondo Beach, California; C. Mitchell, Colorado State University, Fort Collins, Colorado 80523-0002; and D. Sutliff, AYT Corporation, 2001 Aerospace Parkway, Brook Park, Ohio 44142. Project Manager, L.J. Heidelberg, Structures and Acoustics Division, NASA Glenn Research Center, organization code 5940, (216) 433-3859.

12a. DISTRIBUTION/AVAILABILITY STATEMENT
Unclassified - Unlimited
Subject Categories: 07 and 71 Distribution: Nonstandard
Available electronically at http://gltrs.grc.nasa.gov/GLTRS
This publication is available from the NASA Center for AeroSpace Information, (301) 621-0390.

12b. DISTRIBUTION CODE

13. ABSTRACT ***(Maximum 200 words)***

This report details design methods for and feasibility of an Active Noise Control (ANC) system using flush-wall-mounted sensors and actuators to reduce turbofan engine rotor-stator interaction noise. ANC concepts capable of suppressing discrete-tone spinning modes containing several cut-on radial mode were identified, developed analytically, and evaluated. Separate ANC systems that suppressed at least three radial modes in a cylindrical inlet duct and three radial modes in an exhaust annulus were developed. These designs resulted in inlet duct and exhaust duct tests that were performed at NASA on the 4-ft ANC Fan in the NASA Glenn AAPL facility. Effective suppression of 2-BPF spinning mode m=2 tone noise was achieved over a range of fan speeds 1800 to 2450 rpm, where up to 4 radials were present. In the inlet duct, up to 12 dB reduction was obtained for 3 radial modes, and up to 4 dB was obtained with 4 radial modes. In the exhaust duct, up to 15 dB PWL reduction was obtained with either two or three radial modes present. Thus, the ability to suppress multiple radial modes for tones in both the inlet and exhaust ducts has been successfully demonstrated. Implications of ANC system design requirements on installation and system integration issues for ANC systems capable of suppressing higher order radial mode content when applied to a 767 using twin CF6 engines were evaluated analytically. The analytical results indicated an ANC system must be part of an integrated design to be effective.

14. SUBJECT TERMS
Acoustic ducts; Fan noise; Ducted fans

15. NUMBER OF PAGES
155

16. PRICE CODE
A08

17. SECURITY CLASSIFICATION OF REPORT	18. SECURITY CLASSIFICATION OF THIS PAGE	19. SECURITY CLASSIFICATION OF ABSTRACT	20. LIMITATION OF ABSTRACT
Unclassified	Unclassified	Unclassified	